Title

Dielectric Elastomer Based Devices: Compliant Electrodes and Dielectric Elastomer Materials Improvements

Author

Peng, Zihang

Publication Date

2022

Peer reviewed|Thesis/dissertation

UNIVERSITY OF CALIFORNIA

Los Angeles

Dielectric Elastomer Based Devices:

Compliant Electrodes and Dielectric Elastomer Materials Improvements

A dissertation submitted in partial satisfaction of the

requirements of the degree Doctoral of Philosophy

in Materials Science and Engineering

by

Zihang Peng

2022

ABSTRACT OF THE DISSERTATION

Dielectric Elastomers Based Devices:

Compliant Electrodes and Dielectric Elastomer Materials Improvements

by

Zihang Peng

Doctor of Philosophy in Materials Science and Engineering

University of California, Los Angeles, 2022

Professor Qibing Pei, Chair

Dielectric elastomers (DEs) can generate large deformations in response to electric stimuli. A DE film sandwiched between a pair of compliant electrodes behaves as a deformable capacitor. The electrostatic force under an electric field causes the film to shrink in thickness and expand in area. The dielectric elastomer actuator (DEA) technology is superior to most other electrical actuation technologies regarding its large actuation strain, high energy density, light weight, mechanical compliancy, and low cost. However, it has been challenging to transition the DEA technology into practical products due to its low operational stability caused by material limitations (DEs and compliant electrodes) and lack of suitable multilayer fabrication processes.

Carbon nanotubes (CNTs) have been widely used as compliant electrodes for DEAs. However, the sharp tips of CNTs induce corona discharges in air under high electric fields, eventually leading to dielectric breakdown. One focus of this dissertation is on developing a CNT-related compliant electrode with long-term stability and reliability at large strains. A bilayer electrode consisting of an ultra-thin CNT network overcoated by a thin polymer layer is introduced. The thin polymer layer serves as the dielectric barrier to suppress corona discharges of the nanotubes in air. The bilayer electrode is compliant and maintains its conductivity under large deformation. The self-clearing property of this bilayer electrode affords fault tolerance; corona discharge that could potentially leads to dielectric breakdown of the DEA is transformed into small current spikes. With the bilayer electrode, the operation stability of VHB acrylic elastomer-based DEAs is improved to 1000 cycles at 150% area strain under a square-wave voltage and 5.5-hours continuous actuation at a constant voltage.

The VHB acrylic elastomer is a commonly used DE material due to its ability to sustain high electric fields and reach large actuation strains and energy densities. However, high prestrain is required to obtain the high performance. The frames used to support the prestrain limit device flexibility, reduce overall specific energy density, and cause fatigue over time. Therefore, another focus of this dissertation is to synthesize high-performance prestrain-locked VHB DEs. The prestrain-locked free-standing DE films, VHB-IPN-Ps, have lower viscoelasticity and Young's modulus as compared to highly prestrained VHB films. VHB-IPN-Ps respond to electric fields fast and reach large strains at relatively low electric fields. The DEA based on the VHB-IPN-P and the bilayer electrode can be operated over 5000 cycles at strains above 80% under a square-wave voltage stably and reliably. A multilayer stacking process based on VHB-IPN-Ps and the bilayer

electrodes is also developed. This process is a hybrid of wet deposition and solid film lamination and has the potential to be scaled up for the manufacturing of multilayer DEAs.

This dissertation also studies a DE derivative material, a phase-changing bistable electroactive polymer (BSEP), to enable rigid-to-rigid actuation without complex structures. Unlike most BSEPs, which have broad glass transition temperature bands over 30 °C to complete the modulus change, the phase-changing BSEP undergoes reversible melting-crystallization of the polymer chains in a narrow temperature band, resulting in a modulus change within 10 ˚C. A tactile display of Braille standard resolution was explored based on the phase-changing BSEP. It employed 'Prestretch-Pattern-Protect-Release' to pattern the serpentine electrode for Joule heating to administer the phase change under a pneumatic actuation mechanism to deform the polymer at the softened state. This work has improved the phase-changing BSEP to achieve over 1000-folds modulus change within 3 ˚C. A laser-engraving process is adopted to pattern the serpentine electrode for localized Joule heating with high resolution. The resulting tactile display achieves large vertical displacements of the Braille dots and high blocking forces under a low power supply. This tactile display may potentially be made user-safe and cost-effective in various tactile-display-related devices.

The dissertation of Zihang Peng is approved.

Yinmin Morris Wang

Aaswath Pattabhi Raman

Veronica Santos

Qibing Pei, Committee Chair

University of California, Los Angeles

2022

TABLE OF CONTENTS

LIST OF FIGURES

LIST OF TABLES

ACKNOWLEDGEMENT

My honest thanks and acknowledgments give to all the people who provided their generous help in various ways during my five-year study at UCLA.

I would like to thank my advisor, Professor Qibing Pei, for his professional guidance and financial support during my Ph.D. study. Professor Pei has not only offered me inspiring ideas and encouragement in research, but also taught me how to think, analyze, and scientifically solve problems.

I would like to thank Professor Yinmin Morris Wang, Professor Aaswath Raman, Professor Veronica Santos, for being my committee members and for their valuable comments.

Especially, I would like to thank Dr. Kwing Tong, Dr. Yuan Meng, Dr. Ziyang Zhang, Dr. Jason (Zhixin) Xie, and Dr. Yu Qiu for teaching me fundamental skills in the lab and setting up experimental apparatus at the early stage of my Ph.D. study. I would like to thank Dr. Ye Shi for his professional advice in conducting scientific experiments and for critically reviewing my manuscripts for publication. Without him, my research could be far slower. I would like to thank Ms. Ziqing Han for working with me in the lab during the last year of my Ph.D. study. Her help makes my graduation smoother. I would also like to thank the three undergraduates who worked with me, Yanji Li, Norris Chen, and Belinda (Huiying) Wang, for trusting me and helping me with experiments. I would like to give my thanks to Dr. Roger (Hongxiang) Zhao, Dr. Yu Xie, Mr. Hanxiang Wu, Ms. Yuan Zhu, Mr. Yuanxuan Guo, Mr. Hexing Yin, Mr. Jinsung Kim, Mr. Kareem Youssef, Mr. Roshan Plamthottam, Ms. Jianghan Wu, Mr. Jiacheng Fan, Mr. Hao Yu, all the previous lab members and my research collaborators for their help and valuable discussion.

Outside the academic field, I would like to thank Dr. Boris Russ, Dr. Alvin Barlian, and Dr. Bayu Atmaja Thedjoisworo in Apple Inc. for offering the internship opportunity. And thank all the intelligent colleagues who I worked with, for their help. This 6-month internship provided me with insights into the consumer electronics industry and inspired my scoping in career.

A big thanks to my best friends Ms. Bei Zhou and M.D. Naici Liu for always encouraging me, even though we are physically far from each other. A lot of thanks to my best friend at UCLA, Ms. Jin Cai, her kindness keeps warming my heart. The greatest thank to my family, especially to my grandparents and my mom, for their selfless support and unconditional love. I love you so much! I would also like to thank my boyfriend, Mr. Ruiyi Wu, for always being with me and being inclusive of everything about me. Finally, my most special thanks to my lovely pets, Joizze, UU, Yuki, and Zia, you are the best gifts ever. I love you FOREVER!

VITA

2017	B.S., Polymer Materials and Engineering
	Sichuan University
2017-2022	Ph.D. Candidate, Materials Science and Engineering
	University of California, Los Angeles, CA

PUBLICATIONS

Z. Peng, Y. Shi, N. Chen, Y. Li and Q. Pei, Stable and high-strain dielectric elastomer actuators based on a carbon nanotube-polymer bilayer electrode, *Advanced Functional Materials*, 2020, 2008321.

Z. Han**, Z. Peng** and Q. Pei, Hybrid manufacturing of prestrain-locked acrylic dielectric elastomer thin films and multilayer stacks. *In preparation.*

Z. Peng, Y. Shi, Z. Xie, Y. Li, N. Chen and Q. Pei, Self-clearable compliant electrode for dielectric elastomer actuators. *Electroactive Polymer Actuators and Devices (EAPAD) XXIII*, 2021, 115871Y.

Z. Peng, Y. Qiu, Y. Shi, Z. Zhang, A. Alwen, H. Yin and Q. Pei, Bistable electroactive polymers for refreshable tactile displays. *Electroactive Polymer Actuators and Devices (EAPAD) XXI*, 2019, 109662C.

J. Pu, Y. Meng, Z. Xie, **Z. Peng**, J. Wu, R. Plamthottam, W. Yang and Q. Pei, A unimorph nanocomposite dielectric elastomer for large out-of-plane actuation. *Science Advances*, 2022, 8(9).

Y. Zhang, Y. Zhao, **Z. Peng**, B. Yao, Y. Alsaid, M. Hua, D. Wu, Y. Qiu, Q. Pei, X. Zhu, Z. He and X. He, Ultrastretchable polyaniline-based conductive organogel with high strain sensitivity. *ACS Materials Letter*, 2021, 3.

Z. Xie, J. Kim, **Z. Peng**, Y. Qiu and Q. Pei, A 2D refreshable braille display based on a stiffness variable polymer and pneumatic actuation. *Electroactive Polymer Actuators and Devices (EAPAD) XXIII*, 2021, 115870O.

Y. Liu, J. Fan, R. Plamthottam, M. Gao, **Z. Peng**, Y. Meng, M. He, H. Wu, Y. Wang, T. Liu, C. Zhang and Q. Pei, Automatically modulated thermoresponsive film based on a phase-changing copolymer. *Chemistry Materials*, 2021, 33(18).

R. Plamthottam, Y. Shi, E. Askounis, Y. Qiu, **Z. Peng**, J. Kim, K. Youssef and Q. Pei, Dielectric elastomers: new materials and new applications. *Electroactive Polymer Actuators and Devices (EAPAD) XXIII*, 2021, 115870B.

Y. Shi, E. Askounis, R. Plamthottam, T. Libby, **Z. Peng**, K. Youssef, J. Pu and Q. Pei, A processable, high-performance dielectric elastomer and a novel multi-layering process. *Science*, 2022. Accepted.

R. Perez-Gonzalez, **Z. Peng**, D. Camacho, A. Oliva, Q. Pei, A. Zakhidov, A. Encinas and J. Oliva, All solid state stretchable carbon nanotube based supercapacitors with controllable output voltage *Journal of Energy Storage*, 2020, 32.

Y. Zhao, B. Zhang, B. Yao, Y. Qiu, **Z. Peng**, Y. Zhang, Y. Alsaid, I. Frenkel, K. Youssef, Q. Pei and X. He, Hierarchically structured stretchable conductive hydrogels for high-performance wearable strain sensors and supercapacitors. *Matter*, 2020, 3(4).

H. Wang, Y. Meng, Z. Zhang, M. Gao, **Z. Peng**, H. He and Q. Pei, Self-actuating electrocaloric cooling fibers. *Advanced Energy Materials,* 2020, 10(12).

Y. Qiu, E. Askounis, F. Guan, **Z. Peng**, W. Xiao and Q. Pei, Dual-stimuli-responsive polymer composite with ultrawide tunable stiffness range triggered by water and temperature. A*CS Applied Polymer Materials* 2020, 2(5).

Chapter 1 INTRODUCTION AND DISSERTATION OBJECTIVES

1.1 Background and mechanism of dielectric elastomer actuators (DEAs)

Dielectric elastomers (DEs), an important category of electroactive materials, have been widely investigated for use in electromechanical transducers due to their capabilities of achieving large actuation strains and energy densities, and generating high force outputs. [1-3] From the schematic illustration shown in **Figure 1-1**, a DE transducer consists of a sandwiched structure composed by a DE film and a pair of compliant electrodes, and essentially works as a soft and deformable capacitor. The device is in an off-state without an applied voltage, and it reaches an on-state when the voltage is turned on. The charges in the system are rearranged in response to the electrical field. Opposite charges accumulate on the top and bottom of the DE surfaces and build up the electrostatic attraction across the DE film. Like charges are on the same side of the DE surface which induces electrostatic repulsion on each side of the DE surfaces. The synergistic effect of the attraction and repulsion presses the DE film in the electric-field direction and stretches the film perpendicular to the electric-field direction. As a result, the DE film contracts in thickness and expands in area. The driving stress responsible for the phenomenon is the 'Maxwell pressure', which is expressed in (1).

$$p = \varepsilon_0 \varepsilon_r E^2 \quad \text{..... (1)}$$

where ε_0 is the vacuum permittivity, and ε_r is the dielectric constant of the dielectric material. E is the electric field applied across the thickness. This equation is valid if the dielectric constant ε_r is assumed to be constant.

Under a small deformation, the change in thickness (s_z) is given by (2) with the assumptions of linear-elasticity and free boundary approximations: [3-4]

$$s_z = -\frac{p}{Y} = -\frac{\varepsilon_0 \varepsilon_r E^2}{Y} = -\frac{\varepsilon_0 \varepsilon_r \left(V/z\right)^2}{Y} \quad \text{..... (2)}$$

where s_z is the strain in the thickness direction, V is the voltage applied across the DE film, z is the thickness of the DE film and Y is the apparent modulus of the DE film. Assuming the elastomer is incompressible, the strain in the area s_A can be derived as (3):

$$s_A = \frac{1}{1+s_z} - 1 \quad \text{..... (3)}$$

For small strains, the elastic energy density u_e can be estimated as follows:

$$u_e = -\frac{1}{2} p s_z = \frac{1}{2} \frac{(\varepsilon_0 \varepsilon_r)^2 E^4}{Y} = \frac{1}{2} \frac{(\varepsilon_0 \varepsilon_r)^2 \left(V/z\right)^4}{Y} \quad \text{..... (4)}$$

A more useful and simple measurement of performance is the electromechanical energy density e, which can be used to evaluate the amount of electrical energy converted to mechanical energy per unit volume of materials for one cycle:

$$e = -0.5 p \ln(1 + s_z) \quad \text{..... (5)}$$

Under a large strain, as the DE film expands, the thickness strain of the film becomes increasingly negative, and the modulus of the film changes correspondingly. Since the strain calculation is based on Y remaining constant within the small strain range of less than 20%, nonlinear strain functions need to be used to simulate the elastomer stress-strain behavior for strains over 20%. Models applying nonlinear elasticity have been developed previously, such as the Mooney-Rivlin model, [5-6] Ogden model [7-8] and Yeoh model [9] in **Figure 1-2A**. Moreover, a thermodynamic model **(Figure 1-2B)** was developed by Zhao and Suo to study the electrostriction behavior of

elastomers at different strain levels. [10] This model has been widely used by researchers when analyzing elastomers at large deformations.

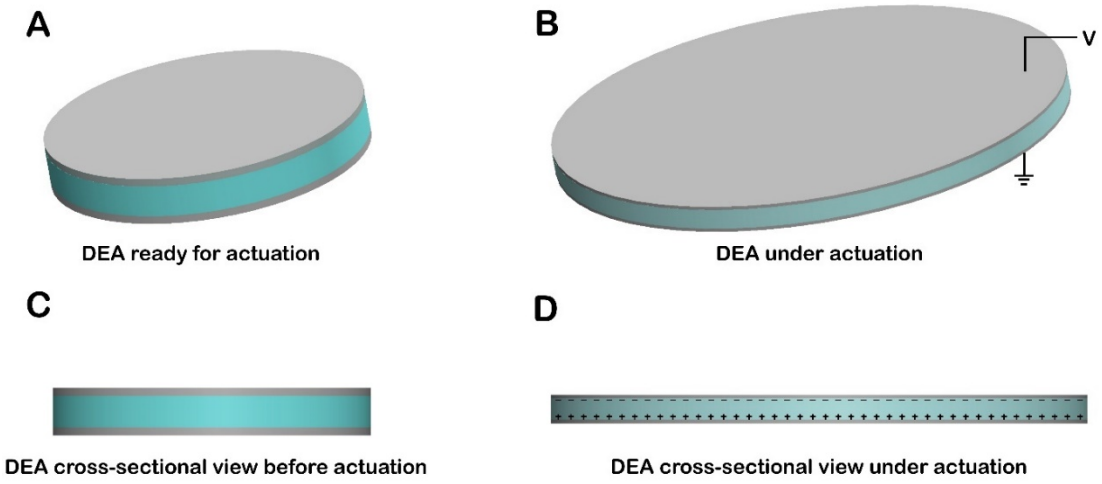

Figure 1-1 Actuation mechanism of a dielectric elastomer actuator. (A) The actuator consists of the DE film (in green) sandwiched between compliant electrodes (in gray) and is ready for actuation. (B) The actuator is driven by a voltage supply and under the actuation state. (C) and (D) show cross-sectional views of the actuator before and under actuation, respectively.

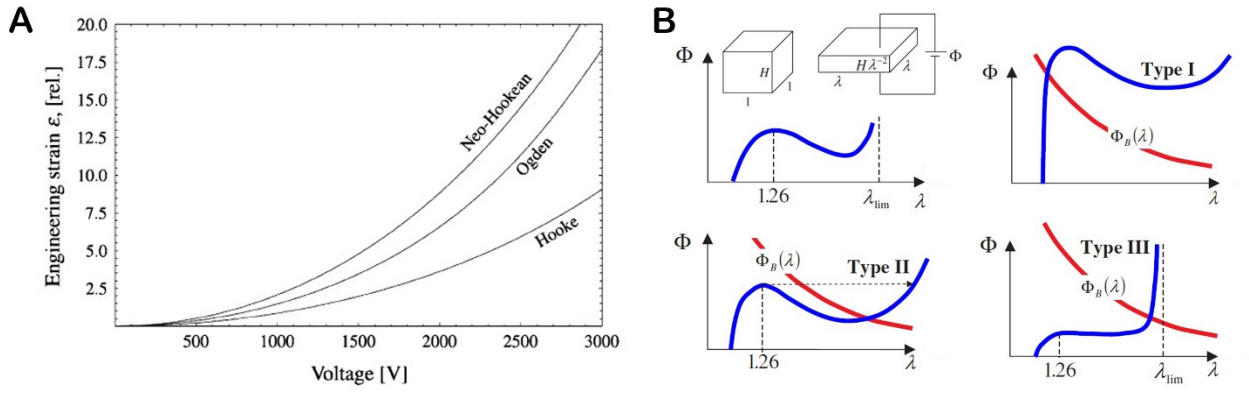

Figure 1-2 (A) DE voltage-engineering strain curves as predicted by different models. (B) A dielectric elastomer membrane subject to a voltage shows reduced thickness and expanded area.

The voltage-stretch curve is typically not monotonic. Three types of dielectrics are distinguished, depending on where the two curves $\Phi(\lambda)$ and $\Phi_B(\lambda)$ intersect. Adopted from Ref [8, 10].

1.2 Dielectric elastomer actuators: compliant electrodes

1.2.1 Overview of the electrodes used for DEAs

Compliant electrodes are used for a wide range of applications, including DEAs. As shown by the illustration of the DEA working mechanism in **Figure 1-1**, the electrode deforms along with the DE film under actuation. To be good electrode candidates of DEAs, the electrodes should be compliant with the DE film, be stretchable to maintain its mechanical integrity under large strain and retain its conductivity to ensure the conductance of the charges on the elastomer surfaces. [2, 11] In addition, the electrode needs to reliably sustain cycles of repetitive stretching in DEA-based practical applications and be suitable for multilayer stacking with the purpose of scaling up the energies and power outputs.

Thin metal films with excellent electrical conductivity have been used as flexible electrodes for decades. However, when used as DEA electrodes, they are too stiff to be stretched to large deformations, limiting the overall actuation performance. Carbon grease, a commonly used carbon-based electrode, is a mixture of carbon black powders and silicone oil. It is compliant with most DE materials and can maintain conductivity at large strains, as shown in **Figure 1-3.** But it is not suitable for fabricating stacking DEAs due to its messy oil form, which can lead to slippage between adjacent DE layers during deformation.

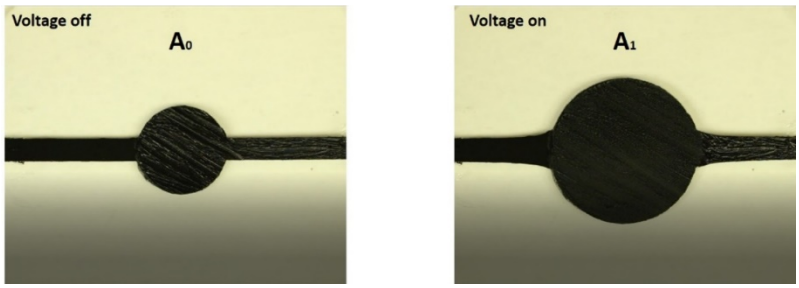

Figure 1-3 The actuator made by 300% biaxially prestretched VHB 4905 and carbon grease electrodes (left). The actuator achieved 200% area expansion under a 3.5 kV applied voltage (right).

Nano-sized electrodes received much attention due to their controllable stiffness, changeable thickness, easy-patterning characteristics, and favorable conductivity.

1.2.2 Silver nanowire electrodes

Silver nanowires (AgNWs), as stretchable nano-sized electrodes, are attractive to researchers due to their outstanding mechanical compliancy, electrical conductivity, and optical transparency. [12-14] As shown in **Figure 1-4**, Hu reported that the transmittance of AgNWs was 92.4% at 50.1 Ω/sq. When used as the DEA electrode, it reached an area strain of 68%. [15] However, the unavoidable drawback is that AgNWs normally show poor stability, such as fragmentation under high temperatures or oxidation over time in air, limiting their applications for use as DEA electrodes.

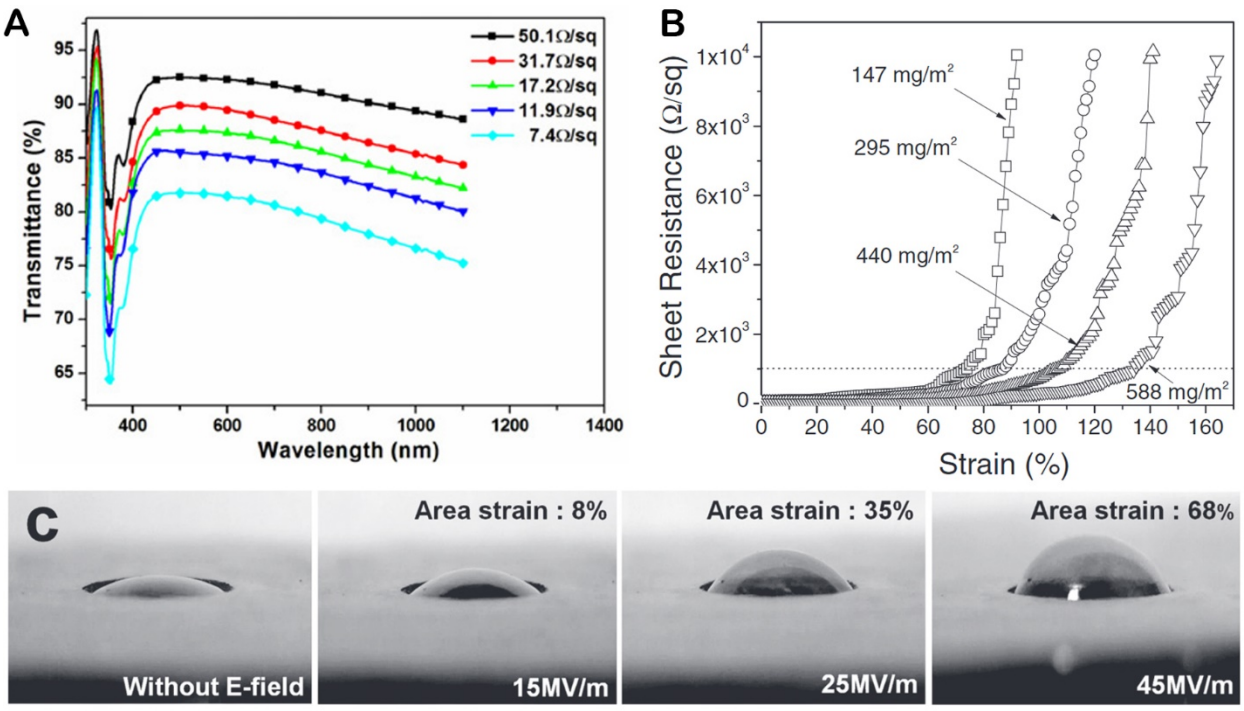

Figure 1-4 (A) Transmission spectra of AgNW coatings on a glass substrate with specified sheet resistance. (B) Evolution of sheet resistance profiles of AgNW composites at increasing strains (C) Actuation performances coupling with AgNW Joule heating electrodes. Adopted from Ref [12, 15].

1.2.3 Carbon nanotube electrodes

Another nano-sized material, carbon nanotubes (CNTs), have been widely studied due to their good thermal stability, favorable mechanical compliancy, and electrical conductivity. Yuan adopted CNTs as the DEA electrode, [16] and the actuator reached an area strain of 200% and exhibited a fault-tolerance property. **Figure 1-5** shows that under a constant voltage, the actuator was actuated to an area strain of 200%. Puncturing the active area of the DE film led to a manually induced localized dielectric breakdown. With the benefit of the CNT fault-tolerance/self-clearing

property, the actuator did not fail but maintained an area strain of 180% after recovering from the breakdown event.

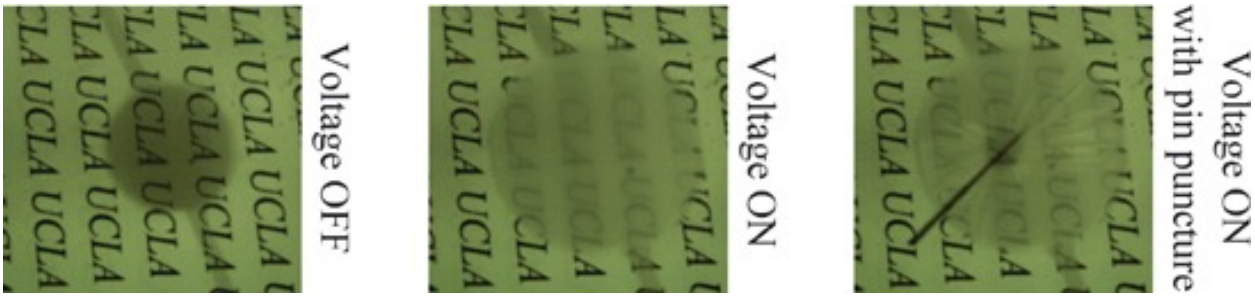

Figure 1-5 Fault-tolerance property of CNT electrodes. An actuator was prepared by using a 300% biaxially prestrained VHB 4910 film and CNT electrode on both surfaces. From left to right: actuator was ready for actuation, actuator was actuated to 200% area strain, actuator was punctured by a pin without terminal breakdown. Adopted from Ref [16].

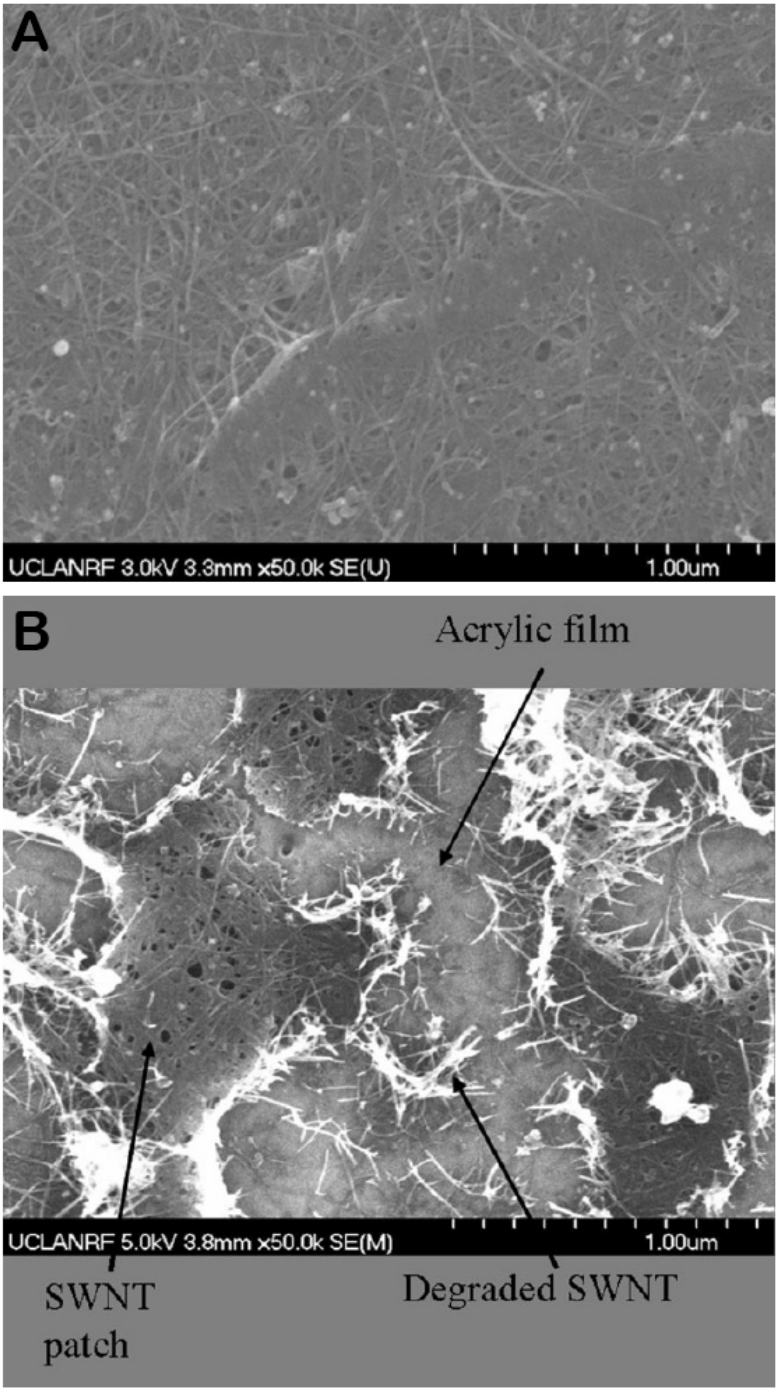

Figure 1-6 SEM images of (A) the SWNT electrode surface before voltage application, and (B) the self-cleared SWNT electrode surface near the fault. Adopted from Ref [16].

However, it is still challenging for CNT-based DEAs to have long-term and stable operations under decent strains. Under the high electrical field, the sharp tips of CNTs can form field amplification, which causes the corona discharge in air leading to dielectric breakdown in the dielectric elastomer film. Although the self-clearable CNTs can prevent the terminal breakdown, but at the cost of a reduced conductive active area. Each breakdown event clears out a small area of the electrode coating (**Figure 1-6**) and eventually, the electrode loses conductivity, and the actuator ceases to function. Some studies have been conducted to address this issue. Yuan proposed that overcoating a layer of dielectric oil to isolate the sharp tips of CNTs from air could suppress continuous corona discharges. The results showed that samples with dielectric oil overcoated on CNT survived longer time under decent actuation strains than samples with CNT electrode. [19] Further improvements are needed since the liquid form of the dielectric oil doesn't fit the stacking DEA configuration. It may leak out during packaging and may cause interlayer slippage under deformation.

1.3 Dielectric elastomer actuators: dielectric elastomer (DE) materials

1.3.1 Overview of DE materials

Dielectric elastomer films play a significant role in the performance of DEAs. An ideal DE film should have a favorable dielectric constant to be actuated at a low electric field and a good mechanical property to reach a large deformation. Three major types of elastomers with different features have been investigated as DE materials, as shown in **Figure 1-7**. Polyurethane elastomers normally have high dielectric constants of over 10 and can be actuated at low electric fields but have difficulty reaching large strains. Silicone elastomers with low viscoelasticity exhibit a fast response speed to electrical fields, operating at high frequencies. The drawback is that silicone elastomers typically have dielectric constants of approximately 3, which requires the application

of high driving electric fields. Polyacrylate elastomers, after a high ratio of prestrain, can achieve area strains of over 200%, and have larger dielectric constants than silicone elastomers. However, they typically have high viscoelasticity, leading to low response speed to electrical signals.

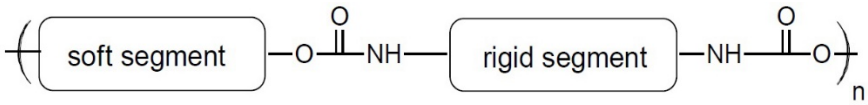

Polyurethane

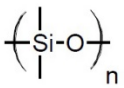

Polydimethylsiloxane (PDMS), a silicone

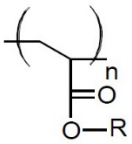

Polyacrylate, R refers to alkyl group or other functional groups

Figure 1-7 Chemical structures of representative DE materials.

1.3.2 Electromechanical instability (EMI)

From the DE actuation mechanism, when a DE film is subjected to a voltage, the thickness of the film decreases, and the area of the film expands. The EMI, also known as the pull-in effect, refers to an excessive decrease in the thickness of the DE film due to an applied voltage. [20-21] After EMI, the electric field across the DE film increases dramatically, which could lead to dielectric breakdown. As shown in **Figure 1-8**, [4] a typical stress-strain curve of the elastomer starts with a rapid increase in stress, followed by a plateau region, then a sharp rise in stress until rupture. If a voltage is applied to the elastomer film, the Maxwell pressure increases quadratically in response

to the electric field. For a sufficiently high driving voltage, the reduction in the film thickness and the increase in the electric field form a positive feedback loop. The DE film continues to be driven thinner and thinner until the localized electric field exceeds its dielectric strength. The intersection of the elastic stress and Maxwell stress shown in **Figure 1-8** indicates the eventual dielectric breakdown. Therefore, EMI severely constrains maximum stable actuation performance of a given material.

1.3.3 Prestrain

Prestrain is an efficient way to suppress EMI. DE films become stiffened after prestraining, and the starting point of the elastic stress-strain curve for this elastomer shifts from origin O to O'. When turning the voltage on, the quadratic Maxwell stress curve starts from O' correspondingly and will be less likely to intersect with the elastic stress-strain curve, offering a more stable actuation performance. Prestrain is important for both acrylate-based and silicone-based films to reach good strains in DEA applications. In 2000, SRI first reported that after prestrained, these two types of elastomers were capable of large actuation strains of above 100%. [1] An easy way of providing prestrain is to mount the stretched DE films onto rigid frames. Unfortunately, this step increases the complexity of actuator fabrication, adds extra weight to the actuation system, decreases the overall specific energy density and causes fatigue. To solve this problem, Ha introduced an interpenetrating network (IPN) from the VHB, [22] which acted as a free-standing DE film and exhibited an electrically induced strain of up to 300%. The IPN was formed by creating a second network inside the highly prestrained VHB matrix. This second network provides an internal supporting force after the removal of the rigid support, therefore, some portion of the prestrain can be preserved, resulting in a rigid-frame-free DE film.

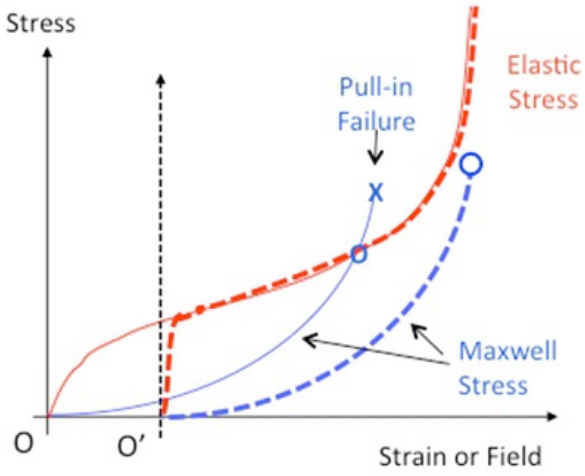

Figure 1-8 Characteristic stress of a DE film as a function of mechanical strain or electric field (constant voltage condition). The chart with origin at O is for a non-prestrained film at O' for the prestrained film. The cross (×) indicates dielectric breakdown and the bar (-) indicates stable actuation strain. Small o and large O represent the apparent breakdown field and actual breakdown strength respectively. Adopted from Ref [4].

1.3.4 Viscoelasticity

Viscoelasticity is a material property that exhibits both viscous and elastic characteristics. It can be characterized by the mechanical loss factor as expressed by (6):

$$\tan \delta_m = \frac{E''}{E'} \quad \text{..... (6)}$$

where E' and E'' are the storage modulus and loss modulus, respectively. A big loss factor of the material leads to a reduced response speed to the stimulus and the stress relaxation over time, and dissipates the electromechanical energy into heat, lowering the overall reliability. For example, the

commonly used acrylic elastomer, VHB, shows a limited maximum response speed in the 10-100 Hz range and a time-dependent strain due to the viscoelastic effect.

1.4 Variable stiffness polymers (VSPs)

1.4.1 Overview of VSPs

As mentioned above, dielectric elastomers are typically soft and can show electrically induced large strains. However, in some applications, smart materials with tunable mechanical properties are desired for changeable working conditions, such as adaptive grippers [24, 25] and wearable electronics. [26] Variable stiffness polymers, as presentative smart materials, have attracted extensive attention due to their excellent adaptivity to changing working conditions. For example, a gripper design using a VSP can vary the stiffness in response to temperature. Both actuators and holding elements are based on controllable stiffness, exploiting their soft state to conform to the object's shape, and their rigid stage to generate a high force. [27-28] Another example is a smart skin based on VSPs that acted as a highly sensitively capacitive touch sensor and conformed to the shape of various surfaces under different working conditions. [29]

1.4.2 Bistable electroactive polymers (BSEPs)

Bistable electroactive polymers (BSEPs) are a unique brand of VSPs and a derivate of dielectric elastomers. They combine the properties of shape memory polymers and dielectric elastomers. As shown in **Figure 1-9**, below the transition temperature, a BSEP acts as a rigid plastic. It becomes soft and turns into a rubbery state above the transition temperature, such that the BSEP is deformed when an external stimulus is applied (either a voltage or an external force). The deformation can be locked by cooling the materials down below the transition temperature; meanwhile, the BSEP becomes rigid again. Removing the stimulus wouldn't make a change to the deformation as the

deformation is ‘locked in’. Reheating the BSEP then can bring it back to the initial non-strain state. The process is reversible, repeatable, and reliable.

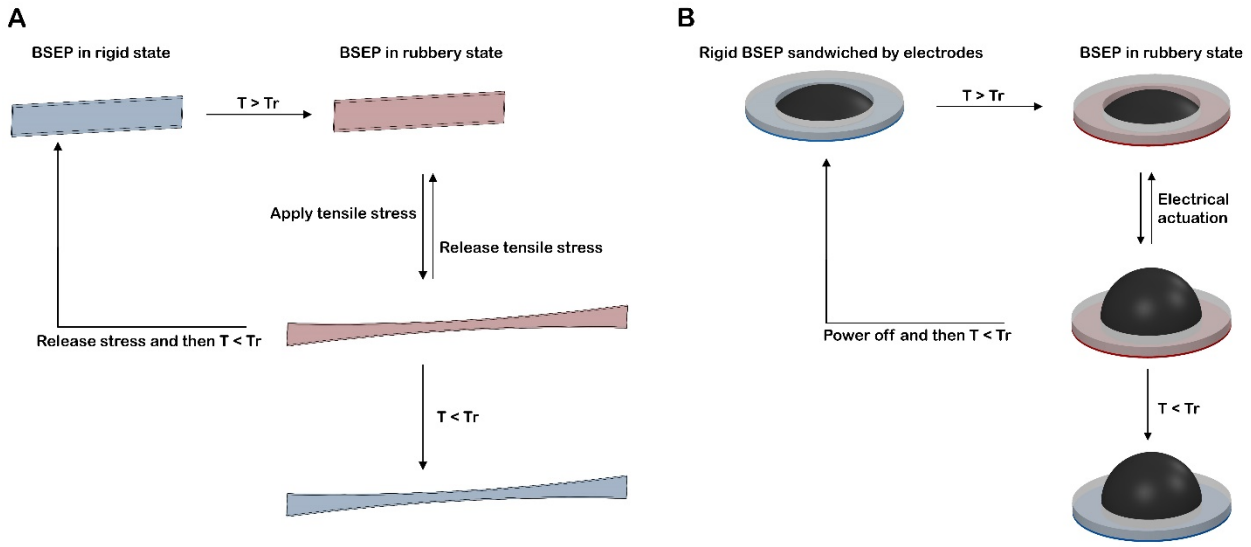

Figure 1-9 (A) BSEP acts as a shape memory polymer and responds to temperature change, along with external tensile stress. (B) BSEP acts as a shape memory polymer and dielectric elastomer material and responds to a temperature change, along with an electrical stimulus.

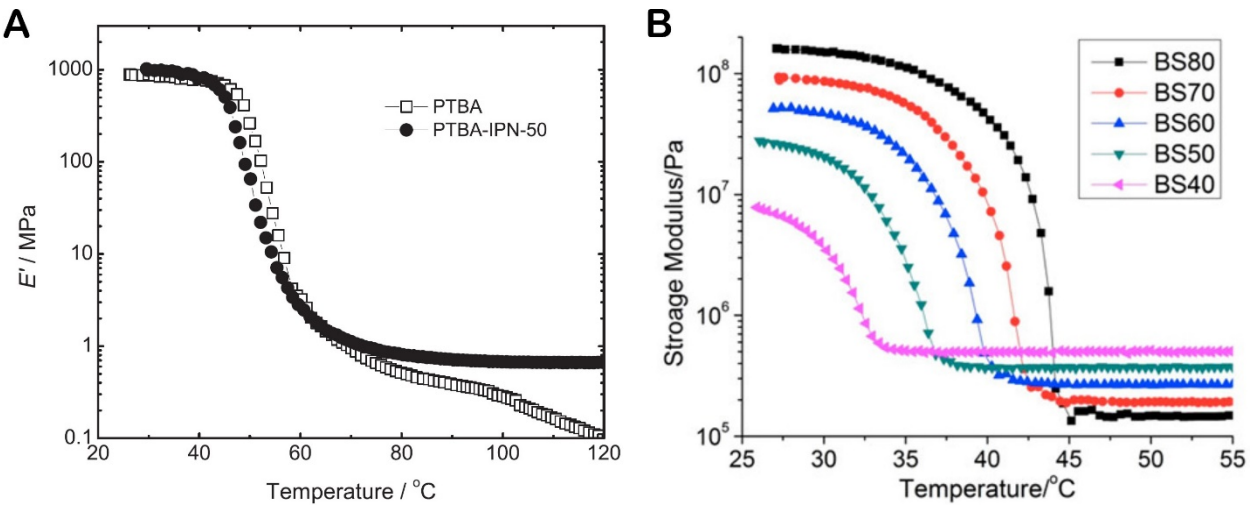

Figure 1-10 Storage modulus vs. temperature for (A) glass-transition BSEP and (B) phase changing BSEP. Adopted from Ref [30, 32].

BSEPs are categorized into two groups according to their physical states: glass transition BSEPs [30, 31] and phase-changing BSEPs. [32, 33] As shown in **Figure 1-10**, one glass transition BSEP, linear thermoplastic poly(tert-butyl acrylate) (PTBA) exhibited a ~10^3 folds storage modulus change within a transition temperature range of ~20 °C. [30] Unlike glass transition BSEPs, the phase-changing BSEP, which was introduced by Ren et al., [32] exhibited a steep change in the modulus within a narrow transition temperature range of 10 °C.

1.5 Motivation of the dissertation

It has been over 20 years since the superior actuation performance of dielectric elastomers was first investigated. Numerous branches of study have emerged in this field, including mechanism studies, mechanics features and modeling exploration, dielectric elastomer and compliant electrode development, and prototype stacking methods of multilayer DEAs for manufacturing. However, for DEAs, from the aspect of both dielectric elastomer materials and compliant electrodes, it has been challenging to realize stable actuation performances under large strains and generate favorable energies durably. Furthermore, a reliable stacking method for multilayer DEAs is urgently needed to meet manufacturing requirements, i.e., scalability and high yield. Therefore, it is of great importance to improve both dielectric and electrode materials, fitting some newly developed multilayer stacking processes for the practical applications of DEAs.

Researchers have used DEA technology for tactile displays, which require a high voltage supply of several kVs in dielectric actuation mechanism. Realistically, this high voltage is not ideal for human-contact devices. Thus, a pneumatic actuation mechanism coupled with a suitable smart material could be a good option for a user-safe tactile display.

1.6 Scope and layout of the dissertation

The dissertation is divided into five chapters.

Chapter 1, the current chapter, gives an overview of the research field, including the background and working mechanism of dielectric elastomer actuators, and the requirements for compliant electrodes and dielectric elastomer materials. Additionally, the need to develop variable stiffness polymers is introduced, especially in describing the advantages of bistable electroactive polymers.

Chapter 2 discusses a novel bilayer electrode for dielectric elastomer actuator applications. This bilayer electrode consists of a thin polymer layer overcoated onto an ultrathin carbon nanotube network and offers an acylate-based actuator with stable and reliable actuation under a large actuation strain.

Chapter 3 describes the hybrid manufacturing of prestrain-locked acrylic dielectric elastomer thin films and multilayer stacks. The synthesized arylate-based DE is free-standing and rigid-frame-free with an interpenetrating-network structure. It is diffused by a plasticizer as additive and shows a fast response speed. The rigid-frame-free IPNs can be fabricated into multilayer DEAs by a hybrid stacking method with a high yield, opening the door for large-scale multilayer DEAs manufacturing.

Chapter 4 presents a prototype of a refreshable tactile display for Braille applications based on a pneumatic actuation mechanism. This device utilizes a phase-changing bistable electroactive polymer and a laser-engraved stretchable Joule heating electrode to realize high-resolution actuation. By exploiting the great stiffness change and large deformation at the rubbery state of the BSEP, the diaphragm dots reach large vertical strokes with high blocking forces.

Chapter 5 provides an outlook for future research and concludes the dissertation.

1.7 References

[1] R. Pelrine, R. Kornbluh, Q. Pei, J. Joseph, High-speed electrically actuated elastomers with strain greater than 100%. *Science* **2000**, 287,836.

[2] R. Kornbluh, R. Pelrine, High-field electrostriction of elastomeric polymer dielectrics for actuation. *Proc. SPIE* **1999**, 3669,146.

[3] R. Pelrine, R. Kornbluh, J. Joseph, Electrostriction of polymer dielectrics with compliant electrodes as a means of actuation. *Sens. Actuators A Phys.* **1998**, 64, 77.

[4] P. Brochu, Q. Pei, Advances in dielectric elastomers for actuators and artificial muscles. *Macromol. Rapid Commun*. **2010**, *31*(1), 10.

[5] E. Yang, M. Frecker, E. Mockensturm, Viscoelastic model of dielectric elastomer membranes. *Proc. SPIE* **2005**, 5759, 82.

[6] P. Sommer-Larsen, G. Kofod, M.H. Shridhar, M. Benslimane, P. Gravesen, Performance of dielectric elastomer actuators and materials. *Proc. SPIE* **2002**, 4695,158.

[7] N. Goulbourne, E. Mockensturm, M. Frecker, A nonlinear model for dielectric elastomer membranes. *J. Appl. Mech.* **2005**, 72, 899.

[8] G. Kofod, Dielectric elastomer actuators. PhD thesis, The Technical University of Denmark, **2001**.

[9] M. Wissler, E. Mazza, Modeling of a pre-strained circular actuator made of dielectric elastomers. *Sens. Actuators A* **2005**, 120,184.

[10] X. Zhao, Z. Suo, Electrostriction in elastic dielectrics undergoing large deformation. *J. Appl. Phys.* **2008**, 104, 123530.

[11] F. Carpi, D. De Rossi, R. Kornbluh, R.E. Pelrine, P. Sommer-Larsen, Dielectric elastomers as electromechanical transducers: fundamentals, materials, devices, models and applications of an

emerging electroactive polymer technology, Elsevier Science, Amsterdam, The Neitherlands, **2011**.

[12] W. Hu, X. Niu, L. Li, S. Yun, Z. Yu, Q. Pei, Intrinsically stretchable transparent electrodes based on silver-nanowire–crosslinked-polyacrylate composites. *Nanotechnology* **2012,** 23(34), 344002.

[13] K. Jun, K. Jongnam, I. Oh. An electroactive and transparent haptic interface utilizing soft elastomer actuators with silver nanowire electrodes. *Small* **2018**, 14(35), 1801603.

[14] D. Langley, G. Giusti, C. Mayousse, C. Celle, D. Bellet, J. Simonato, Flexible transparent conductive materials based on silver nanowire networks: a review. *Nanotechnology* **2013**, 24(45), 452001.

[15] S. Yun, X. Niu, Z. Yu, W. Hu, P. Brochu, Q. Pei, Compliant silver nanowire-polymer composite electrodes for bistable large strain actuation. *Adv. Mater.* **2012**, 24, 1321.

[16] W. Yuan, L. Hu, Z. Yu, T. Lam, J. Biggs, S. Ha, D. Xi, B. Chen, M. Senesky, G. Grüner, Q. Pei, Fault-tolerant dielectric elastomer actuators using single-walled carbon nanotube electrodes. *Adv. Mater.* **2008**, *20*(3), 621.

[17] W. Yuan, L. Hu, S. Ha, T. Lam, G. Grüner, Q. Pei, Self-clearable carbon nanotube electrodes for improved performance of dielectric elastomer actuators. *Proc. SPIE* **2008**, 6927, 69270P.

[18] W. Yuan, L. Hu, P. Brochu, X. Niu, Q. Pei, Fault-tolerant silicone dielectric elastomers. *Int. J. Smart Nano Mater.* **2010**, 40-52.

[19] W. Yuan, P. Brochu, S. Ha, Q. Pei, Dielectric oil coated single-walled carbon nanotube electrodes for stable, large-strain actuation with dielectric elastomers. *Sens. Actuators A* **2009**, 155(2), 278.

[20] Z. Suo, Theory of dielectric elastomers. *Acta Mechanica Solida Sinica* **2010**, 23(6), 549.

[21] X. Zhao, Z. Suo. Theory of dielectric elastomers capable of giant deformation of actuation. *Phys. Rev. Lett.* **2010**, 104(17), 178302.

[22] S. Ha, W. Yuan, Q. Pei, R. Pelrine, S. Stanford, Interpenetrating networks of elastomers exhibiting 300% electrically-induced area strain. *Smart Mater Struct.* **2007**, 16, S280

[23] Q. Pei, R. Pelrine, M. Rosenthal, S. Stanford, H. Prahlad, and R. Kornbluh. Recent progress on electro elastomer artificial muscles and their application for biomimetic robots. *Proc. SPIE* **2004**, 5385, 41.

[24] E. Brown, N. Rodenberg, J. Amend, A. Mozeika, E. Steltz, M. Zakin, H. Lipson, H. Jeager, Universal robotic gripper based on the jamming of granular material. *Proc. Natl. Acad. Sci.* 2010, 107, 18809.

[25] O. Araromi, I. Gavrilovich, J. Shintake, S. Rosset, M. Richard, V. Gass, H. Shea, Rollable multisegment dielectric elastomer minimum energy structures for a deployable microsatellite gripper. *IEEE/ASME Trans. Mechatronics* **2014**, 20, 438.

[26] J. Heo, J. Eom, Y. Kim, S. Park, Recent progress of textile-based wearable electronics: a comprehensive review of materials, devices, and applications. *Small* **2008**, 14(3), 1703034.

[27] J. Shintake, V. Cacucciolo, D. Floreano, H. Shea, Soft robotic grippers. *Adv. Mater.* **2018**, 30(29), 1707035.

[28] J. Shintake, S. Rosset, B. Schubert, D. Floreano, H. Shea, Versatile soft grippers with intrinsic electroadhesion based on multifunctional polymer actuators. *Adv. Mater.* **2016**, 28(2), 231.

[29] Q. Yu, S. Ma, Q. Pei, A self-conformable smart skin with sensing and variable stiffness functions. *Adv. Intell. Syst.* **2019**, 1(5), 1900054.

[30] Z. Yu, W. Yuan, P. Brochu, B. Chen, Z. Liu, Q. Pei, Large-strain, rigid-to-rigid deformation of bistable electroactive polymers. *Appl. Phys. Lett.* **2009**, *95* (19), 21.

[31] X. Niu, X. Yang, P. Brochu, H. Stoyanov, S. Yun, Z. Yu, Q. Pei, Bistable large-strain actuation of interpenetrating polymer networks. *Adv. Mater.* **2012**, *24* (48), 6513.

[32] Z. Ren, W. Hu, C. Liu, S. Li, X. Niu, Q. Pei, Phase-changing bistable electroactive polymer exhibiting sharp rigid-to-rubbery transition. *Macromolecules* **2016**, *49* (1), 134.

[33] Y. Qiu, Z. Lu, Q. Pei, Refreshable tactile display based on a bistable electroactive polymer and a stretchable serpentine Joule heating electrode. *ACS Appl. Mater. Interfaces* **2018**, *10*, 24807.

Chapter 2 STABLE AND HIGH-STRAIN DIELECTRIC ELASTOMER ACTUATORS BASED ON A CARBON NANOTUBE-POLYMER BILAYER ELECTRODE

2.1 Background of this study

2.1.1 Dielectric elastomer actuators (DEAs) and compliant electrodes

Dielectric elastomer actuators (DEAs) based on acrylic elastomers have attracted increasing interests due to their large actuation strain and high energy density. Combined with the features of mechanical compliancy, no noise, light weight and low cost, DEAs have been explored for applications such as biomimetic robotics, [6-10] tactile displays, [11-14] tunable optics, [15-16] and microfluidics.[17-18] However, the acrylic-based DEAs show poor reliability and durability, [19] especially under large strain due to operation close to the dielectric breakdown field of the elastomer films and limited compliancy and continuity of the electrode. [19-21] Defects formed during film processing, such as voids, uneven thickness, particles, and stress concentration, also cause actuators' premature failure at voltages significantly lower than the voltage determined from the elastomer's field strength due to local electrical breakdown. [22-24] To tackle this problem, various compliant electrodes have been explored to self-clear the localized breakdown sites [23, 25-26] (also knowns as self-healing electrodes [27]), thus dramatically extending the lifetime of DEAs by surviving a certain number of localized breakdown events. For examples, doped conductive polymers, e.g. poly(3-dodecyloxylthiophene) (P3DOT) and polyaniline (PANi), exhibit self-clearing capability by isolating the defects. [28-29] However, they are unstable when exposed to heat or electric field, which hinders long-term stability. Liquid electrolytes may be used as self-healing electrodes, but their applications may be limited by leakage of the liquid and packaging issues. [30] Compared with the liquid electrolytes, gel electrolytes have recently received extensive attention

because of their improved processability and self-healing capability. [31-33] Nevertheless, their self-healing processes always take more than ten hours to complete, [34-35] which may be too long for reactivating the DEAs.

2.1.2 A single-walled carbon nanotube (SWNT) as a compliant electrode for DEAs

Single-walled carbon nanotube (SWNT) stands out as a promising electrode for DEAs due to the formation of a high mechanically compliant and electrically conductive network, high environmental stability, ease of processing and patterning. [4-5, 36-39] In particular, the self-clearing ability of SWNT electrodes has been demonstrated to significantly improve the actuation performances for both acrylic elastomer and silicone elastomer based actuators. [20, 23, 27, 40-41] However, major challenges remain. The nanotubes have sharp tips which can induce corona discharging of the surrounding air at the high electric field as the field is amplified at the sharp tips. [23, 41] While the localized electrical breakdown of the DEA caused by the corona discharge can be self-healed, the electrode gradually loses conductivity after multiple electrical breakdown-clearing events, and the actuator eventually ceases to actuate. To address this issue, dielectric oil was used to cover the porous SWNT network and shield the sharp tips from the air. The resulting DEAs showed improved lifetime under large-strain actuation. [24] Similar to the liquid electrolytes, the dielectric oil may leak out and may swell the underlying dielectric elastomer films to cause unwanted side effects and limit its processability.

2.1.3 A single-walled carbon nanotube (SWNT) overcoated by a polymer layer as compliant electrode for DEAs

In this work, we introduce a polyurethane latex dispersion in water (water-based polyurethane, or WPU shown in **Figure 1B**) to overcoat the SWNT electrode to shield the sharp tips after drying.

This WPU has good compatibility with the SWNT network as it can be used as an effective surfactant to disperse SWNT in polar solvents such as water and isopropanol (IPA). A diluted solution of the WPU in water/IPA can thus penetrate into the SWNT network, squeeze the air out of the network, and isolate the SWNT electrode from surrounding air. By coating a dilute WPU solution over a pre-formed SWNT network, an interpenetrating bilayer structure is obtained which retains the high electrical conductivity of the interconnected SWNT network while the pores and the outer surface of the SWNT network are covered by the WPU matrix. This interpenetrating bilayer electrode may also prevent the sliding of the nanotubes at large strain deformation, and therefore maintains the conductive network better than a bare SWNT network. DEAs based on this bilayer electrode and acrylic elastomers have been successfully actuated to strains as high as 225% in area expansion. Furthermore, the bilayer electrode is also demonstrated to effectively suppress corona discharge during high-strain actuation and exhibit self-clearing capability, thereby achieving stable actuation at 150% area strain.

2.2 Experimental design

2.2.1 Materials preparation

SWNT solution was prepared similarly as our previous research.[34, 48] 7 mg P3 SWNT (Carbon Solution, Inc.) was dispersed into 2 mL deionized water and 20 mL isopropanol (IPA). The mixture was bath-sonicated for 120 min, then centrifuged at 9000 rpm for 18 min. The supernatant SWNT solution was used for spraying. 35 wt % WPU (UD-410, Bond Polymers International) was diluted by IPA into 1 wt %. 100 parts of urethane diacrylate (CN9021, Sartomer), 0.25 part of 2,2-dimethoxy-2-phenylacetophenone (DMPA), and 0.125 part of benzophenone (BP) was mixed and diluted by IPA into 1 wt %. These clear mixtures were ready for spraying. The 1.3 wt % PEDOT:

PSS aqueous solution (Clevios PH 1000) was diluted by IPA into 0.1 wt% and vigorously stirred at room temperature for 5 minutes before spraying.

2.2.2 Actuator fabrication

For SWNT samples, the SWNT solution was spray-coated on both sides of the acrylic elastomer film (3M 4905VHB, 200% biaxially prestretched), by using an airbrush (Paasche Airbrush Company) to the sheet resistance of 100±5 kΩ/□. Both surfaces of VHB film were covered by shadow masks to get the overlapped circular active area and contact leads. The spraying rate of the SWNT solution was controlled at 1 mL min^{-1}, and the acrylic elastomer film was fixed onto a hot plate at 75 °C during spraying. For bilayer electrode samples, following by the described processes of fabricating SWNT samples, diluted WPU, CN9021, or PEDOT solution was spray-coated onto surfaces. The SWNT+WPU samples were left on the hot plate at 75 °C for 30 min to dry out the water residual after spraying. The SWNT+CN9021 samples were UV cured immediately and then annealed on the hot plate at 60 °C for 2 hours. High voltage (Trek, Inc) was applied via the two electrical leads to drive the sandwich-structured actuators.

2.2.3 Actuation stability and duration

Under the square-wave voltage, prepared actuators were connected directly to the power supply. Under the constant voltage, prepared actuators were connected in series with 50 MΩ current-limiting resistors, Keithley 2000 multimeter, and a high-voltage power supply. The current-limiting resistors were used to protect the multimeter from high current caused by the rupture of acrylic film. Circuits for both measurements were shown in **Figure 2-8**. The chronoamperic curves were recorded by Keithley 2000 multimeter, and the corresponding actuation strains were

monitored by a webcam. They were controlled by the LabView software. $(a_1-a_0)/a_0 \times 100\%$ is the programmed equation to calculate area actuation strains.

2.2.4 Estimated thickness of spray-coated polymers on the SWNT layer

Approximate thicknesses of the sprayed-coated solid layer were determined by measuring the volume of the sprayed solution and by assuming the following:

(1) The total sprayed region is around 4 inch x 2 inch, i.e. 51.6 cm^2 in area.

(2) The thickness is constant throughout the sprayed area.

(3) 50% of the solution is not deposited to the target area.

(4) The density of the elastomer film is around 1 g/cm^3 determined from the measured weight of a thick free-standing film and the dimensions of the film.

Using these assumptions and the concentration of the dispersion (1 wt% in the solvent), the thicknesses of 0.5 mL sprayed solution is around 480 nm. After overcoating an extra solid polymer layer, the resistance of the electrode was almost unchanged.

2.2.5 Samples preparation for SEM measurements

The SEM measures for samples of polymer outer surfaces and SWNT inner interfaces (facing substrate) are prepared as follows.

Polymer outer surfaces:

(1) Spray coat SWNT solution onto a PET substrate.

(2) Overcoat polymer solution onto the SWNT electrode.

(3) Samples are ready for SEM measurements.

SWNT inner interfaces:

(1) Spray coat SWNT solution onto a glass slide.

(2) Overcoat polymer solution onto the SWNT electrode.

(3) Laminate a PET substrate with the SWNT+polymer deposited glass slide and following by the vacuum-press.

(4) Peel the transferred SWNT+polymer from the glass slide.

(5) Samples are ready for SEM measurements.

2.3 Results and discussions

2.3.1 Electrode preparation, actuation performance and microstructures

The fabrication of the acrylic-based actuator with SWNT+WPU bilayer electrode is illustrated in **Figure 2-1A**. The process starts with spray-coating SWNT solution onto prestretched VHB films with masks, followed by spray-coating the diluted solution of WPU onto the SWNT electrode to form the thin polymer layer. The bilayer electrode was applied on both sides of VHB and separately connected to the positive and negative sides of the power supply. When a voltage is on, an electric field is applied across the DE film, the electrostatic attraction between opposite charges and the electrostatic repulsion between like charges generate stress on the film, forcing the film to contract in thickness and expand in area. The bilayer electrode, both the WPU layer and the SWNT network expand and contract in sync with the VHB film. The WPU was used to fabricate the bilayer electrode due to its high compliancy, ease of processing, and compatibility with multiple materials. [42-44] The WPU film is elastic with a low modulus on the order of 10^5 Pa and high

stretchability up to 900% strain (**Figure 2-1B**). Strong bonding was reported to form between WPU and VHB. [42] Two other polymers with distinctive properties were also investigated in comparison to WPU. CN9021 (difunctional acrylic ester resin) was investigated as the thin polymer layer because it's a widely studied DE material with high actuation performances. [45-46] PEDOT:PSS was also selected for the bilayer electrode fabrication since it has been adopted for composite electrodes for high strains. [42, 47]

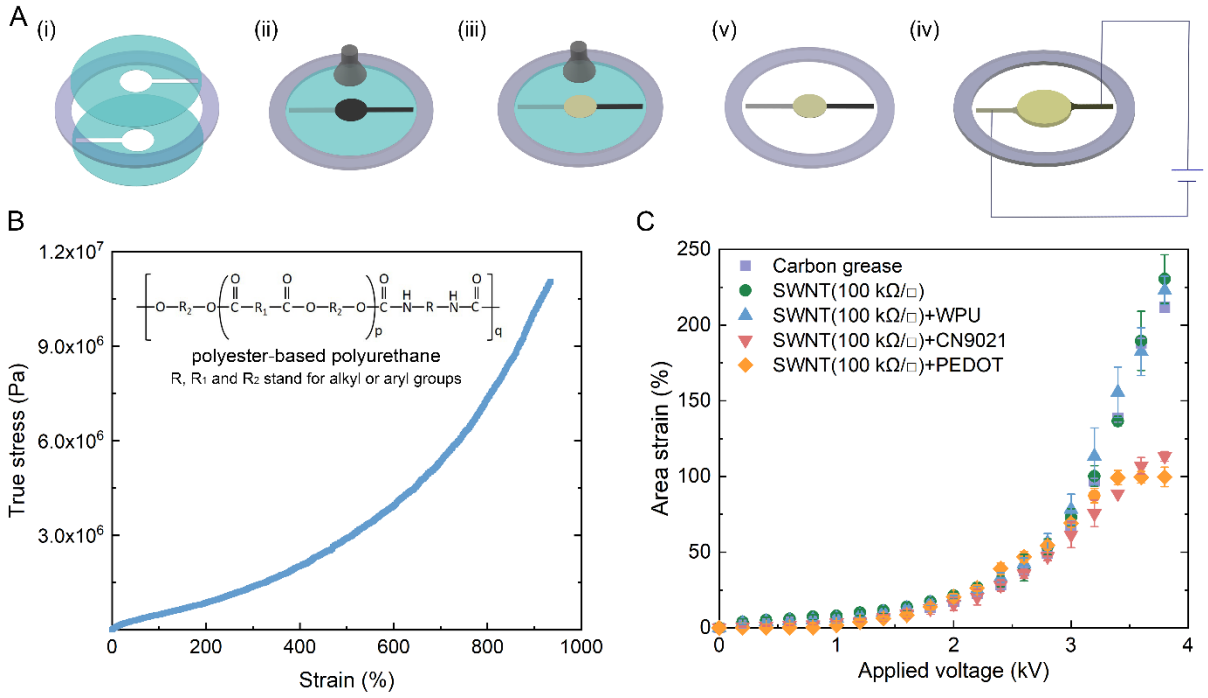

Figure 2-1 (A) Fabrication processes for 200% biaxially prestretched VHB-based DEAs with compliant electrodes. (i) Attaching masks on both sides of prestretched VHB film. (ii) Spraying SWNT solution on both sides of the mask-covered acrylic film. (iii) Spraying diluted WPU, CN9021, or PEDOT solutions, followed by UV curing for CN9021 or heating for WPU layers. (iv) The actuator is ready for testing. (v) The area expansion performance under an applied voltage. (B) Chemical structure of polyester-based WPU and its stress-strain curve. (C) Electrically induced strain as a function of applied ramping-up voltage on a 200% biaxially pre-stretched VHB film

with carbon grease, SWNT, SWNT+WPU, SWNT+CN9021, and SWNT+PEDOT electrodes on both surfaces. For each electrode, five samples were tested. Each sample was actuated for one cycle at each 0.2 kV increment from 0 kV to 3.8 kV. Error bars indicate the standard deviation.

In our experiments, the sheet resistance of the SWNT is controlled to 100±5 kΩ/□ (**Figure 2-2A**), since the thicker, stiffer SWNT electrode could increase the elastic stress of the actuator and impede the actuation strain, while the thinner one may lose electrical conductivity under large actuation strain (**Figure 2-2B-C**).[23] The thicknesses of WPU, CN9021 and PEDOT polymer layers are controlled to be less than 480 nm in order to minimize the mechanical impedance. The estimation of the thickness is shown in the 2.2.4. After overcoating an extra solid polymer layer, the resistance of the electrodes was almost unchanged.

A

Sheet resistance (kΩ/□)	99.5	99.6	98.7	101.6	103.7	96.9	101.5	103.8	96.3	102.3

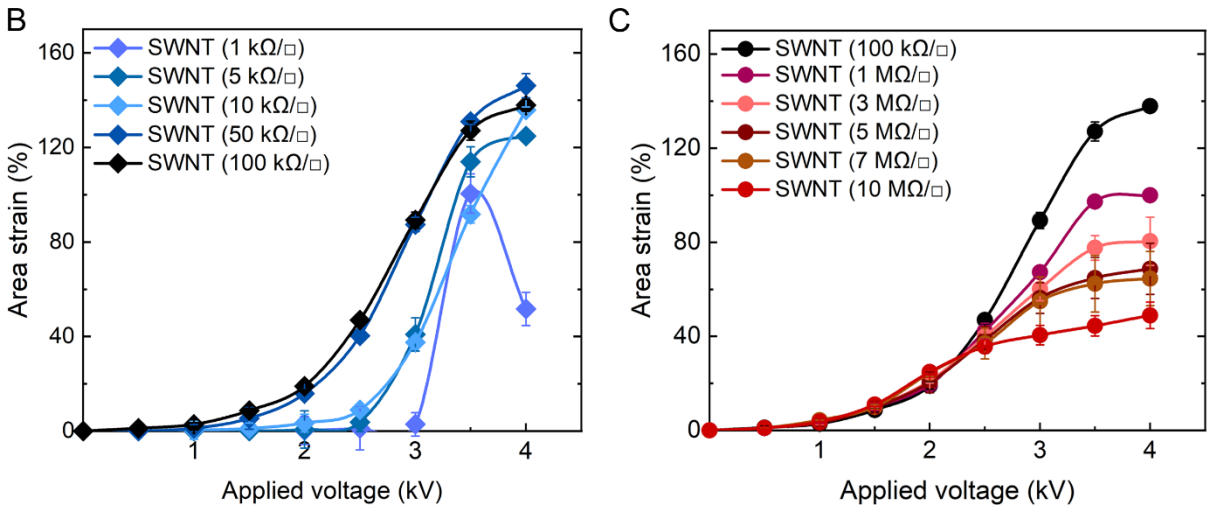

Figure 2-2 (A) Measured sheet resistances of different regions of prepared SWNT electrode with a circular diameter in 1 inch. (B-C) Electrically induced strain as a function of applied ramping-up voltage on a 300% biaxially pre-stretched VHB film with different thicknesses of SWNT

electrodes on both surfaces. For each electrode, five samples were tested. Each sample was actuated for one cycle at each 0.5 kV increment from 0 kV to 4 kV. Error bars indicate the standard deviation.

Figure 2-1C shows the actuation strains of DEAs with different electrodes including SWNT+WPU, SWNT+CN9021, and SWNT+PEDOT under the ramping-up voltages. The actuation properties of DEAs with commonly used single-layer electrodes including carbon grease and SWNT are also presented for comparison. DEAs with pure SWNT and carbon grease electrodes reached similar area strains of around 225% at 3.8 kV as expected.[23] DEAs with the SWNT+WPU electrodes can also achieve a 225% actuation strain at 3.8 kV. However, actuators with SWNT+CN9021 and SWNT+PEDOT electrodes only achieved actuation strains of 115% and 100% under 3.8 kV and the strains maintained with even higher voltage.

To explore the mechanisms behind the actuation properties of DEAs with different electrodes, we used SEM to investigate their microstructures and studied the mechanical properties of bilayer electrodes. **Figure 2-3C** and **2-3D** showed that uniform WPU coating was formed on both the outer and inner surfaces of the SWNT network, which indicates the WPU diluted solution is able to penetrate into the SWNT network during spray coating. The reason is that WPU shows good compatibility with SWNT, which was demonstrated by our control studies (**Figure 2-4**). As a result, the thin WPU layer not only covers but also fully wraps the SWNT network and thus shields the nanotubes' sharp tips from the air and prevents the sliding of the networks while retaining its conductivity under large strain. Moreover, this thin WPU layer is as compliant as non-prestretched VHB films, as shown in the stress-strain curve (**Figure 2-5A**). The table in **Figure 2-5B** compares the modulus of 200% biaxially pre-stretched VHB and WPU films,[48] and it shows that the WPU film has the same modulus magnitude (10^5 Pa) as the 200% uniaxially pre-stretched VHB film,

indicating that the overcoated WPU layer does not add substantial stiffness to the actuators. Thus, the bilayer SWNT+WPU electrode is chosen to improve the actuation stability and durability of acrylic-based DEAs.

For SWNT+CN9021 electrodes, the polymer agglomerates, and bare SWNT can be found under SEM, as shown in **Figure 2-3C** and **2-3D**. The agglomerates were formed because of the poor compatibility between hydrophobic CN9021 and hydrophilic SWNT network. Even diluted by IPA, CN9021 chains can only partially penetrate the SWNT network during spray coating, thus resulting in agglomerates of CN9021, and bare SWNT without polymer cover. Under high driving voltage, the areas with and without CN9021 agglomerates experienced different strains due to mechanical impedance and thus limited the actuation performance. We measured the conductivity of SWNT+CN9021 electrodes at 115% strain and found that it had become non-conductive (**Figure 2-6B**). Different from CN9021, the PEDOT formed a uniform layer and successfully penetrated into the SWNT network after its aqueous solution was spray-coated. However, the stiff PEDOT layer formed cracks at high strain (**Figure 2-6A**), which eventually broke the electrode network and limited the actuation strain (**Figure 2-1C** and **Figure 2-6D**). The resistances of both samples with SWNT+PEDOT and PEDOT electrodes (**Figure 2-6B**) were too large to be measured at around 100% and 15% area strain, respectively.

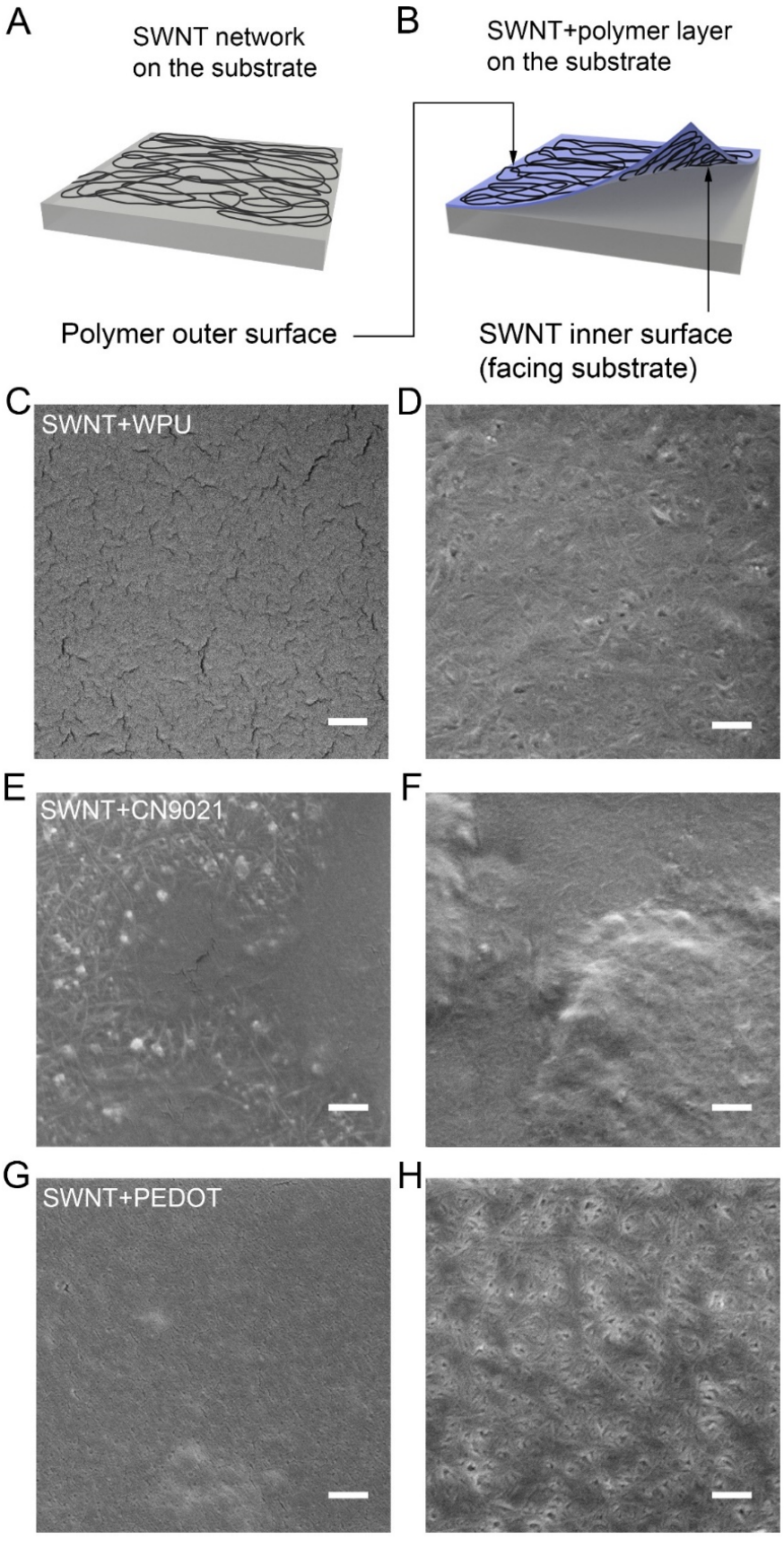
A
SWNT network
on the substrate
B
SWNT+polymer layer
on the substrate
Polymer outer surface
SWNT inner surface
(facing substrate)
C
SWNT+WPU
D
E
SWNT+CN9021
F
G
SWNT+PEDOT
H

Figure 2-3 Schematic illustrations of deposited SWNT electrode on the substrate (A) and SWNT+polymer bilayer electrode on the substrate (B). SEM images of deposited bilayer compliant electrodes for polymer outer surfaces (C, E, G) and the SWNT inner surface facing the substrate (D, F, H), respectively. (C) and (D) are for SWNT+WPU electrode, (E) and (F) are for SWNT+CN9021 electrode, (G) and (H) are for SWNT+PEDOT electrode. Scale bars are 200 nm.

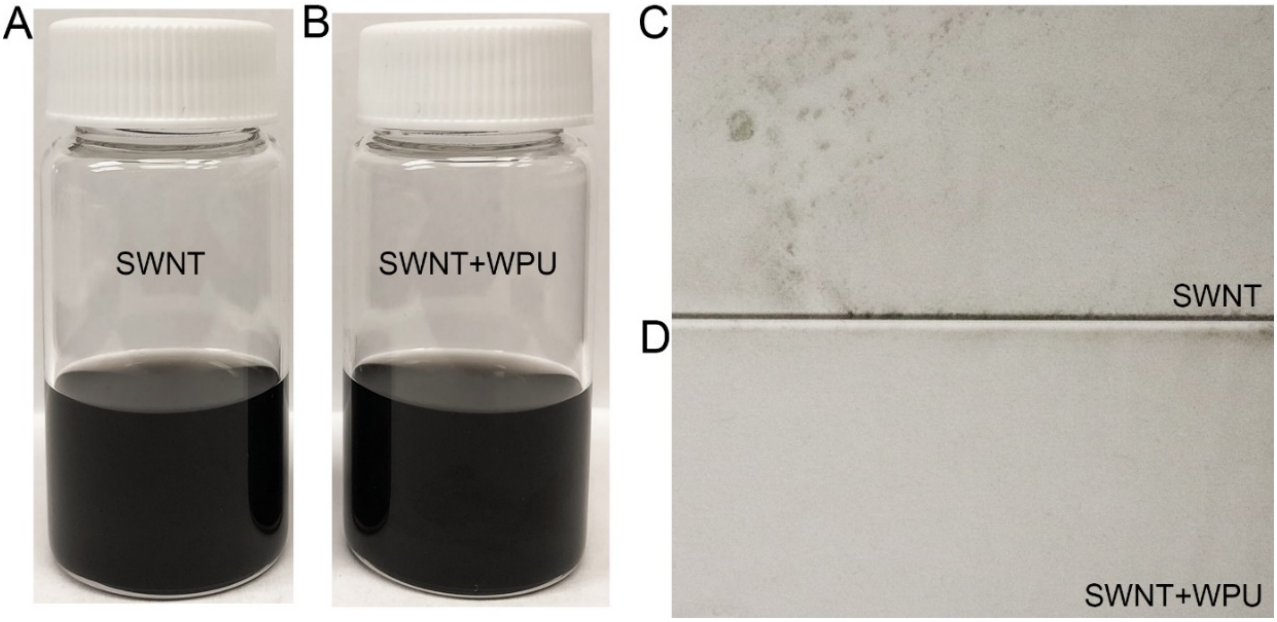

Figure 2-4 Dispersions of SWNT (A) and SWNT+WPU (B) in water/IPA. Photographs of the costings on glass formed by casting 1 mL of the SWNT (C) and SWNT+WPU (D) dispersions on glass substrate and subsequently air drying at room temperature.

The actuation-strain studies indicated that an ideal protective polymer thin layer should have both good compatibility with SWNT network and lower stiffness than DE films. The WPU is successfully used as the thin layer without sacrificing the actuation performance of VHB because WPU chains can easily penetrate SWNT network and form a uniform layer. The layer is also compliant enough to allow the full strain of VHB. As for comparisons, the CN9021 layer shows

non-uniformity while the PEDOT layer has high stiffness, thus leading to limited actuation properties of DEAs.

A

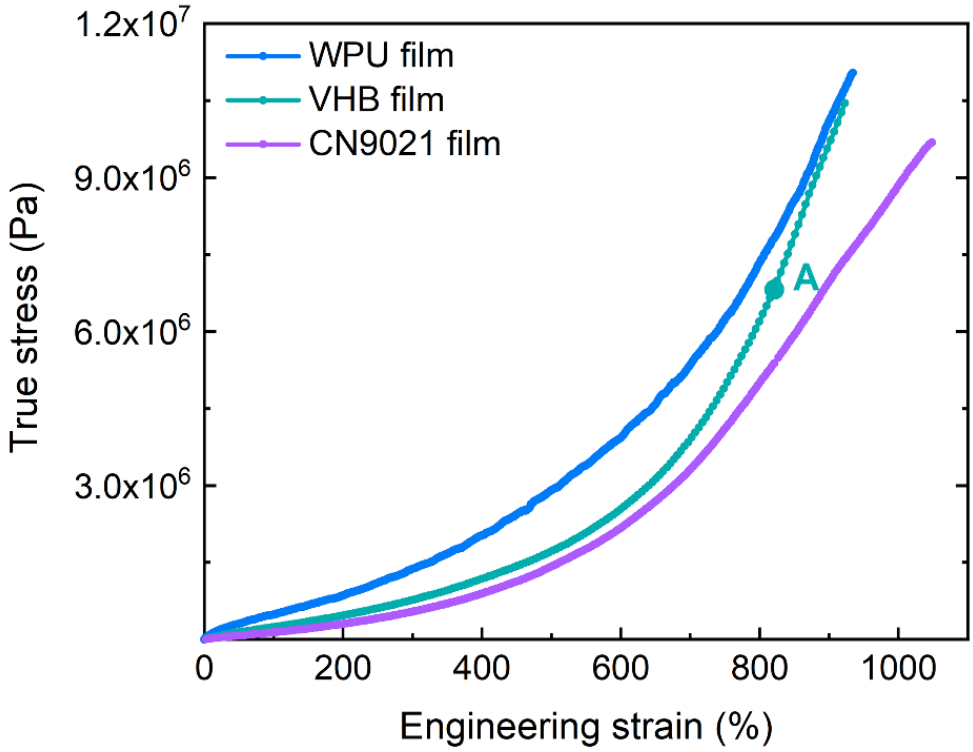

B

	WPU film	200% biaxially prestretched VHB film	CN9021 film
Modulus (10^5 Pa)	2.76	2.80	0.43

Figure 2-5 (A) True tress-strain curves for non-pre-stretched VHB film and WPU film. Point A indicates the strain at 800% on VHB film. (B) Table of the young's modulus of 200% biaxially prestretched VHB film (estimated) and WPU film (vendor sheet).

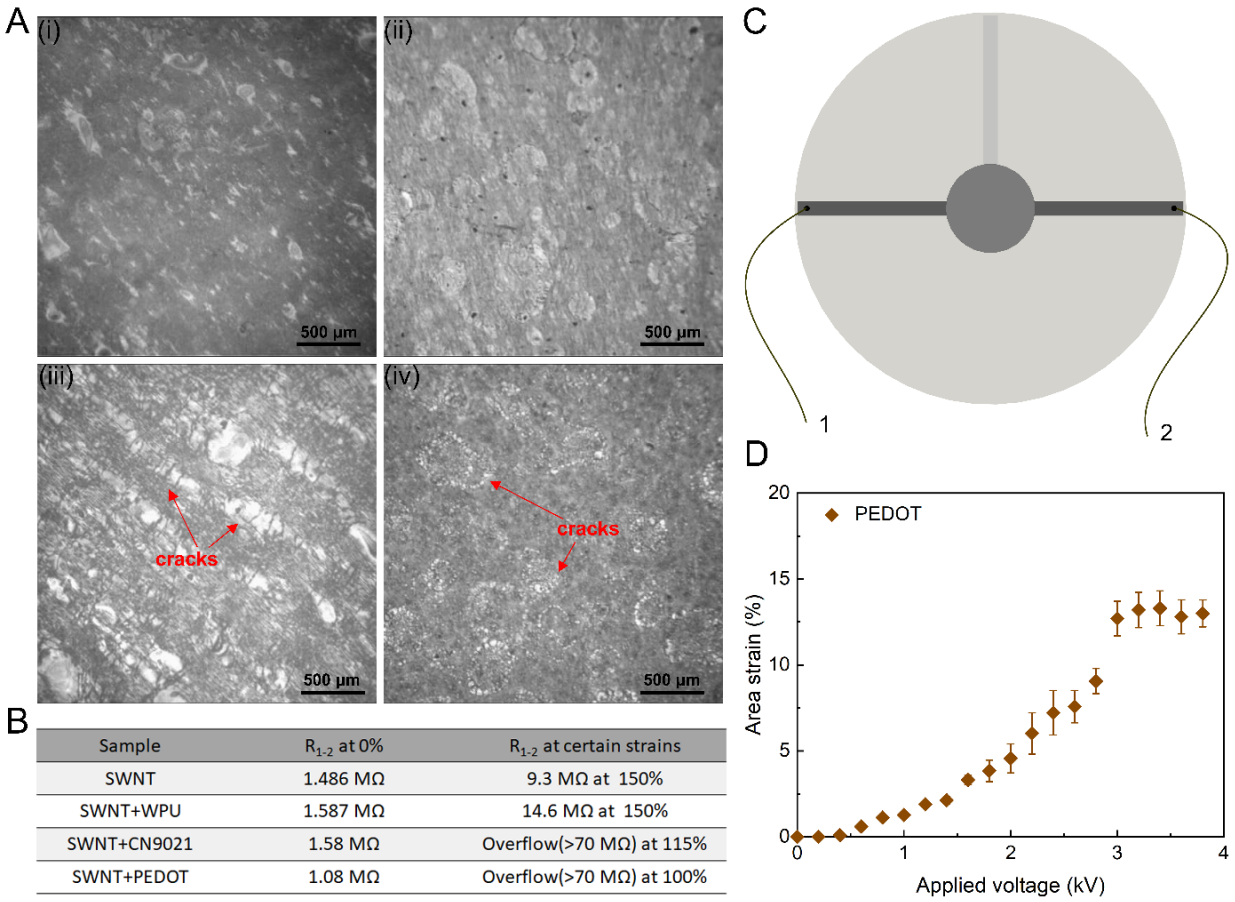

Sample	R_{1-2} at 0%	R_{1-2} at certain strains
SWNT	1.486 MΩ	9.3 MΩ at 150%
SWNT+WPU	1.587 MΩ	14.6 MΩ at 150%
SWNT+CN9021	1.58 MΩ	Overflow(>70 MΩ) at 115%
SWNT+PEDOT	1.08 MΩ	Overflow(>70 MΩ) at 100%

Figure 2-6 (A) Microscopic images of spray-coated PEDOT and SWNT+PEDOT electrodes on prestretched VHB film. PEDOT ((i) and (iii)) and SWNT+PEDOT ((ii) and (iv)) electrodes before and after one cycle of electrical actuation. (B) Table of resistances' change without electrical actuation and with electrically actuation strain. The measured resistance is between wire 1 and wire 2 in (C). (D) Electrically induced strain as a function of applied ramping-up voltage on a 200% biaxially pre-stretched VHB film with PEDOT electrodes on both surfaces. Five samples were tested. Each sample was actuated for one cycle at each 0.2 kV increment from 0 kV to 3.8 kV. Error bars indicate the standard deviation.

2.3.2 Actuation stability measurements

In order to measure the actuation stability, DEAs with SWNT+WPU, SWNT and carbon grease electrodes were driven by a 3 kV square-wave signal at a frequency of 0.05 Hz (**Figure 2-7A**). The circuit design for the measurements is shown in **Figure 2-8A**. The actuation strain is recorded by measuring the strain gap between the highest and lowest values. The SWNT+WPU based actuators can run for at least 1000 cycles with an actuation strain of 150% in area without fluctuation. The actuator with the SWNT electrode had a shorter lifetime of 725 cycles with decreased actuation strain. The actuator with the carbon grease electrode showed the lowest actuation stability which broke after 375 cycles, though its actuation strain slightly increased from 150% to 170%. This slight increase denotes the side effect of the permeation of silicone oil into VHB film and softening it.[24] The cyclic-actuation results demonstrated that the SWNT+WPU bilayer electrode provides actuators long lifetime and large actuation strain. As comparisons, the carbon grease electrode showed no self-clearing effect so that any localized breakdown would fail the actuators. The SWNT electrode with self-clearing capability sustains more cycles, but the unavoidable corona discharge in the air caused by sharp tips on nanotubes results in unstable actuation strain.

To further demonstrate the actuation stability of the SWNT+WPU electrode and understand the mechanisms, we conducted actuation tests under a constant voltage to test the actuation durability. **Figure 2-7B** to **2-7D** show the real-time actuation strain and the corresponding chronoamperic curves under a constant voltage of 3 kV for actuators with the SWNT+WPU, SWNT, and carbon grease electrodes, respectively. **Figure 2-8B** illustrates the circuit design for applying the constant voltage. Actuators show consistent responses in the case of measured area strain and current. Upon applying 3 kV, the actuation strains increased dramatically, then stabilized. Meanwhile, the

currents rose sharply to 10-15 μA and subsequently leveled off at 1-3 μA. The sharp current increase is due to the flow of charge onto the active area, and the stabilized current is the current across the acrylic film. For each type of electrodes, five samples were measured, and all of them showed a similar actuation trend under the consistent actuation condition.

For the SWNT+WPU electrode, both the real-time actuation strain and the corresponding chronoamperic curves were smooth under a constant voltage. No apparent fluctuation in actuation strain and current for at least 20,000 s (5.5 hours) indicates that the overall actuation performance is very stable during the continuous actuation. The SWNT electrode exhibited a similar trend as the SWNT+WPU sample within the first 100 s to 2000 s, the area strain and current stabilized at 190% and 3 μA, respectively. However, the area strain started to drop at around 2100 s along with the current jumping to 31 μA. The measured actuation strain gradually decreased from 185% to 20% after 15,000 s of the continuous actuation. Beyond 15,000 s, applying a voltage higher than 3 kV did not change the actuation strain, which means the actuator did not function anymore. The carbon grease electrode-based actuator showed even worse actuation stability with a sudden drop of area strain from 160% to 0% and a jump of current from 2 μA to 32 μA at 7500 s. At this stage, the electrode shorted through the acrylic film due to the localized electrical breakdown, and the film broke.

The localized electrical breakdown did not cause terminal failure or burning of the DE film for the SWNT electrode-based actuators, due to the self-clearing capability of the SWNT electrode which isolates the breakdown sites from the remaining conductive areas. However, the sharp tips of the nanotubes in the SWNT network could amplify the electric field and trigger more frequent corona discharging of the surrounding air which lead to localized electrical breakdown events in the dielectric elastomer film. Each breakdown event clears out a small area of the SWNT coating and

eventually, the SWNT electrode loses conductivity, and the actuator ceases to function. With the overcoated WPU thin layer on the self-clearable SWNT, this corona discharge issue is solved effectively. The sprayed water-based polyurethane solution penetrates the SWNT porous network, squeezes air out from the network, and shields SWNT networks from the air. As a result, corona discharge in the air is hugely quenched, meaning that the risk of failure caused by localized electrical breakdown is reduced a lot so that a long lifetime (more than 20,000 s) under considerable area strain (over 150%) can be easily realized.

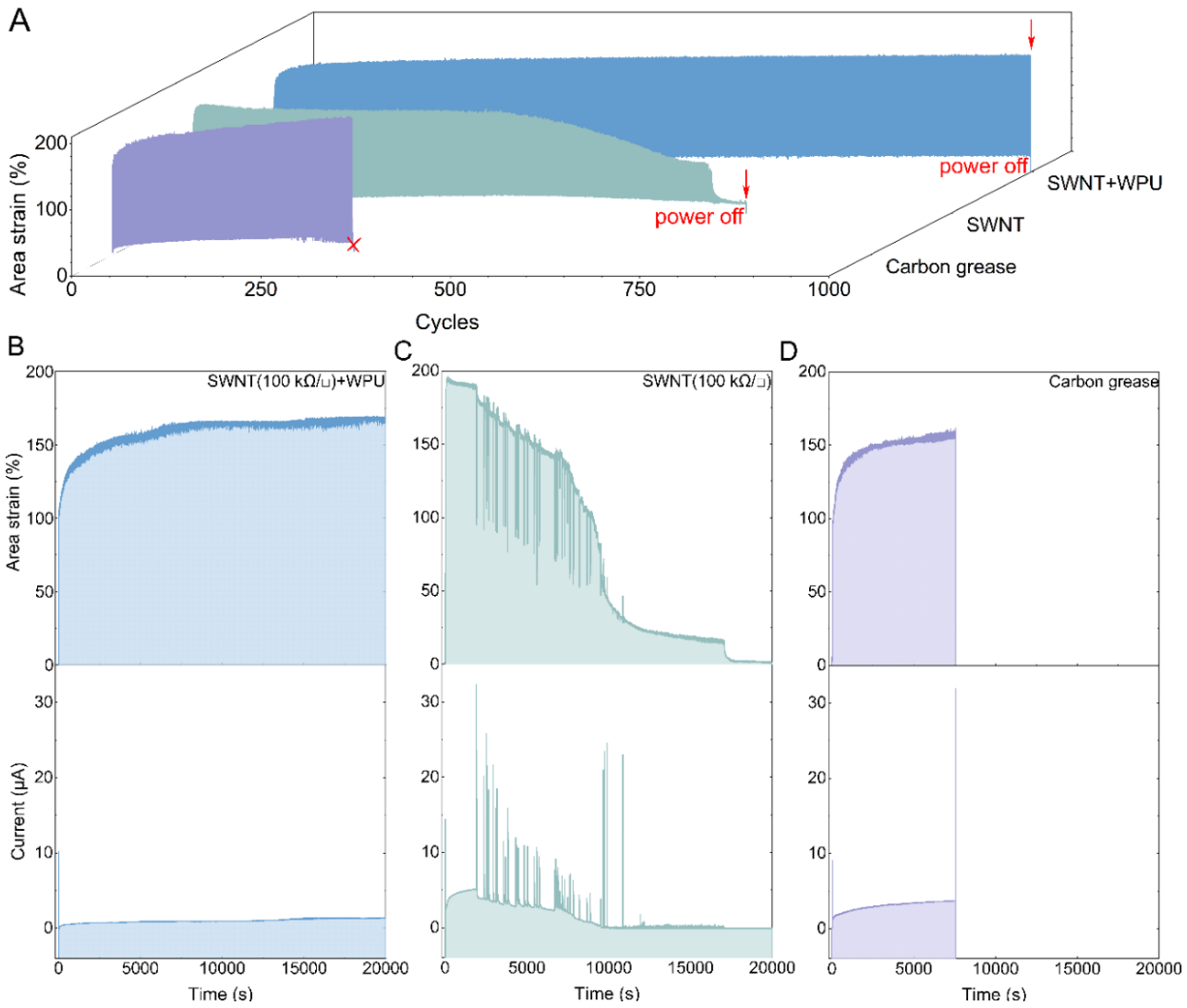

Figure 2-7 (A) Actuation stability tests under 3 kV square-wave voltage at 0.05 Hz for 200% biaxially pre-stretched VHB-based DEAs with SWNT+WPU, SWNT and carbon grease electrodes. Actuation stability tests under 3 kV constant voltage for 200% biaxially pre-stretched VHB-based DEAs with (B) SWNT+WPU, (C) SWNT and (D) carbon grease electrodes. Real-time actuation strain and corresponding current across the actuators were measured.

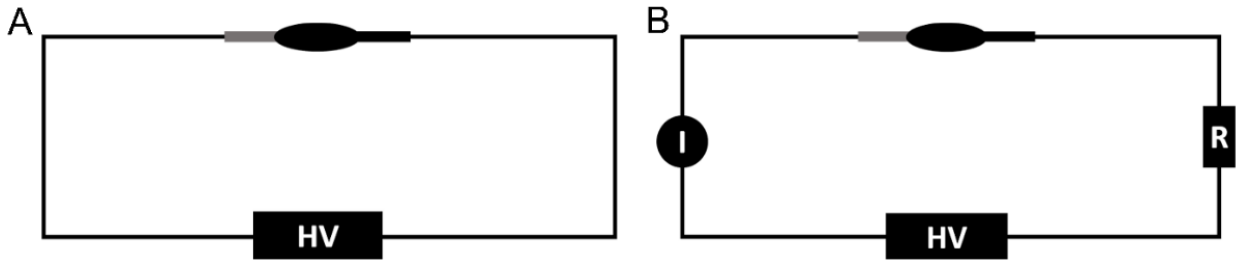

Figure 2-8 Circuit designs for actuation stability measurements under (A) square-wave voltage and (B) constant voltage. The circular expansion actuator, current-limiting resistor (R) with the resistance of 50 MΩ, and Keithley 2000 multimeter (I) were connected in series with high voltage power supply (HV). The actuation strain was recorded by a webcam, which was controlled and processed by LabView software.

2.3.3 Self-clearing capability

The new compliant SWNT+WPU electrode shows self-clearing capability under even harsher conditions, such as the higher applied voltage, at which electrical breakdown in the air becomes unavoidable. **Figure 2-9A** is the actuation stability test of an SWNT+WPU-based actuator under 3.4 kV pulse voltage at 0.05 Hz. The overall actuation performance was fairly stable, except that there was a drop in the actuation strain at around 783rd cycle, and multiple seconds later, this actuator restarted working normally and carrying a hole. This hole is formed by the self-clearing process on the breakdown site (**Figure 2-9A** (ii, iii)).

The continuous actuation test further proved the SWNT+WPU electrode's self-clearing capability. **Figure 2-9B** is the actuator's real-time actuation strain and the corresponding chronoamperic curves under a constant voltage of 3.4 kV. Upon the power on, there was a sharp increase in current to 7 μA, which then reduced and stabilized at 1.5 μA. Meanwhile, the corresponding area strain increased dramatically and stabilized at 215%. Both curves were smooth during actuation until

6200 s. The current-time and strain-time curves showed a sudden jump to 42 μA and drop to 105%, respectively. Later on, they returned to the specific stabilized values, i.e., 1.5 μA and 215%. Another huge fluctuation showed similar trends like the above described in current and area strain at 7200 s. The two high current spikes indicate the circuit shorts, i.e., electrical breakdown. This electrical breakdown did not cause the actuator's failure owing to the self-clearing capability of electrode materials.

To confirm the self-clearing capability of SWNT+WPU electrodes, we conducted puncturing experiments on DEAs with SWNT+WPU electrodes at working states. One SWNT+WPU-based DEA was driven to 140% actuation strain by a constant voltage. A sewing needle punctured the film, induced a sudden circuit short, and caused the shrinkage of actuation strain. Nevertheless, the actuator recovered to almost the same actuation strain after the electrode completed the self-clearing process. Multiple punctures did not affect the overall actuation strain. **Figure 2-9C** shows the captured images from the self-clearing video and the SEM image of the formed hole through puncturing the actuator by applying a constant voltage. The sizes of the holes formed after self-clearing processes can be variable. When the hole is too big, it might lead to the DE film's rupture due to the prestrain.

Following the two large spikes in **Figure 2-9B**, some tiny spikes of current appeared, indicating minor electrical breakdown events. Unlike the SWNT sample, those electrical breakdown events that happened in the SWNT+WPU sample did not cause gradually decreased actuation strain. The subdued spikes, rather than large spikes in the current curve, underlie the benefit of having the WPU thin solid layer in a similar fashion as having a dielectric oil overcoating on the SWNT electrode (see **Figure 2-10**). The tips of the nanotubes could amplify the electric field and cause the corona discharge in the air at high voltages. The thin WPU layer not only isolates the SWNT

network from air, it also serves as a dielectric barrier and distributes charges over a larger surface area rather than accumulating at a nanotube tip, thus transforming a corona discharge into silent, or subdued discharges. [24, 49-52] Therefore, this WPU dielectric layer helps weaken or suppress the corona discharge impact.

As such, the combination of the self-clearable SWNT electrode with a dry and thin polymer layer, which is compliant and compatible with the SWNT electrode, i.e., is stretchable and can penetrate and cover the electrode network thoroughly from the air, should offer actuators the stable actuation performance.

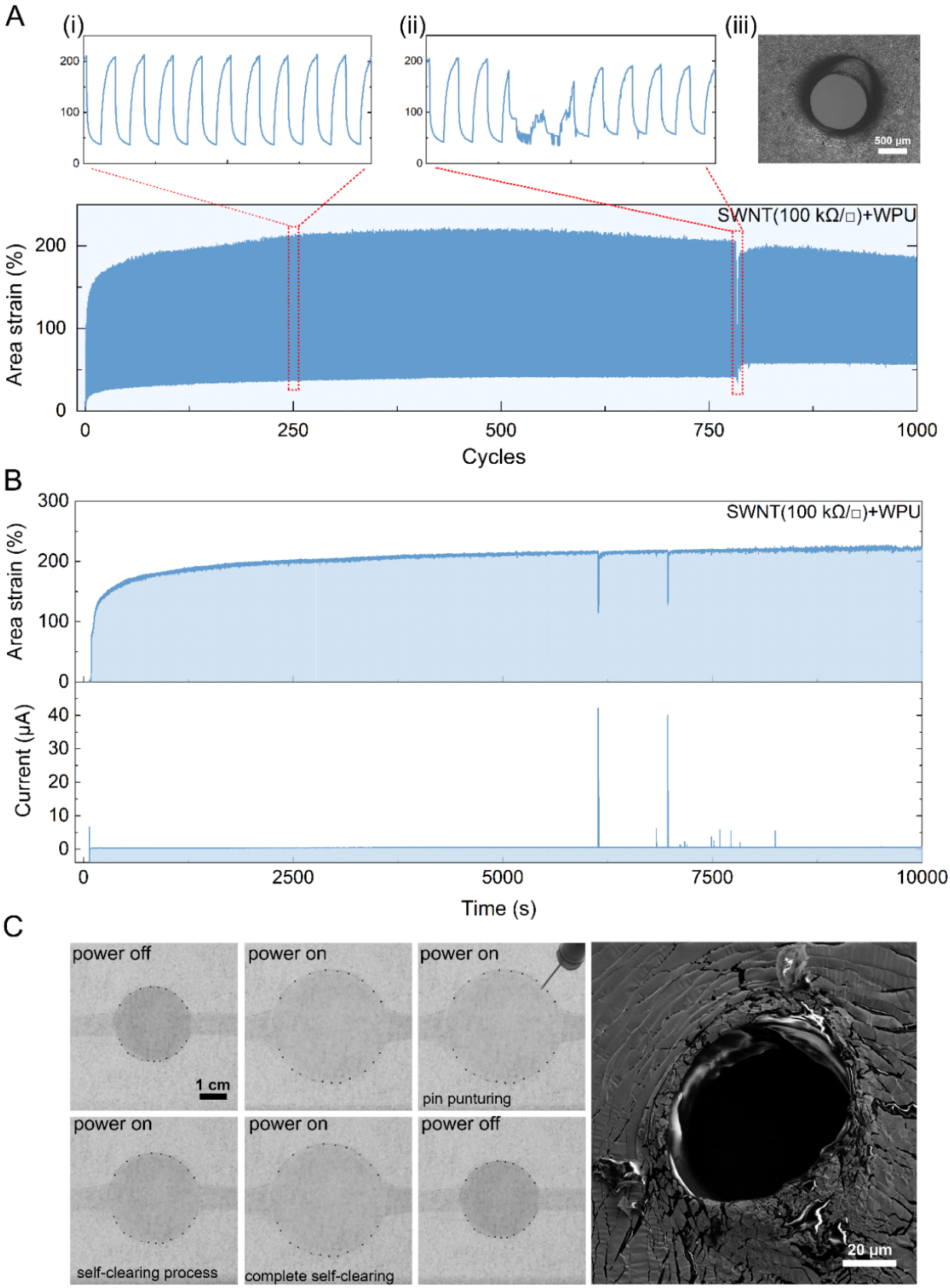
A
(i)
(ii)
(iii)
200
100
0
500 μm
SWNT(100 kΩ/□)+WPU
Area strain (%)
200
100
0
0
250
500
750
1000
Cycles
B
SWNT(100 kΩ/□)+WPU
Area strain (%)
300
200
100
0
Current (μA)
40
30
20
10
0
0
2500
5000
7500
10000
Time (s)
C
power off
1 cm
power on
power on
pin punturing
power on
self-clearing process
power on
complete self-clearing
power off
20 μm

Figure 2-9 (A) Real-time actuation strain under 3.4 kV square-wave voltage at 0.05 Hz. Zoom-in figure of the area strain drop and recovery under pulse-voltage actuation from 240th to 250th (i) and 780th to 790th cycles (ii). (iii) Microscopic image of the formed hole through self-clearing process. (B) Real-time actuation strain and corresponding current under 3.4 kV constant voltage for 200% biaxially pre-stretched VHB-based DEAs with SWNT+WPU electrode. (C) Captured images from the self-clearing video in supporting information, and SEM images of formed holes through puncturing under constant-voltage actuation.

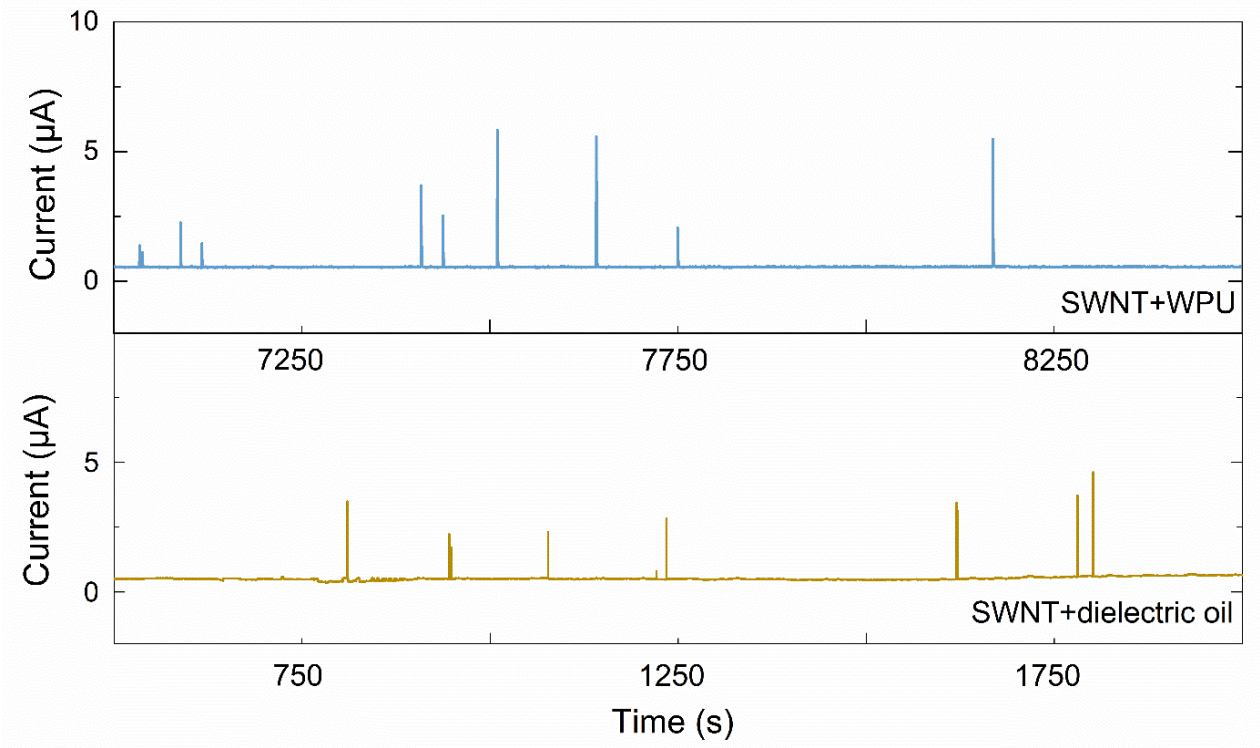

Figure 2-10 Real-time currents across actuators during large-strain actuation at a constant voltage for 200% biaxially pre-stretched VHB-based DEAs with SWNT+WPU and SWNT+dielectric oil electrode, respectively.

2.4 Conclusions

An interpenetrating bilayer compliant electrode has been prepared by over-coating a thin polymer layer of WPU on the SWNT network. This bilayer electrode is stretchy to obtain an actuation strain of 225% under 3.8 kV. It exhibits self-clearing ability in the event of a dielectric breakdown at high strains to avoid terminal breakdown. Operating at a 150% actuation strain under a constant voltage, the actuator shows high stability for at least 5.5 hours. Under a square-wave voltage operation at 150% actuation strain at 0.05 Hz, the actuation was stable for 1000 cycles. This bilayer electrode has resolved the actuation instability issue from the use of bare SWNT electrode, as the SWNTs' sharp tips in the bilayer electrodes are embedded in the dielectric WPU layer. The corona discharging caused by the exposed nanotube tips may have been transformed into silent, subdued dischargings. The improved actuation stability should be an important development to move the DEAs closer to practical applications, where their large actuation strains may be unleashed.

2.5 References

[1] R. Kornbluh, R. Pelrine, Q. Pei, Dielectric elastomer produces strain of 380%. *EAP Newsletter* **2002**, 2.

[2] R. Pelrine, R. Kornbluh, Q. Pei, J. Joseph, High-speed electrically actuated elastomers with strain greater than 100%. *Science* **2000**, 287, 836.

[3] F. Carpi, I. Anderson, S. Bauer, G. Frediani, G. Gallone, M. Gei, C. Graaf, C. Jean-Mistral, W. Kaal, G. Kofod, M. Kollosche, R. Kornbluh, B. Lassen, M. Matysek, S. Michel, S. Nowak, B. O'Brien, Q. Pei, R. Pelrine, B. Rechenbach, S. Rosset, H. Shea, Standards for dielectric elastomer transducers. *Smart Mater. Struct.* **2015**, 24.

[4] P. Brochu, Q. Pei, Dielectric elastomers for actuators and artificial muscles. Electroactivity in

polymeric materials, *Springer* **2012**,1.

[5] Y. Qiu, E. Zhang, R. Plamthottam, Q. Pei, Dielectric elastomer artificial muscle: materials innovations and device explorations. *Accounts Chem. Res.* **2019**, 52, 316.

[6] I. A. Anderson, T. A. Gisby, T. G. McKay, B. M. O'Brien, E. P. Calius, Multi-functional dielectric elastomer artificial muscles for soft and smart machines. *J. Appl. Phys.* **2012**, 112, 041101.

[7] J. Eckerle, S. Stanford, J. Marlow, R. Schmidt, S. Oh, T. Low, S. V. Shastri, Biologically inspired hexapedal robot using field-effect electroactive elastomer artificial muscles, Smart structures and materials 2001: Industrial and commercial applications of smart structures technologies, *Proc. SPIE* **2001**, 4332, 269.

[8] Q. Pei, R. Pelrine, S. Stanford, R. Kornbluh, M. Rosenthal, Electroelastomer rolls and their application for biomimetic walking robots. *Synthetic Met.* **2003**, 135, 129.

[9] S. K. Mitchell, X. Wang, E. Acome, T. Martin, K. Ly, N. Kellaris, V. G. Venkata, C. Keplinger, An Easy-to-Implement Toolkit to Create Versatile and High-Performance HASEL Actuators for Untethered Soft Robots. *Adv. Sci.* **2019**, 6, 1900178.

[10] Y. Chen, H. Zhao, J. Mao, P. Chirarattananon, E. F. Helbling, N.S. P. Hyun, D. R. Clarke, R. J. Wood, Controlled flight of a microrobot powered by soft artificial muscles. *Nature* **2019**, 575, 324.

[11] B. Chen, J. J. Lu, C. H. Yang, J. H. Yang, J. Zhou, Y. M. Chen, Z. Suo, Highly stretchable and transparent ionogels as nonvolatile conductors for dielectric elastomer transducers. *ACS Appl. Mater. Interfaces* **2014**, 6, 7840.

[12] S. Yun, S. Park, B. Park, S. K. Park, H. Prahlad, P. Von Guggenberg, K. U. Kyung, Polymer-based flexible visuo-haptic display. *IEEE ASME Trans. Mechatron.* **2014**, 19, 1463.

[13] H. Boys, G. Frediani, S. Poslad, J. Busfield, F. Carpi, A dielectric elastomer actuator-based tactile display for multiple fingertip interaction with virtual soft bodies. *Electroactive Polymer Actuators and Devices (EAPAD)*, **2017**, 101632D.

[14] A. Marette, A. Poulin, N. Besse, S. Rosset, D. Briand, H. Shea, Flexible zinc–tin oxide thin film transistors operating at 1 kV for integrated switching of dielectric elastomer actuators arrays. *Adv. Mater.* **2017**, 29, 1700880.

[15] J. Li, Y. Wang, L. Liu, S. Xu, Y. Liu, J. Leng, S. Cai, A biomimetic soft lens controlled by electrooculographic signal. *Adv. Funct. Mater.* **2019**, 29, 1903762.

[16] S. Shian, R. M. Diebold, D. R. Clarke, Tunable lenses using transparent dielectric elastomer actuators. *Opt. Express* **2013**, 21, 8669.

[17] D. McCoul, Q. Pei, Tubular dielectric elastomer actuator for active fluidic control. *Smart Mater. Struct.* **2015**, 24, 105016.

[18] S. Solano-Arana, F. Klug, H. Mößinger, F. Förster-Zügel, H. F. Schlaak, A novel application of dielectric stack actuators: a pumping micromixer. *Smart Mater. Struct.* **2018**, 27, 074008.

[19] J. S. Plante, S. Dubowsky, Large-scale failure modes of dielectric elastomer actuators. *Int. J. Solids Struct.* **2006**, 43, 7727.

[20] H. Stoyanov, P. Brochu, X. Niu, C. Lai, S. Yun, Q. Pei, Long lifetime, fault-tolerant freestanding actuators based on a silicone dielectric elastomer and self-clearing carbon nanotube compliant electrodes. *RSC Adv.* **2013**, 3, 2272.

[21] P. Lochmatter, G. Kovacs, Design and characterization of an active hinge segment based on soft dielectric EAPs. *Sensor Actuat. A-Phys.* **2008**, 141, 577.

[22] J. D. Vogan, Development of dielectric elastomer actuators for MRI devices. *MS Thesis*, Department of Mechanical Engineering, Massachusetts Institute of Technology, Cambridge, USA,

2004.

[23] W. Yuan, L. B. Hu, Z. B. Yu, T. Lam, J. Biggs, S. M. Ha, D. J. Xi, B. Chen, M. K. Senesky, G. Grüner, Q. Pei, Fault-tolerant dielectric elastomer actuators using single-walled carbon nanotube electrodes. *Adv. Mater.* **2008**, 20, 621.

[24] W. Yuan, P. Brochu, S. M. Ha, Q. Pei, Dielectric oil coated single-walled carbon nanotube electrodes for stable, large-strain actuation with dielectric elastomers. *Sensor Actuat. A-Phys.* **2009**, 155, 278.

[25] G. K. Lau, S. C. K. Goh, L. L. Shiau, Dielectric elastomer unimorph using flexible electrodes of electrolessly deposited (ELD) silver. *Sensor Actuat. A-Phys.* **2011**, 169, 234.

[26] S. Rosset, H. R. Shea, Flexible and stretchable electrodes for dielectric elastomer actuators. *Appl. Phys. A-Mater.* **2013**, 110, 281.

[27] W. Yuan, P. Brochu, H. Zhang, A. Jan, Q. Pei, Long lifetime dielectric elastomer actuators under continuous high strain actuation. *Electroactive Polymer Actuators and Devices (EAPAD)*, **2009**, 72870O.

[28] W. Yuan, T. Lam, J. Biggs, L. Hu, Z. Yu, S. Ha, D. Xi, M. K. Senesky, G. Grüner, Q. Pei, New electrode materials for dielectric elastomer actuators. *Electroactive Polymer Actuators and Devices (EAPAD)*, **2007**, 65240N.

[29] T. Lam, H. Tran, W. Yuan, Z. Yu, S. Ha, R. Kaner, Q. Pei, Polyaniline nanofibers as a novel electrode material for fault-tolerant dielectric elastomer actuators. *Electroactive Polymer Actuators and Devices (EAPAD)*, **2008**, 69270O.

[30] S. Li, M. Jiang, Y. Xie, H. Xu, J. Jia, J. Li, Developing high-performance lithium metal anode in liquid electrolytes: challenges and progress. *Adv. Mater.* **2018**, 30, 1706375.

[31] T. P. Huynh, P. Sonar, H. Haick, Advanced materials for use in soft self-healing devices. *Adv.*

Mater. **2017**, 29, 1604973.

[32] X. Cheng, J. Pan, Y. Zhao, M. Liao, H. Peng, Gel polymer electrolytes for electrochemical energy storage. *Adv. Energy Mater.* **2018**, 8, 1702184.

[33] L. M. Zhang, Y. He, S. Cheng, H. Sheng, K. Dai, W. J. Zheng, M. X. Wang, Z. S. Chen, Y. M. Chen, Z. Suo, Self-healing, adhesive, and highly stretchable ionogel as a strain sensor for extremely large deformation. *Small* **2019**, 15, 1804651.

[34] X. Li, L. Liu, X. Wang, Y. S. Ok, J. A. W. Elliott, S. X. Chang, H. J. Chung, Flexible and self-healing aqueous supercapacitors for low temperature applications: polyampholyte gel electrolytes with biochar electrodes. *Sci. Rep.* **2017**, 7, 1685.

[35] Y. Cao, T. G. Morrissey, E. Acome, S. I. Allec, B. M. Wong, C. Keplinger, C. Wang, A transparent, self-healing, highly stretchable ionic conductor. *Adv. Mater.* **2017**, 29, 1605099.

[36] Y. Qiu, Z. Lu, Q. Pei, Refreshable tactile display based on a bistable electroactive polymer and a stretchable serpentine Joule heating electrode. *ACS Appl. Mater. Interface* **2018**, 10, 24807.

[37] H. Wang, Y. Meng, Z. Zhang, M. Gao, Z. Peng, H. He, Q. Pei, Self-actuating electrocaloric cooling fibers. *Adv. Energy Mater.* **2020**, 10, 1903902.

[38] M. Duduta, R. J. Wood, D. R. Clarke, Multilayer dielectric elastomers for fast, programmable actuation without prestretch. *Adv. Mater.* **2016**, 28, 8058.

[39] H. Sun, X. You, Y. Jiang, G. Guan, X. Fang, J. Deng, P. Chen, Y. Luo, H. Peng, Self-healable electrically conducting wires for wearable microelectronics. *Angew. Chem. Int. Edit.* **2014**, 53, 9526.

[40] W. Yuan, H. Li, P. Brochu, X. Niu, Q. Pei, Fault-tolerant silicone dielectric elastomers. *Int. J. Smart Nano Mater.* **2010**, 1, 40.

[41] M. Duduta, E. Hajiesmaili, H. Zhao, R. J. Wood, D. R. Clarke, Realizing the potential of

dielectric elastomer artificial muscles. *P. Natl. Acad. Sci USA* **2019**, 116, 2476.

[42] P. Li, Y. Wang, U. Gupta, J. Liu, L. Zhang, D. Du, C. C. Foo, J. Ouyang, J. Zhu, Transparent soft robots for effective camouflage. *Adv. Funct. Mater.* **2019**, 29, 1901908.

[43] P. Li, D. Du, L. Guo, Y. Guo, J. Ouyang, Stretchable and conductive polymer films for high-performance electromagnetic interference shielding. *J. Mater. Chem. C* **2016**, 4, 6525.

[44] R. Zhou, P. Li, Z. Fan, D. Du, J. Ouyang, Stretchable heaters with composites of an intrinsically conductive polymer, reduced graphene oxide and an elastomer for wearable thermotherapy. *J. Mater. Chem. C* **2017**, 5, 1544.

[45] X. Niu, X. Yang, P. Brochu, H. Stoyanov, S. Yun, Z. Yu, Q. Pei, Bistable large-strain actuation of interpenetrating polymer networks. *Adv. Mater.* **2012**, 24, 6513.

[46] X. Niu, H. Stoyanov, W. Hu, R. Leo, P. Brochu, Q. Pei, Synthesizing a new dielectric elastomer exhibiting large actuation strain and suppressed electromechanical instability without prestretching. *J. Polym. Sci. Pol. Phys.* **2013**, 51, 197.

[46] Y. Wang, C. Zhu, R. Pfattner, H. Yan, L. Jin, S. Chen, F. Molina-Lopez, F. Lissel, J. Liu, N. I. Rabiah, Z. Chen, J. W. Chung, C. Linder, M. F. Toney, B. Murmann, Z. Bao, A highly stretchable, transparent, and conductive polymer. *Sci. Adv.* **2017**, 3, e1602076.

[47] F. B. Albuquerque, H. Shea, Influence of humidity, temperature and prestretch on the dielectric breakdown strength of silicone elastomer membranes for DEAs. *Smart Mater. Struct.* **2020**.

[48] B. Eliasson, U. Kogelschatz, Nonequilibrium volume plasma chemical processing. *IEEE Trans. Plasma Sci.* **1991**, 19, 6.

[49] B. Eliasson, U. Kogelschatz, Modeling and applications of silent discharge plasmas. *IEEE Trans. Plasma Sci.* **1991**, 19, 2.

[50] U. Kogelschatz, B. Eliasson, W. Egli, Dielectric-barrier discharges. Principle and applications. *Le Journal de Physique IV* **1997**, 07, C4.

[51] U. Kogelschatz, Dielectric-barrier discharges: their history, discharge physics, and industrial applications. *Plasma Chem. Plasma P.* **2003**, 23, 1.

[52] Z. Peng, Y. Qiu, Y. Shi, Z. Zhang, A. Alwen, H. Yin, R. Plamthottam, Z. Ren, Q. Pei, Bistable electroactive polymers for refreshable tactile displays. *Electroactive Polymer Actuators and Devices (EAPAD) XXI*, **2019**, 109662C.

Chapter 3 HYBRID MANUFACTURING OF PRESTRAIN-LOCKED ACRYLIC DIELECTRIC ELASTOMER THIN FILMS AND MULTILAYER STACKS

3.1 Background of this study

3.1.1 Dielectric elastomers (DEs)

Dielectric elastomers earned the name of 'artificial muscle' due to their capability of matching human muscles' performance in terms of the large actuation strain, high work density, and good mechanical compliance. [1-5] A DE film can act as a deformable capacitor after sandwiching between compliant electrodes. [6] Applying a voltage across the DE film, the electric field would rearrange the charges, i.e., like charges accumulate on the same side of the DE film and repel each other, at the same time, the opposite charges locate on the opposite side of the DE film and attract each other. As a result, the DE film expands in area and contracts in the thickness direction.

The majority of applications have been explored based on the actuation mechanism, such as tactile displays, [7-9] tunable optics, [10, 11] and biomimetic robotics. [12-15] It was known that DE materials play the central role in achieving good operation performances. Commercially available 3M VHB acrylate adhesives stand out as one of the most promising DE materials due to their large electrically induced strain. A highly prestretched VHB film can reach 380% actuation strains and 3.4 J/g elastic energy density. [3, 16, 17] However, two major problems exist for VHB-based actuators, limiting their further applications. One is that a rigid frame is always required to support the mechanical prestrain. This rigid structure increases the total mass of the DE actuators, diminishes the device flexibility, reduces the overall specific energy density and causes fatigue. [1, 18] Another

one is that the intrinsic high viscoelasticity from these acrylate films results in a low response speed to an electric field. [19, 20]

3.1.2 Improved acrylate VHBs

Interpenetrated polymer networks (IPNs) from VHBs were reported to be able to lock the prestrain, realizing rigid-frame-free DE films. [21-24] An IPN structure is typically a composite system of polymers, within which at least one polymer is crosslinked in the immediate presence of the others. Introducing a multifunctional monomer additive into a highly prestrained VHB film, subsequently curing the system, a second elastomeric network will be formed within the VHB matrix. When removing the rigid frame used to support the prestrain, the highly prestrained VHB tends to contract, compressing the second network until the two networks are in balance, resulting in a preserved prestrain. One of our previous studies showed that the free-standing VHB-IPNs using a trifunctional monomer as an additive achieved the maximum strains of over 200%. [1, 15]

However, VHB-IPN films exhibited a temperature-dependent elasticity, thus strongly affecting the responded strain in terms of the electric field due to the inherent viscoelastic loss. [1, 18, 19] An efficient way of increasing the response speed is to add plasticizers. [18, 25, 26] Plasticizers are small molecules with low glass transition temperatures. When embedded and distributed into a polymer matrix, they can separate polymer chains via creating more free volume to weaken the intermolecular interaction and increase chain mobility. [26] At the same time, the overall glass transition temperature of the polymer/plasticizer system will be lower than the polymer itself due to the induced low-glass-transition-temperature plasticizer.

3.1.3 Multilayer stacking

Multilayer stacking has been adopted on DEAs to scale up the energy and force output, especially when a lower voltage is required for a practical purpose. [2, 27, 28] But it has been a big challenge to find a reliable way to stack thin elastomer films with large-scale manufacturing, either because of the low yield or process complexity. So far, there are two general categories for DEA multilayer fabrication, i.e., based on wet DE films and based on dry DE films. An example of the former one is to stack the DEAs by repeating the processes of spin-coating or blade-coating and curing, i.e., spin-coat or blade-coat a layer of liquid polymer precursor, cure, apply electrode, spin-coat or blade-coat the second layer of liquid precursor, cure, apply electrode, spin-coat or blade-coat the third layer of liquid precursor…[29-31] Depending on the required number of layers, the processes are repeated a number of times. For fabricating multiple layers, the repeated steps of coating and curing are too complex to be adopted for manufacturing. Multilayer stacking based on dry films refers to that all required DE films have been cured and are ready for stacking, this results in faster manufacturing. Furthermore, the stacks' quality control should be better due to the 'screening' of avoiding using the defective films prior to stack. For examples, one multilayer DEA was fabricated by folding and compacting a monolithic structure of an electrode-patterned DE sheet directly [32] and another was made by several sub-processes of folding DE and patterning electrode on that DE layer. [33] But achieved actuators made by the above processes didn't show ideal actuation performances. This is possibly due to the intrinsic DE material properties. [33] Therefore, selecting high-performance DE films for stacking is crucial. The VHB-IPN films were reported to be free-standing and showed a great actuation strain. [21, 22] Kavocs targeted the prefabricated VHB-IPN films for multilayer stacking through a simple piling-up configuration. [34] The multilayer actuator, at activation, was able to lift 1 kg of mass, reaching 10% contraction. However, according to what

they mentioned, due to the pile-up design, the system essentially had no structural integrity unless the electrostatic field was applied. At the inactivation state, the actuator tended to delaminate under loading.

3.1.4 Prestrain-locked dielectric elastomers (VHB-IPN-Ps) and novel stacking adoption

To overcome the bulky prestraining structure and the intrinsic viscoelasticity of acrylate elastomers, while utilizing them to fabricate multilayer DEAs, we developed hybrid manufacturing, which combines prestrain-locked high-performance dielectric elastomer (VHB-IPN-P) thin films and multilayer stacks. This hybrid approach optimizes actuators' overall actuation performance, avoids the mechanical prestraining structure, and offers efficient multilayer stacking. We induced a bifunctional monomer (HDDA) as the additive to the highly prestrained VHB matrix and coupled it with a plasticizer to prepare the prestrain-locked dielectric elastomers (VHB-IPN-Ps). The cured bifunctional monomers formed a second network within the VHB matrix and served as internally mechanical support after removing the external prestraining structure, locking the residual prestrain when the tension in the VHB matrix and compression in the secondary poly (HDDA) network were balanced. The plasticizer was then diffused into the interpenetrated system to lower the glass transition temperature by separating polymer chains and creating more free volume inside of the polymers. As a result, the DE film was softened, showing a low modulus and viscoelasticity. The VHB-IPN-P films reached a greater actuation strain under the same condition than those of VHBs or VHB-IPNs and exhibited a significantly faster actuation response than the other two. Furthermore, by coating a carbon nanotube-polymer bilayer electrode, the VHB-IPN-P actuators showed a much more stable and durable actuation than actuators with only a single layer electrode (CNT). Moreover, a hybrid stacking method based on the VHB-IPN-P and bilayer electrode was developed successfully, it offers structural integrity with strong interlayer bonding and provides

fast manufacturing to produce scalable multilayer stacks. The 4-layer stack prepared by the hybrid manufacturing showed a comparable actuation performance and response speed as the single VHB-IPN-P film. With high repeatability, processing quality, and yield, we believe the hybrid stacking opens the door for large-scale multilayer DEAs' manufacturing.

3.2 Experimental design

3.2.1 Raw materials

4910 VHB adhesives were purchased from 3M. Urethane diacrylate (UDA, CN9021), dibutoxyethoxyethyl formal (DBEF), Isopropyl alcohol (IPA), tetrahydrofuran (THF), butyl acrylate (BA), neopentyl glycol propoxylate diacrylate (PNPDA), bifunctional 1,6-hexandiol diacrylate (HDDA), 2,2-dimethoxy-2-phenylacetophenone (DMPA) and benzophenone (BP) were purchased from Sigma Aldrich and used as received. Single-walled carbon nanotubes (CNTs, P3-SWNT) were purchased from Carbon Solutions, Inc.

3.2.2 VHB-IPN preparation

Firstly, 3M VHB 4910 with the original thickness of 1 mm was stretched to 400% x 400% biaxial prestrain. The film thickness after prestrain became 40 μm. Then, the HDDA solution (mixed with 1% DMPA and 0.5% BP, diluted with acetone into 2 wt%) was sprayed uniformly to the prestretched VHB film. The actual spraying HDDA amount was estimated as 1.15 μl/cm^2. The VHB film diffused by HDDA monomers was then UV cured on a UV curing conveyor equipped with a 2.5 W/cm^2 Fusion 300s UV curing bulb for 2 passes at a speed of 12 ft/min and 3 passes 15 ft/min to form the IPN structure. The cured film was then transferred to the stretcher to initiate the releasing process. The releasing stopped when visible wrinkles appeared. This rigid-frame-free and free-standing VHB-IPN film was then preserved with around 275% x 275% area prestrain.

3.2.3 VHB-IPN-P preparation

VHB-IPN-P preparation started with the VHB-IPN film. After relaxing the VHB-IPN film to 275% x 275% prestrain, DBEF (weight ratio of IPN: DBEF = 2:1, diluted with acetone) was then sprayed onto the released film. The film was then left overnight to have DBEF diffused completely.

3.2.4 Fabrication of single-layer actuator based on VHB-IPN or VHB-IPN-P films

Actuators with carbon nanotube electrode

CNT solution, which was prepared by referring to our previous study, [35] was diluted with deionized water and IPA, and uniformly sprayed onto the uncured IPN film. The approximate sheet resistance was 50-100 kΩ/sq. After depositing the electrodes, the film underwent UV curing and releasing. For actuators based on VHB-IPN, the free-standing film was then cut to make the diaphragm actuation samples. For actuators based on VHB-IPN-P, DBEF solution was sprayed on the released film and left overnight before cutting. The active area of actuators was 0.33 inches in diameter.

Actuators with carbon nanotube/polymer bilayer electrode

Actuators with bilayer electrodes followed a similar process as the way of fabricating actuators with CNT electrode, the only difference was that after depositing the CNT electrode, a polymer precursor solution was sprayed onto the CNT electrode. The polymer precursor solution was prepared by mixing CN9021, BA, PNPDA, DMPA, and BP together and then diluted by acetone in 2 wt%. After depositing the bilayer electrodes, the film underwent UV curing and releasing. For actuators based on VHB-IPN, the free-standing film was then cut to make the diaphragm actuation

samples. For actuators based on VHB-IPN-P, DBEF solution was sprayed on the released film and left overnight before cutting. The active area of actuators was 0.33 inches in diameter.

3.2.5 Fabrication of multilayer VHB-IPN-P actuators

Each pre-stacking DE film was prepared as the procedure above. 20 wt% HDDA was sprayed onto 400% x 400% biaxial prestrained VHB 4910 to serve as the pre-stacking film (VHB-HDDA). These films were then adhered onto the supporting substrate (Teflon wrapped with heavy duty tape, ①) and the sacrificial substrate (Teflon, ②). The electrodes were deposited on to the active area of ② through a mask. The achieved ②/VHB-HDDA film was then aligned onto the ①/VHB-HDDA film and placed in the laminating vacuum chamber. The chamber was vacuumed, and the samples were laminated under a pressure of 4 kg/cm^2 for 2 min. The Teflon (②) was peeled off from the supporting substrate (①) and a 2-layer stacked VHB-HDDA films were left on the supporting substrate. The process was then repeated until the certain number of layers was achieved. The stack was then UV cured by 8 passes at a speed of 15 ft/min and transferred to the stretcher for relaxing. 50 wt% DBEF was sprayed onto the released stacking film afterwards and left overnight. The film was them cut to make diaphragm samples. Sliver glue was applied to cover the exposed conductive edges.

3.3 Results and discussions

3.3.1 Materials synthesis, actuator fabrication and actuation performance

An actuator can exhibit an out-of-plane actuation with a voltage applied when there is an edge constraint. We adopted the diaphragm actuation method to evaluate the actuation performances of VHB-IPN and VHB-IPN-P based actuators. **Figure 3-1A** illustrates the VHB-IPN-P synthesis and **Figure 3-1B** describes the fabrication processes of actuators. A 400% x 400% prestretched VHB

film was mounted on an acrylic frame. Diluted HDDA solution was sprayed on the entire area of the prestretched VHB film. With the small molecular weight, the HDDA monomers would diffuse into the VHB film. Electrode solution was then deposited onto the film covered by a mask. The film was UV cured to have a second network of poly (HDDA) formed within the VHB matrix. The cured VHB-IPN film was placed and adhered to a stretcher, then the rigid acrylic frame was removed to initiate the release. The releasing process stopped when visible wrinkles appeared on the film. The HDDA, when highly crosslinked, exhibited Young's modulus of 930 ± 12 MPa, [36] therefore, can provide certain internal mechanical support to the highly prestrecthed VHB matrix. As the prestraining structure was removed from the VHB-IPN film, the contraction from the prestretched VHB matrix would cause compression in the poly (HDDA) network. When the tension within the VHB matrix was balanced with the compression in the second network, there would be a preserved strain. The preserved strain depends on the induced HDDA amount into the matrix. **Table 3-1** lists the preserved strains corresponding to the added HDDA amounts. We selected the spraying HDDA amount of 1.15 μl/cm^2, which offered a preserved biaxial strain of 275%, since, from our previous studies, this preserved strain was investigated to sustain a relatively high dielectric breakdown field with a high strain. [22] The VHB-IPN-P film was made by adding DBEF as a plasticizer into the VHB-IPN film to soften the system. After DBEF's complete diffusing, the actuator based on VHB-IPN-P film was ready to test.

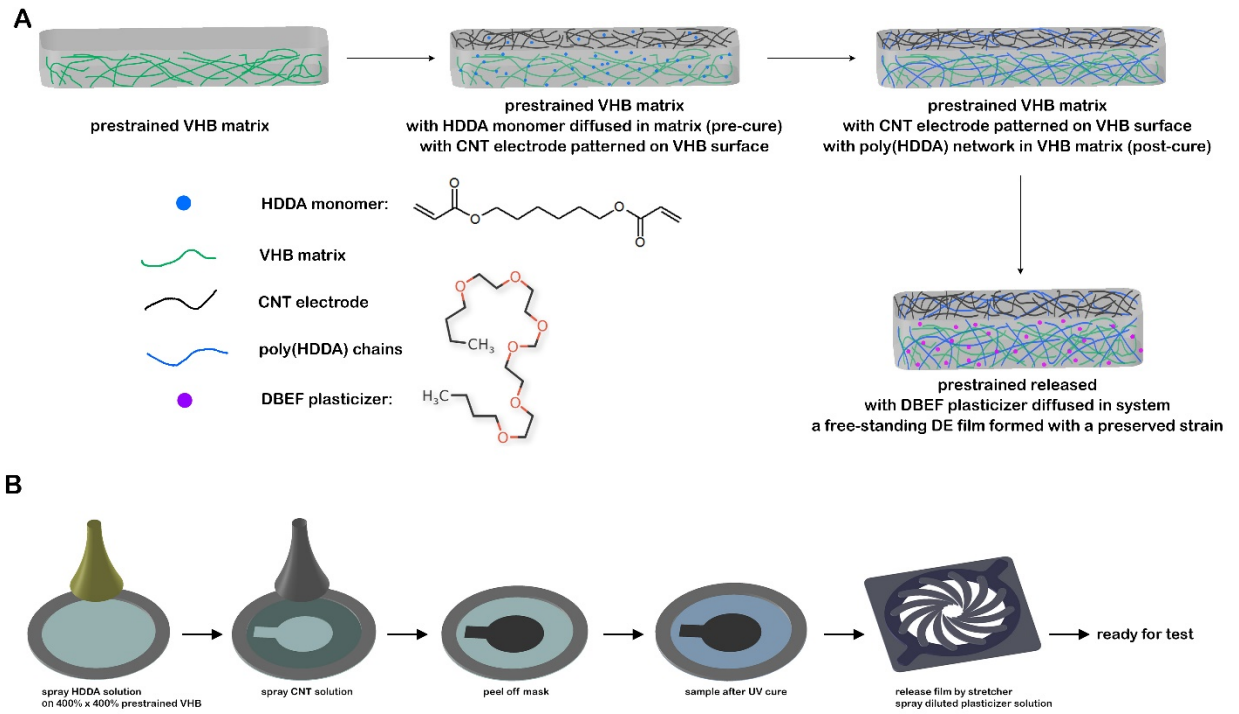

Figure 3-3 (A) Schematic illustration of synthesizing VHB-IPN-P, the original film was 400% x 400% biaxially prestretched. (B) Fabrication processes of VHB-IPN-P-based actuators.

Table 3-1 Experimental conditions and film thickness determinations.

Experimental conditions		IPN thickness after releasing (μm)	
Actual spraying HDDA amount (μl/cm^2)	Preserved prestrain (From 400% to % biaxially) [a]	Measured by digital micrometer	Estimated from preserved prestrain [b]
1.15	275 ± 3	82 ± 3	85
1.53	290 ± 10	80 ± 10	78.4
2.20	300 ± 10	76 ± 3	74.5

[a] Calculation approach: mark red dots (3 inch) onto the prestretched film, measure the distance after releasing and calculate the preserved prestrain.

[b] See below calculation details.

The estimated IPN film thickness was obtained by the following calculations.

$$t_{\text{VHB 400\% prestrain}} = t_{\text{VHB 4910}} \times \frac{1}{(1+400\%)^2} = 40\ \mu\text{m}$$

$$t_{\text{HDDA}} = \frac{A \times t_{\text{VHB 400\% prestrain}} \times \rho_{\text{VHB}} \times V_{\text{HDDA}}}{A \times \rho_{\text{HDDA}}} = t_{\text{VHB 400\% prestrain}} V_{\text{HDDA}} \frac{\rho_{\text{VHB}}}{\rho_{\text{HDDA}}}$$

A is the area of the DE film. Take HDDA amount of 1.15 µl/cm^2 as an example, $t_{\text{HDDA}} = 7.68\ \mu\text{m}$. Then, the estimated thickness can be calculated by below.

$$t_{\text{estimated}} = \left(t_{\text{VHB 400\% prestrain}} + t_{\text{HDDA}}\right) \times \frac{(1+400\%)^2}{(1+\text{preserved prestrain})^2}$$

Where preserved prestrain was determined by the above approach, which is 275%. Therefore, the estimated thickness was 85 µm by using given data.

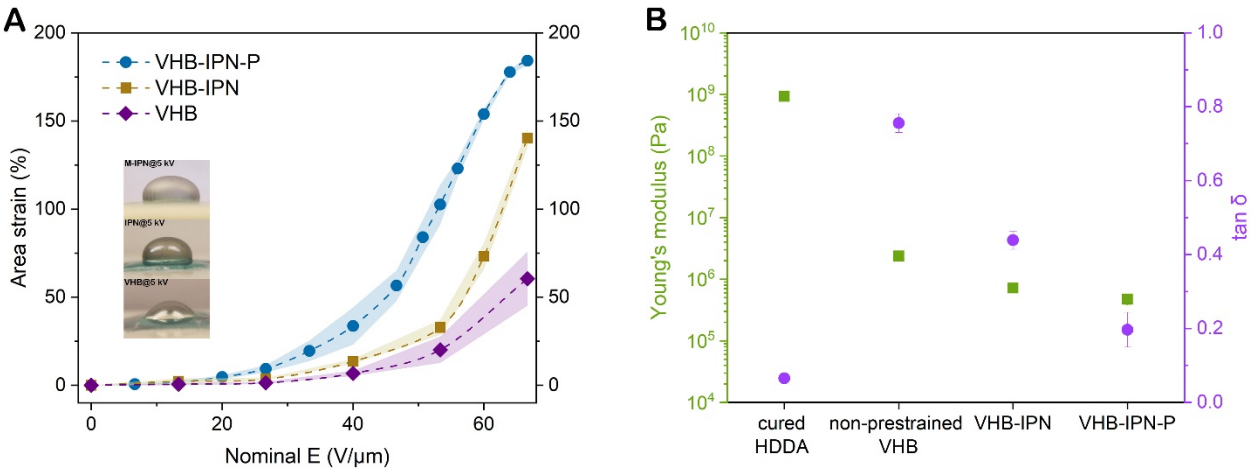

Figure 3-2 (A) Electrically induced actuation strains as a function of applied nominal electric fields on VHB, VHB-IPN, and VHB-IPN-P, with CNT as the electrodes. For each type, five samples were tested. Error-bar bands indicate the standard derivations. (B) Young's modulus and

tan δ for cured HDDA, non-prestrained VHB, VHB-IPN, and VHB-IPN-P at 1Hz under room temperature.

Figure 3-2A shows the actuation strains of VHB (250% biaxially prestretched)-based, VHB-IPN-based and VHB-IPN-P-based DEAs driven by ramping up nominal electric field. The actuators used the CNT as electrodes, and their sheet resistances were controlled to 62 ± 10 kΩ/□ after UV curing and became 78 ± 10 kΩ/□ under the persevered strain states. The measured thickness of VHB after 250% biaxial prestrain was ~82 μm and ~82 μm for both VHB-IPN and VHB-IPN-P. At a nominal electric field of ~66 V/μm, VHB samples reached an area strain of 60%, and VHB-IPN samples had a 140% area strain. Whereas VHB-IPN-P samples exhibited an actuation strain of 185% at the same nominal electric field. Besides, VHB-IPN-P samples reached a larger strain than the other samples when the same nominal electric field were applied. Starting from ~40 V/μm, the VHB-IPN-P samples exhibited at least 30% more strains than other samples at the similar nominal electric field. This is possiblely due to the plasticizer additive softening the polymer chains within the elastomers. From **Figure 3-2B and Figure 3-3**, VHB-IPN-P films have the lowest Young's modulus and highest dielectric constant among the candidates. Thus, they could deform more under similar electric fields based on the actuation mechanism. [1,3]

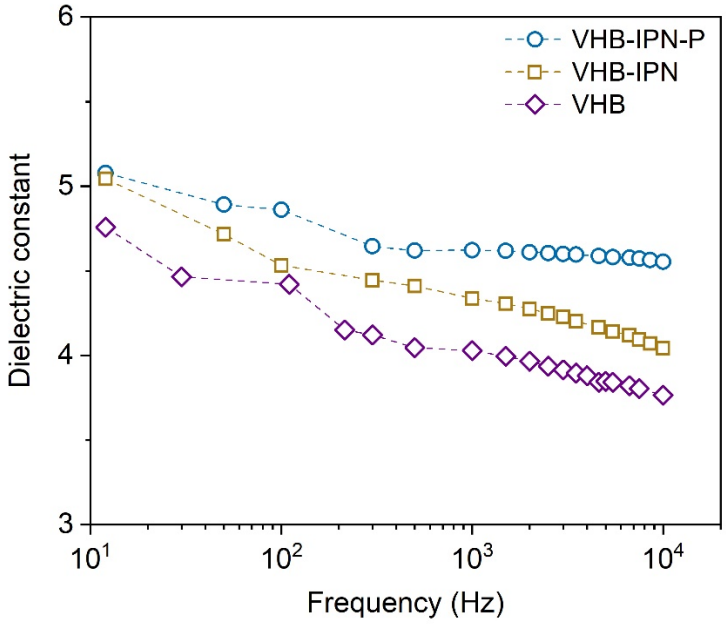

Figure 3-3 Dielectric constants of VHB-IPN-P, VHB-IPN and 250% biaxial prestrained VHB films at variable frequencies.

Viscoelasticity, characterized by the energy loss factor tan δ, is the key to the actuation response speed. A high viscoelastic loss causes great energy loss and low response speed. From **Figure 3-2B**, VHB elastomers have a tan δ of 0.76. VHB-IPN elastomers have a decreased tan δ of 0.44 due to that the added HDDA component typically has a low energy loss factor. [37] While both loss factors are much higher than VHB-IPN-Ps with 0.19. The tan δ difference helps us to visualize that the actuation response speed for VHB-IPN-Ps should be faster than the other two. To validate our assumption, we compared the actuation response speed between VHB, VHB-IPN, and VHB-IPN-P samples. In **Figures 3-4A, B and C,** the samples were driven by the square-wave voltage with increasing frequencies from 0.1 Hz to 2 Hz. All the samples showed a similar decreasing trend in strain. For the VHB-based actuator, the actuation expansion reduced from 67% at 0.1 Hz to 24% at 2 Hz under 5 kV square-wave voltage maintaining only 35% of the initial strain. VHB-

IPN-based actuator started with an area expansion of 139% at 0.1 Hz and underwent a steep strain decrease to 47% in area at 2 Hz under 4.8 kV square-wave voltage. While the decrease was much more moderate for VHB-IPN-P-based actuators, i.e., reduced from 182% at 0.1 Hz to 172% at 2 Hz under 4.5 kV square-wave voltage, maintaining 90% of the initial strain. The results are strong proof that adding a plasticizer can dramatically lower the viscoelasticity and increase the actuation response speed of the elastomers for reaching an efficient actuation performance.

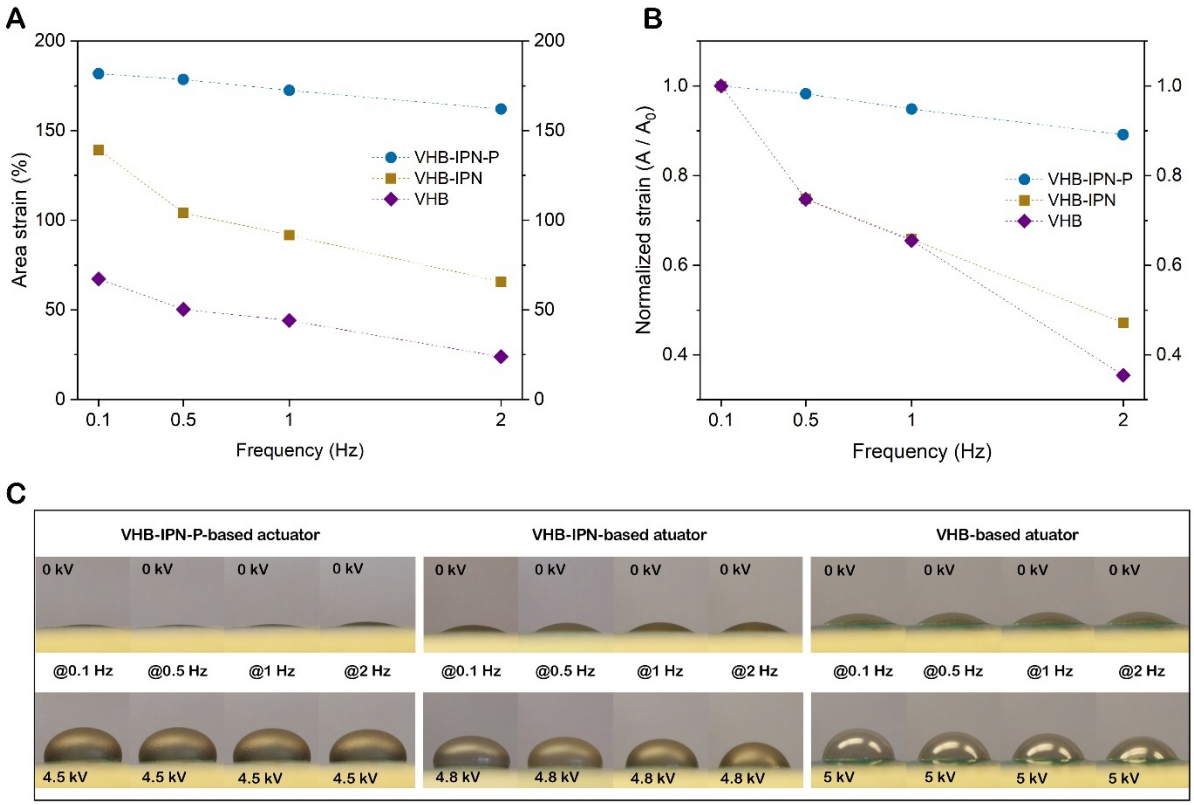

Figure 3-4 (A) Measured area strain and (B) the normalized strain (A/A_0) of VHB-IPN-P, VHB-IPN, and VHB under square-wave voltage (between 0 kV and 4.5 kV for VHB-IPN-P, between 0 kV and 4.8 kV for VHB-IPN, and between 0 kV and 5 kV for VHB) at 0.1 Hz, 0.5 Hz, 1 Hz and 2 Hz. The electrode are CNTs with 78 ± 10 kΩ/□. (C) Captured photos during the square-wave

volage actuation at 0 kV (upper) and specified high voltage (lower). Note that at high frequencies, the films may not recover their fully relaxed shape at 0 kV.

Actuation stability is crucial for practical applications. We adopted the method from our previous study by overcoating a thin polymer layer above the ultra-thin CNT electrode in order to suppress the corona discharge of CNTs' sharp tips under high electric fields,[35] therefore, achieving a stable and durable actuation. **Figure 3-5** compared the actuation stability of VHB-IPN-P-based actuators with a single-layer electrode, i.e., CNT electrode only, and with a bilayer electrode, i.e., CNT electrode overcoated by a thin polymer layer. An actuator fabricated with VHB-IPN-P/single-layer electrode was driven to an area strain of ~120% at 1 Hz. The strain decreased dramatically within 500 cycles to ~15%, an 87.5% strain drop from the initial point. Whereas for the VHB-IPN-P actuator with a bilayer electrode, the strain had only a ~10% drop at the 500th cycle, reduced moderately from ~120% area expansion to ~80% after 5,000 cycles, and was able to continue functionalizing. This improved actuation stability offered by the bilayer electrode matches our previous results. The thin polymer layer can isolate the CNT network from the air, thus preventing the corona discharge and exhibiting a stable actuation.

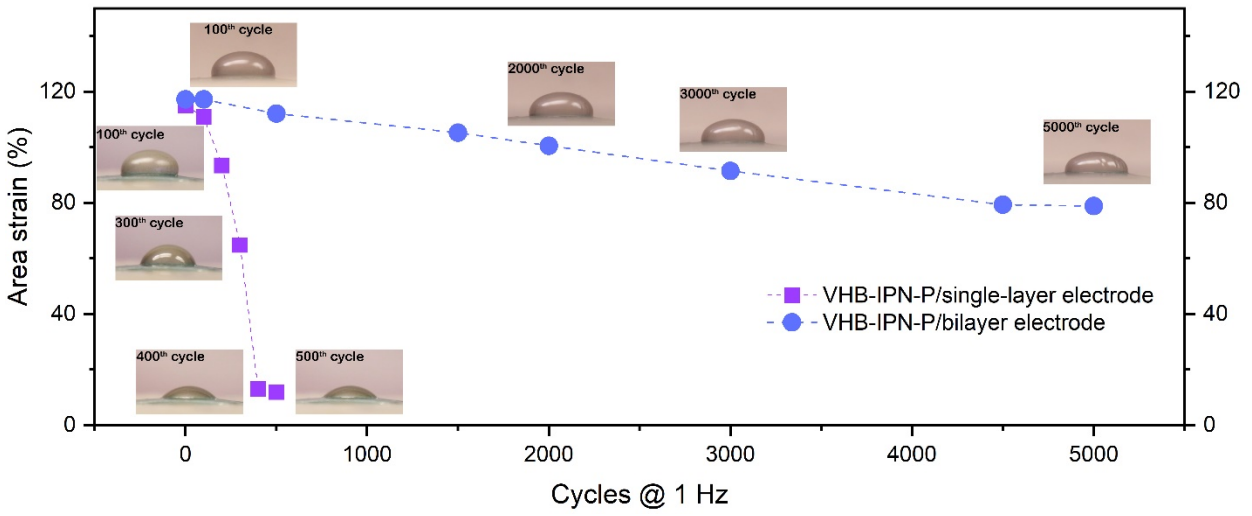

Figure 3-5 Actuation stability test under 4.2 kV square-wave voltage at 1 Hz for VHB-IPN-P-based actuators with the single-layer electrode, i.e., CNT, and the bilayer electrode, i.e., CNT and a thin polymer layer. This polymer precursor is the mixture of CN9021, BA, PNPDA, and photoinitiators.

With the advantages of large actuation strain, fast response speed, and stable actuation operation, we explored VHB-IPN-P in the ball-tossing application to visualize the power output and energy density. As shown in **Figure 3-6**, an aluminum ball was able to be tossed to a certain height when turning the voltage off from on. At the static actuation state under 4.5 kV, the areal actuation strain was ~150% after putting the aluminum ball on top of the actuator surface. The energy density of the actuator was then calculated to be 0.214 MJ/m^3. From our experiment, the 91 mg ball was tossed up to a height of 6.5 cm, reaching potential energy of 0.058 mJ according to the U = mgh, where U is the potential energy, m is the ball mass, g is the gravity acceleration, and h is the tossed height. The achieved energy conversion from the electromechanical energy to the potential energy was then calculated to be 6.5%.

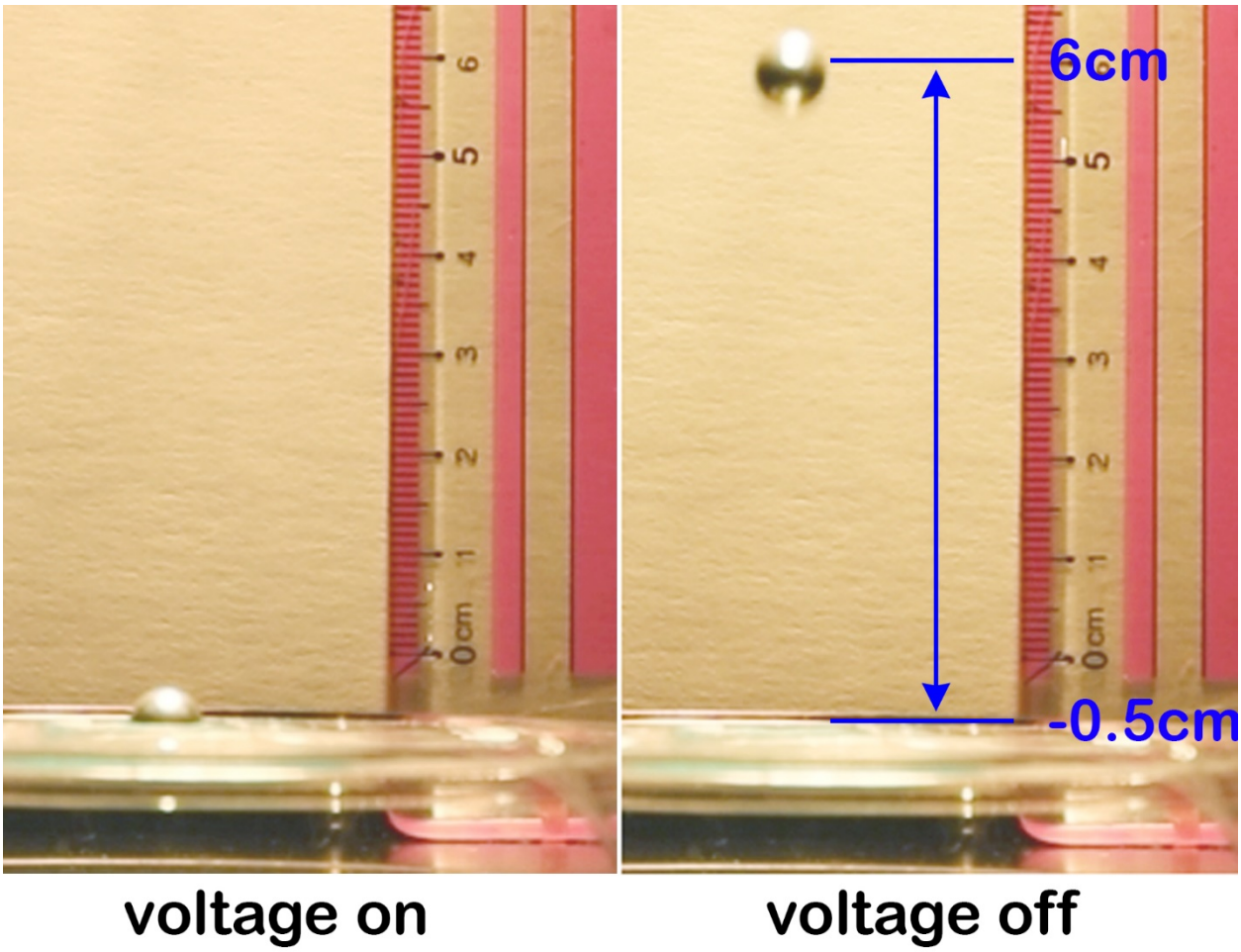

Figure 3-6 Captured photos during the ball-tossing experiment. The actuator was made by VHB-IPN-P and the bilayer electrode.

3.3.2 Multilayer actuator fabrication and actuation performance

We developed a novel stacking process for VHB-IPN-P films to scale up the energy output. This method is easy and convenient to stack multilayers and has a high yield, and it is not limited to VHB-IPN-P films but applicable for other DE films with prestraining. Here, we demonstrate the method by fabricating 2x2 actuators with VHB-IPN-P films. As illustrated in **Figure 3-7**, the overall steps consist of three major parts: film preparation, multilayer stacking, and stack releasing. The film preparation processes include the sample preparation from a single prestained VHB film

(sprayed HDDA solution already) to an electrode-patterned DE film, for stacking purposes. Firstly, we laser cut the Teflon sheet into the certain shape shown in the figure. The one wrapped with packaging tape was used as the supporting substrate and the one without packaging tape wrapping was used as the sacrificial substrate. Secondly, both supporting and sacrificial substrates were laminated onto prestrained VHB films (fixed by acrylic frames), respectively. Next, the mask was attached to the VHB on the sacrificial substrate for electrode depositing. The samples were then ready for multilayer stacking. The stacking processes started with laminating the 1-layer VHB (on supporting substrate), and 1-layer VHB patterned with CNT electrode (on sacrificial substrate) in a vacuum laminator. After the lamination process was done, gently peeled off the sacrificial substrate, then a 2-layer stack was left on the supporting substrate. Laminating another 1-layer VHB (patterned with CNT electrode, on sacrificial substrate) on the 2-layer stack in the vacuum laminator and peeling off the sacrificial substrate would give a 3-layer stacking actuator. Depending on the required layers, the processes can be repeated reliably to an n-layer stack. After the n-layer stack was completed, placed it under a UV light to fully cure the HDDA. Then transferred it onto a stretcher (same as the one used for making the VHB-IPN-P film), peeled off the supporting substrate, sprayed bilayer electrode on the top and bottom side of the n-layer stack, and started releasing until visible wrinkles appeared. Then, transferred the released stack to an acrylic frame, sprayed the diluted plasticizer solution, and left it overnight for complete diffusion. The 2x2 multilayer stack can then be cut into four actuators and ready for testing **(Figure 3-9A)**.

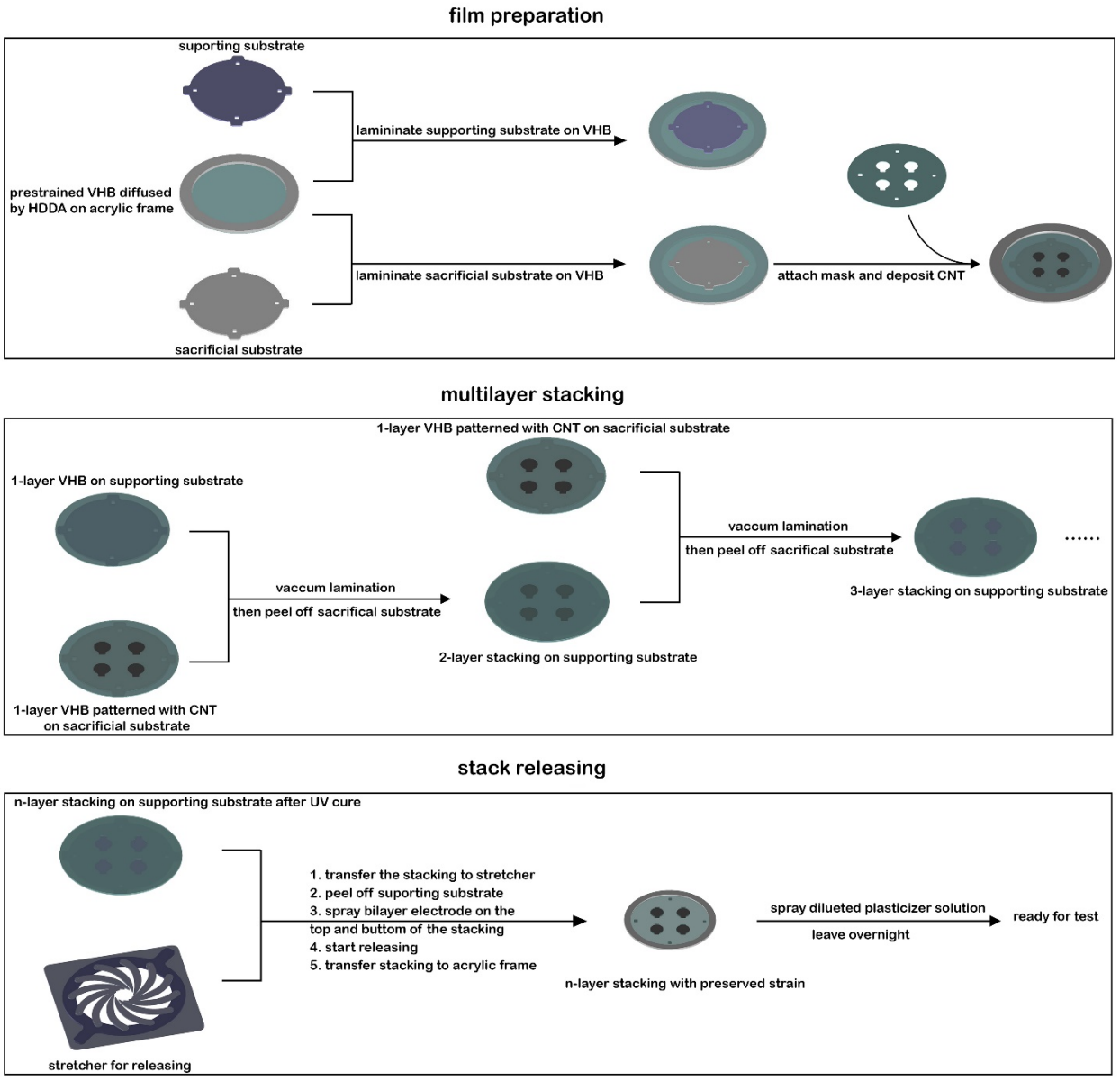

Figure 3-7 Hybrid stacking processes for multilayer stacking DEAs. The fabrication consists of three parts: film preparation, multilayer stacking and stack releasing.

In order to investigate the bonding strength between layers, we soaked a 2-layer VHB-IPN-P stack into a polar solvent, THF. Meanwhile, we prepared two sets of samples as references. One was a 2-layer stack of 250% biaxially prestrained VHB by laminating two VHB films in the laminator with the same laminating condition used for our VHB-IPN-P samples. Another one was made by

laminating two single VHB-IPN films (both were fully cured before laminating) with the same laminating parameters. Three sets of stacks were soaked in THF. In **Figure 3-8A**, after 30-minutes of soaking, the 2-layer VHB stack broke into several pieces, this is probably due to a high ratio of swollen breaking the VHB matrix. The 2-layer VHB-IPN stack didn't break into pieces but the two layers of VHB-IPN films delaminated automatically after 30 minutes. While the 2-layer stack prepared by our hybrid process didn't show delamination and cannot be peeled off from each other after 24-hours of soaking. The soaking results proved that the VHB-IPN-P stack had strong inter-layer bonding. For either the VHB stack or VHB-IPN stack, there should only exist physical bonding between interlayers according to the preparation processes, therefore, the polar solvent could easily destroy the stacking structures. But for the VHB-IPN-P stack, there could be the chemical bonding between interlayers, which helped the stacking structure to survive in the polar solvent. Looking into the sample preparation processes, HDDA monomers were diffused within in prestrained VHB matrix, the DE films were then placed into the laminator. The laminating pressure squeezed the matrix and could dislocate some HDDA monomers accordingly to interlayers. Therefore, under UV curing, partial HDDA polymerization reactions could occur between interlayers, forming the interlayer bonding chemically, resulting in structural integrity, as seen in **Figure 3-8B** of the cross-sectional SEM image.

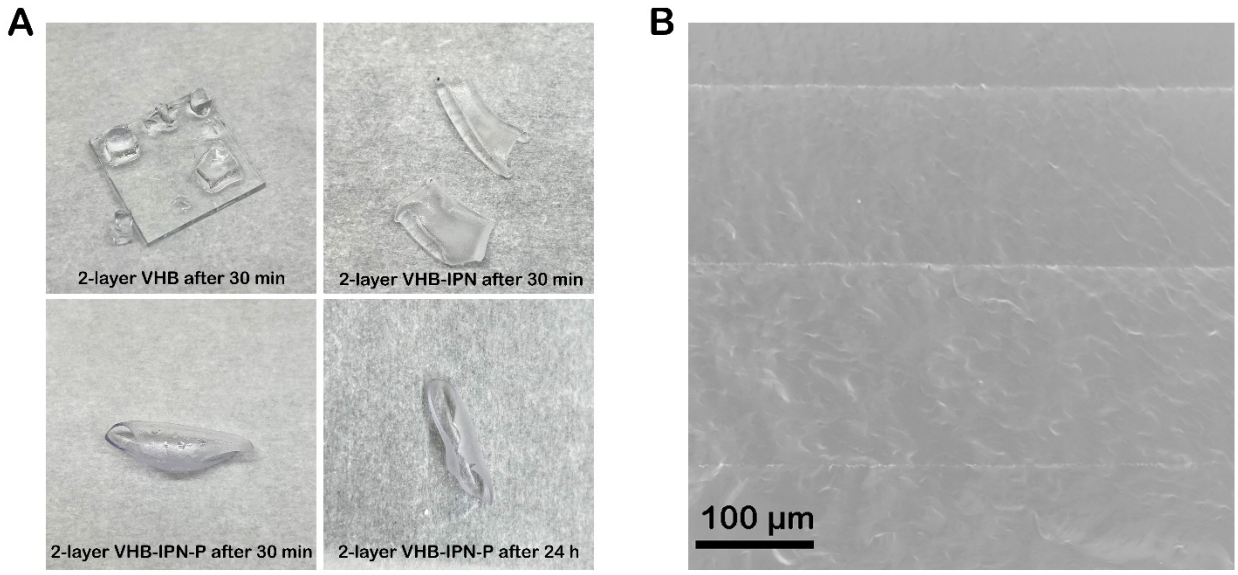

Figure 3-8 (A) Photos of 2-layer stacks (2-layer VHB stack, 2-layer VHB-IPN stack, and 2-layer VHB-IPN-P stack) after soaking in tetrahydrofuran (THF). (B) SEM image of the cross-sectional view of a 7-layer stack based on VHB-IPN-P, with CNT as the interlayer electrode.

We compared the electrically induced actuation strains between actuator based on VHB-IPN-P (1-layer) and its 4-layer stack (**Figure 3-9B**). At low nominal fields, the 4-layer stack shows a similar trend as the VHB-IPN-P single film under, both exhibited small strains, and the actuation strains increased with increasing nominal fields. When they were driven under high nominal electrical fields, the 4-layer stack reached slightly smaller strains than VHB-IPN-P. This is possibly due to the slight misalignment during stacking, causing the reduced overlapping area of electrode, therefore, the actual active area of the stack could be smaller than that of a single DE film, leading to a lower strain.

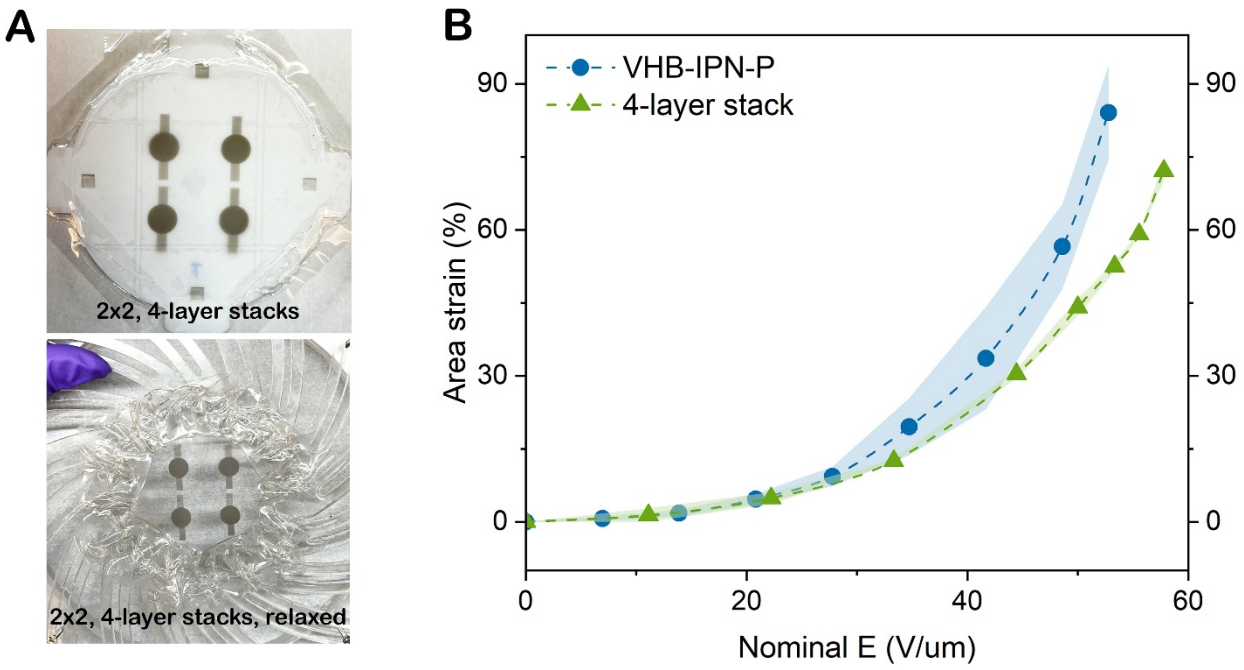

Figure 3-9 (A) Photos of the 4-layer stack with 2x2 actuators. (B) Electrically induced actuation strains as a function of applied nominal electric fields on a single-layer VHB-IPN-P and its 4-layer stack. For each type, five samples were tested. Error-bar bands indicate the standard derivations. Actuators used CNT as the interlayer electrode and CNT/polymer as the outer electrode.

Furthermore, in **Figure 3-10**, the 4-layer stack was able to show a comparable response speed as the VHB-IPN-P single film. Their strain drop ratios from 0.1 Hz to 2 Hz were ~15%. Both the VHB-IPN-P and its 4-layer stack can maintain 40% of the initial strains at 10 Hz, which is far better than other reported acrylate-based DEAs.

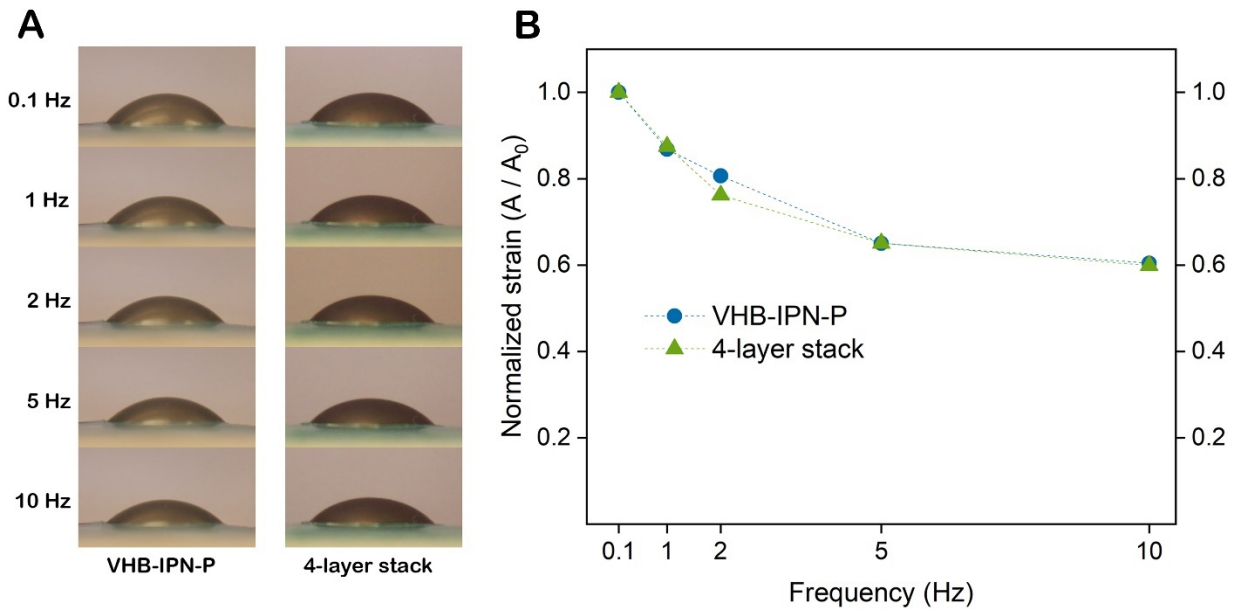

Figure 3-10 (A) Captured photos and (B) normalized strain under variable actuation frequencies for actuators made by single-layer VHB-IPN-P and its 4-layer stack under 3.8 kV square-wave voltage at 0.1 Hz, 1 Hz, 2 Hz, 5 Hz and 10 Hz. (C) Captured photos during the square-wave volage actuation at 3.8 kV. With CNT as the interlayer electrode and bilayer as the outer electrode.

3.4 Conclusions

A prestrain-locked high-performance arylate thin DE film has been developed. The prestrain-locked DEs (VHB-IPN-Ps) have small viscoelasticity with a tan δ of 0.19 and low Young's modulus of 0.4 MPa, therefore respond to electric fields fast: maintaining 90% of the initial strain when frequency increased from 0.1 Hz to 2 Hz. Under ramping-up nominal electric fields, starting from ~40 V/μm, VHB-IPN-P reached over 30% more strain than VHB-IPNs and VHBs. Besides, the actuator made by the VHB-IPN-P and bilayer electrode was demonstrated to be operated stably and reliably under a decent strain. The 4-layer stack by the hybrid stacking processes exhibited comparable actuation performance and response speed as single-layer VHB-IPN-P actuator. Multilayer stacking processes were explored successfully with high repeatability, processing

quality, and yield. This hybrid stacking approach show potential for scalable manufacturing of multilayer DEAs.

3.5 References

[1] P. Brochu, Q. Pei, Dielectric elastomers for actuators and artificial muscles. In Electroactivity in polymeric materials, *Springer* **2012**,1.

[2] M. Duduta, E. Hajiesmaili, H. Zhao, R. Wood, D. Clarke, Realizing the potential of dielectric elastomer artificial muscles. *Proc. Natl. Acad. Sci.* **2019**, 116(7), 2476.

[3] R. Pelrine, R. Kornbluh, Q. Pei, J. Joseph, High-speed electrically actuated elastomers with strain greater than 100%. *Science* **2000**, 287(5454), 836.

[4] R. Pelrine, R. Kornbluh, G. Kofod, High-strain actuator materials based on dielectric elastomers. *Adv. Mater.* **2000**, 12(16), 1223.

[5] F. Madsen, A. Daugaard, S. Hvilsted, A. Skov, The current state of silicone-based dielectric elastomer transducers. *Macromol. Rapid Commun.* **2016**, 37(5), 378.

[6] F. Carpi, I. Anderson, S. Bauer, G. Frediani, G. Gallone, M. Gei, C. Graaf, C. Jean-Mistral, W. Kaal, G. Kofod, M. Kollosche, R. Kornbluh, B. Lassen, M. Matysek, S. Michel, S. Nowak, B. O'Brien, Q. Pei, R. Pelrine, B. Rechenbach, S. Rosset, H. Shea, Standards for dielectric elastomer transducers. *Smart Mater. Struct.* **2015**, 24(10), 105025.

[7] B. Chen, J. Lu, C. Yang, J. Yang, J. Zhou, Y. Chen, Z. Suo, Highly stretchable and transparent ionogels as nonvolatile conductors for dielectric elastomer transducers. *ACS Appl. Mater. Interfaces* **2014**, 6(10), 7840.

[8] H. Boys, G. Frediani, S. Poslad, J. Busfield, F. Carpi, In A dielectric elastomer actuator-based tactile display for multiple fingertip interaction with virtual soft bodies, *SPIE* **2017**, 451.

[9] A. Marette, A. Poulin, N. Besse, S. Rosset, D. Briand, H. Shea, Flexible zinc–tin oxide thin film transistors operating at 1 kV for integrated switching of dielectric elastomer actuators arrays. *Adv. Mater.* **2017**, 29(30), 1700880.

[10] J. Li, Y. Wang, L. Liu, S. Xu, Y. Liu, J. Leng, S. Cai, A biomimetic soft lens controlled by electrooculographic signal. *Adv. Funct. Mater.* **2019**, 29(36), 1903762.

[11] S. Shian, R. Diebold, D. Clarke, Tunable lenses using transparent dielectric elastomer actuators. *Opt. Express* **2013**, 21(7), 8669.

[12] Y. Chen, H. Zhao, J. Mao, P. Chirarattananon, E. Helbling, N. Hyun, D. Clarke, R. Wood, Controlled flight of a microrobot powered by soft artificial muscles. *Nature* **2019**, 575 (7782), 324.

[13] S. Mitchell, X. Wang, E. Acome, T. Martin, K. Ly, N. Kellaris, V. Venkata, C. Keplinger, An easy-to-implement toolkit to create versatile and high-performance HASEL actuators for untethered soft robots. *Adv. Sci*. **2019**, 6(14), 1900178.

[14] I. Anderson, T. Gisby, T. McKay, B. O'Brien, E. Calius, Multi-functional dielectric elastomer artificial muscles for soft and smart machines. *J. Appl. Phys.* **2012**, 112(4), 041101.

[15] J. Eckerle, S. Stanford, J. Marlow, R. Schmidt, S. Oh, T. Low, S. Shastri, Biologically inspired hexapedal robot using field-effect electroactive elastomer artificial muscles, Smart structures and materials 2001: Industrial and commercial applications of smart structures technologies, *SPIE* **2001**, 269.

[16] R. Kornbluh, R. Pelrine, Q. Pei, R. Heydt, S. Stanford, S. Oh, J. Eckerle, In Electroelastomers: applications of dielectric elastomer transducers for actuation, generation, and smart structures, Smart Structures and Materials 2002: Industrial and Commercial Applications of Smart Structures Technologies, *SPIE* **2002**, 254.

[17] R. Kornbluh, R. Pelrine, Q. Pei, Dielectric elastomer produces strain of 380%. *EAP Newsletter* **2002**, 2(2), 10.

[18] Y. Qiu, E. Zhang, P. Plamthottam, Q. Pei, Dielectric elastomer artificial muscle: materials innovations and device explorations. *Acc. Chem. Res.* **2019**, 52(2), 316.

[19] G. Kofod, R. Kornbluh, R. Pelrine, P. Sommer-Larsen, In Actuation response of polyacrylate dielectric elastomers, Smart Structures and Materials 2001: Electroactive Polymer Actuators and Devices, *SPIE* **2001**, 141.

[20] J. Biggs, K. Danielmeier, J. Hitzbleck, J. Krause, T. Kridl, S. Nowak, E. Orselli, X. Quan, D. Schapeler, W. Sutherland, Electroactive polymers: developments of and perspectives for dielectric elastomers. *Angew. Chem. Int. Ed.* **2013**, 52(36), 9409.

[21] S. Ha, W. Yuan, Q. Pei, R. Pelrine, S. Stanford, Interpenetrating polymer networks for high-performance electroelastomer artificial muscles. *Adv. Mater.* **2006**, 18(7), 887.

[22] S. Ha, W. Yuan, Q. Pei, R. Pelrine, S. Stanford, Interpenetrating networks of elastomers exhibiting 300% electrically-induced area strain. *Smart Mater. Struct.* **2007**, 16(2), S280.

[23] P. Brochu, X. Niu, Q. Pei, In Acrylic interpenetrating polymer network dielectric elastomers for energy harvesting, *SPIE* **2011**, 67.

[24] P. Brochu, H. Stoyanov, X. Niu, Q. Pei, All-silicone prestrain-locked interpenetrating polymer network elastomers: free-standing silicone artificial muscles with improved performance and robustness. *Smart Mater. Struct.* **2013**, 22(5), 055022.

[25] Q. Pei, R. Pelrine, M. Rosenthal, S. Stanford, H. Prahlad, R. Kornbluh, In recent progress on electroelastomer artificial muscles and their application for biomimetic robots, Smart Structures and Materials 2004: Electroactive Polymer Actuators and Devices (EAPAD), *International Society for Optics and Photonics* **2004**, 41.

[26] H. Zhang, L. Düring, G. Kovacs, W. Yuan, X. Niu, Q. Pei, Interpenetrating polymer networks based on acrylic elastomers and plasticizers with improved actuation temperature range. *Polym. Int.* **2010**, 59(3), 384.

[27] S. Rosset, H. Shea, Small, fast, and tough: shrinking down integrated elastomer transducers. *Appl. Phys. Rev.* **2016**, 3(3), 031105.

[28] T. McKay, S. Rosset, I. Anderson, H. Shea, Dielectric elastomer generators that stack up. *Smart Mater. Struct.* **2013**, 24(1), 015014.

[29] M. Duduta, R. Wood, D. Clarke, Multilayer dielectric elastomers for fast, programmable actuation without prestretch. *Adv. Mater.* **2016**, 28(36), 8058.

[30] H. Schlaak, M. Jungmann, M. Matysek, P. Lotz, In novel multilayer electrostatic solid state actuators with elastic dielectric, Smart Structures and Materials 2005: Electroactive Polymer Actuators and Devices (EAPAD), *SPIE* **2005**,121.

[31] Z. Li, P. Dong, T. Shi, C. Tang, C. Bian, H. Chen, In elastomeric electrode and casting process for manufacturing multilayer dielectric elastomer actuators, Electroactive Polymer Actuators and Devices (EAPAD), *International Society for Optics and Photonics* **2018**, 1059414.

[32] F. Carpi, C. Salaris, D. De Rossi, Folded dielectric elastomer actuators. *Smart Mater. Struct.* **2007**, 16(2), S300.

[33] J. Maas, D. Tepel, T. Hoffstadt, Actuator design and automated manufacturing process for DEAP-based multilayer stack-actuators. *Meccanica* **2015**, 50(11), 2839.

[34] G. Kovacs, L. Düring, S. Michel, G. Terrasi, Stacked dielectric elastomer actuator for tensile force transmission. *Sens. Actuators, A* **2009**, 155(2), 299.

[35] Z. Peng, Y. Shi, N. Chen, Y. Li, Q. Pei, Stable and high-strain dielectric elastomer actuators based on a carbon nanotube-polymer bilayer electrode. *Adv. Funct. Mater.* **2021**, 31(9), 2008321.

[36] E. Manias, J. Chen, N. Fang, X. Zhang, Polymeric micromechanical components with tunable stiffness. *Appl. Phys. Lett.* **2001**, 79(11), 1700.

[37] H. Kilambi, S. Reddy, L. Schneidewind, T. Lee, J. Stansbury, C. Bowman, Design, development, and evaluation of monovinyl acrylates characterized by secondary functionalities as reactive diluents to diacrylates. *Macromolecules* **2007**, 40(17), 6112.

Chapter 4 A BISTABLE ELECTROACTIVE POLYMER FOR REFRESHABLE TACTILE DISPLAYS

4.1 Background of this study

4.1.1 Electroactive polymers (EAPs)

Among all the electroactive polymers (EAPs) investigated, dielectric elastomers (DEs) stand out by exhibiting a unique combination of properties, including large strains, fast response, high energy densities, mechanical compliancy, and low cost. [1-4] For example, when sandwiched with compliant electrodes, the acrylic elastomer, 3M VHB 4910, can reach 100% or greater area expansion with a maximum elastic energy density of 3.4 J/g under high driving voltages. However, the extraordinarily large actuation strain is obtained at the sacrifice of materials' mechanical stiffness which in turn hinders the applications of the DE actuators in adaptive structures. In addition, high voltages are required to maintain the large deformation, leading to significant energy consumption, material fatigue, and a reduced lifetime.

4.1.2 Bistable electroactive polymers (BSEPs)

Bistable electroactive polymers (BSEPs) can amalgamate the shape memory property with dielectric elastomers to obtain rigid-to-rigid actuation [5-6] owing to their temperature dependent stiffness. The mechanical properties can dramatically change along with varied temperature. [5,7] The BSEP is rigid below its transition temperature, while above this temperature, it behaves like a dielectric elastomer and exhibits large electrically induced actuation strain and high dielectric field strength. The deformation can be locked by cooling the BSEP below its transition temperature during which the polymer turns stiff again. The transition temperature of BSEP is also tunable.

Fast response and low energy consumption can be achieved with narrowed transition temperature range. These features render the BSEP a promising smart material candidate for the fabrication of Braille electronic readers.

4.1.3 Braille devices

Braille has been the media to educate blind children literacy. There are 1.3 million legally blind individuals in the Unites States and among them 55,000 are children. [8,9] Despite the advancements in smartphones and tablets, a tactile version with comparable compactness and low cost serving the vision impaired population is not available on the market. The technical challenge has been the creation of a suitable actuation mechanism that produces larger deformation with a sufficiently high blocking force. [10]

4.1.4 BSEPs for Braille application

Here, we report a refreshable tactile display with Braille standard resolution that combines the specific actuation feature of BSEP with the Joule heating of a serpentine-patterned carbon nanotube (CNT) electrode. [10] The system can be heated up to 70 °C under 30 V voltage in less than 1 s. The blocking force is 51 grams after the BSEP film is cooled down. The out-of-plane displacement induced by pneumatic pump is 0.5 mm. The demonstrated 3 x 2 pneumatic tactile device can be operated for over 100,000 cycles.

4.2 Experimental design

4.2.1 Raw materials

Urethane diacrylate (UDA, catalog name: CN9021) was obtained from SARTOMER and used as received. Stearyl acrylate (SA), acrylic acid (AA), 2,2-Dimethoxy-2-phenylacetophenone

(DMPA), benzophenone (BP), and isopropyl alcohol (IPA) were purchased from Sigma-Aldrich and used as received. Single-walled carbon nanotubes (catalog name: P3-SWNT) were purchased from Carbon Solutions, Inc.

4.2.2 Joule heating serpentine CNT (S-CNT) fabrication

The carbon nanotube (CNT) dispersion solution was made by mixing 7 mg of P3-SWNT powder, 1 ml water, and 20 ml IPA. The mixture was bath sonicated for 90 min to get a stable dispersion. Aggregates were disposed using centrifuge at 8000 rpm for 15 min. The resulting supernatant is then ready for spray coating. The stretchable S-CNT was fabricated by spray coating carbon nanotube solution on glass substrate followed by laser engraving process.

4.2.3 S-CNT patterned BSEP thin film preparation

BS80 prepolymer solution was made by mixing 80 parts (by weight) of SA, 20 pats of UDA, 10 parts of AA, 1 part of DMPA, and 0.5 part of BP at 60 °C. BS70 prepolymer solution was made by mixing 70 parts (by weight) of SA, 30 pats of UDA, 10 parts of AA, 1 part of DMPA, and 0.5 part of BP at 60 °C. BS60 prepolymer solution was made by mixing 60 parts (by weight) of SA, 40 pats of UDA, 10 parts of AA, 1 part of DMPA, and 0.5 part of BP at 60 °C. BS50 prepolymer solution was made by mixing 50 parts (by weight) of SA, 50 pats of UDA, 10 parts of AA, 1 part of DMPA, and 0.5 part of BP at 60 °C.

The prepolymer solution was then injected between a pair of glass slides on a hot plate with two strips of tape as spacers. One piece of glass substrates was with S-CNT pattern. In the device assembling, 40, 90 and 170 μm thick spacers were used to prepare the BSEP film. The prepolymer was then cured through a UV curing conveyor equipped with a Fusion 300S type “H” UV curing

bulb for about 3min. Then the film with S-CNT pattern can be gently peeled off the glass slide after it cooled down to room temperature.

4.3 Results and discussions

4.3.1 Mechanical properties of the BSEP Polymer

Utilizing techniques derived in our previous research, modified BSEP films comprising stearyl acrylate (SA) and a urethane diacrylate oligomer (UDA) were synthesized. The resulting SA-UDA copolymers were characterized using a dynamic mechanical analyzer (DMA) at a temperature ramping rate of 2 °C/min from 25 to 55 °C at the mechanical loading frequency of 1 Hz. **Figure 4-1A** shows that below the transition temperature, the BSEP films exhibits storage modulus on the order of 70-200 MPa which is caused by the crystalline aggregates of hard stearyl acrylate (SA) segments. When they are heated above the transition temperature, BSEP films show a dramatic decline in storage modulus due to melted crystalline aggregates. This rigid-to-rubbery transition can be completed within 3 °C and the storage modulus maintains stable at even higher temperatures, which is beneficial for stable electrical or pneumatic actuation with large deformation. The transition temperature of the BSEP could be tuned by varying the ratios of SA: UDA; higher SA: UDA ratios resulted in larger storage moduli in the rigid state as the percent of crystallinity increased. A modulus change of more than 1000 folds can be achieved within 3 ˚C. The stress-strain curves of the BSEPs were obtained at 60 °C to maintain their rubbery states. Samples with dimensions of 3 mm width, 6 mm length and 170 μm thickness were tested at a stretch rate of 3.33 mm/s. The tensile strengths are 0.26 MPa and 1.87 MPa for BS80 and BS60 along with increasing tear strain from 191% to 233%, respectively. Results in **Figure 4-1B** and **Table 4-1** show that a

larger amount of UDA contributes to higher toughness, however, diminishes the modulus at the rigid state. Further, the copolymers soften at lower temperature as the UDA content is increased.

Table 4-1 Mechanical properties of SA-UDA Copolymers at 60 °C.

Sample	Elongation at break (%)	Tensile strength (MPa)
BS50	235	2.64
BS60	233	1.87
BS70	227	1.01
BS80	191	0.26

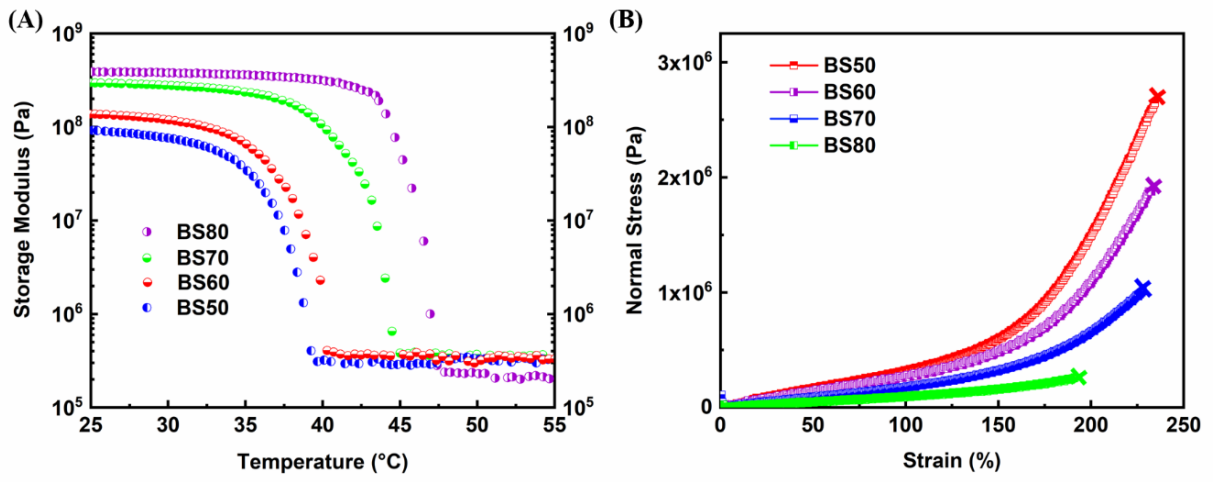

Figure 4-1 Mechanical properties of SA-UDA copolymers. (A) Evolution of storage modulus measured by DMA with temperature ramping from 25 °C to 55 °C at 2 °C/min. (B) Stress-strain curves at 60 °C.

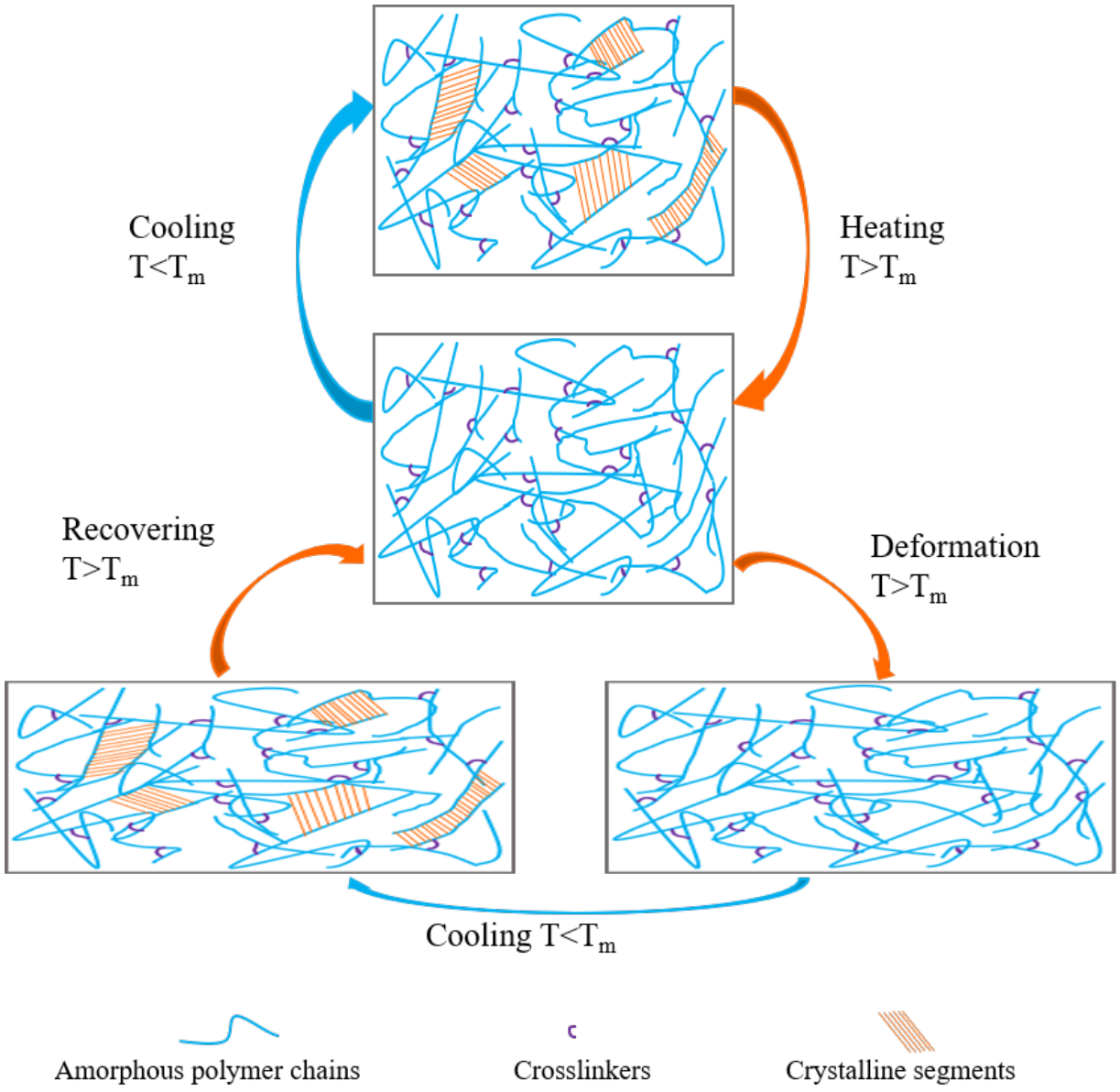

Figure 4-2 Schematic illustration of rigid-to-rigid actuation mechanism of BSEP.

4.3.2 Shape memory property

The variable stiffness and actuation of BSEP are illustrated in **Figure 4-2**. The BSEP comprises crystalline aggregates of the long alkyl side chains in a crosslinked polymer matrix, which makes the polymer film translucent. [12-14] The BSEP turns clears and rubbery after the crystalline aggregates are melted. This deformation can be preserved by cooling down the material due to re-

crystallization of the long alkyl chains. Reheating the polymer above T_m recovers its original shape. **Figure 4-3** shows the shape memory property of BS60. Two BS60 strips of 1 cm width were marked with two parallel blue tapes gapping 2 cm (**Figure 4-3A**). The left strip served as reference, while the right one was heated to 70 °C during which it turned from translucent to transparent (**Figure 4-3B**). The heated strip was stretched to a 100% strain, and then cooled down to ambient temperature. The deformation was locked. The strain fixity rate was close to 100% after removing the load (**Figure 4-3C**). Full recovery of the original shape and translucency was obtained by a reheating-cooling cycle.

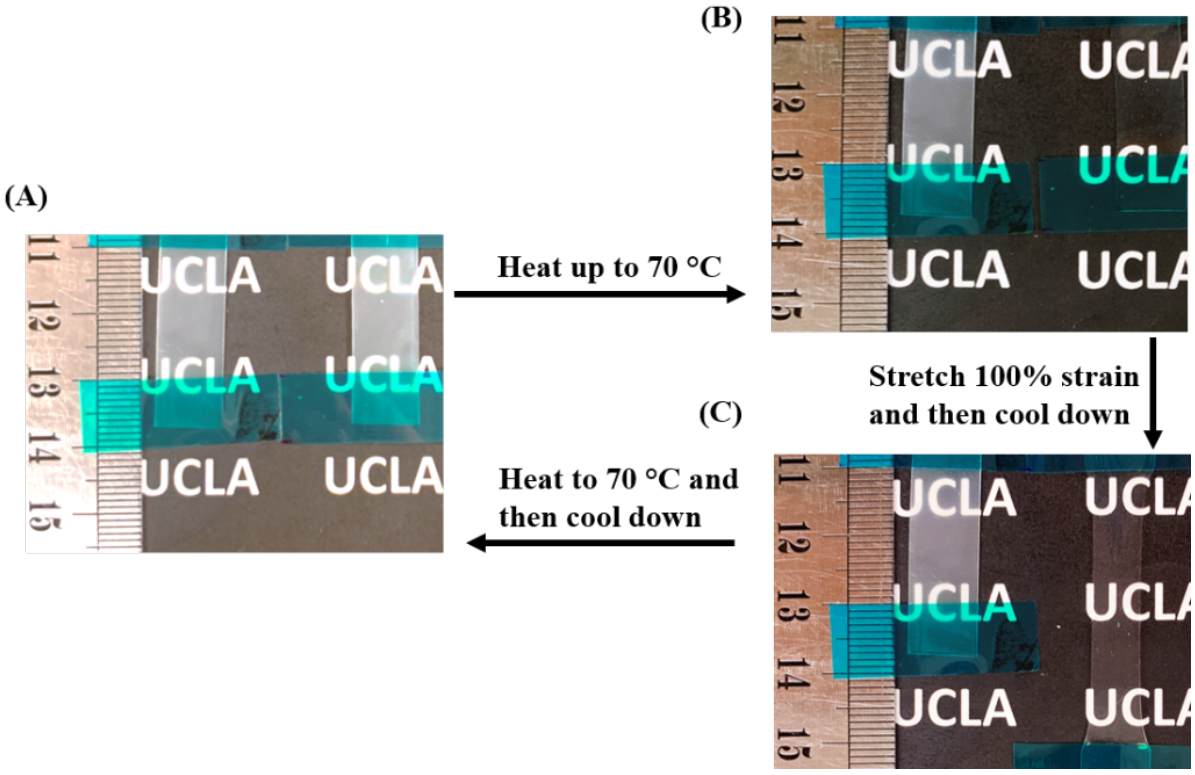

Figure 4-3 Demonstration of shape memory effect of BSEP. (*left*: reference sample without any treatment; *right*: testing sample going through heating-stretching-cooling cycle)

4.3.3 Device fabrication and actuation performance

The one-cell tactile display contains two major parts: BSEP active film and pneumatic system. BSEP active film was made by BSEP film and carbon nanotube electrode. The functional BSEP film was sandwiched by two double-sided Kapton^{TM} tape and the Joule heating serpentine CNT (S-CNT) electrode was fabricated by spray coating carbon nanotube solution reported in our previous research [10, 15-16] on glass substrate followed by laser engraving. The pneumatic system consists of a pneumatic chamber and a miniature pump. The pneumatic chamber with size of 40 mm x 40 mm x 10 mm and chamber cover were built by 3D printing and were sealed to ensure an airtight environment as shown in **Figure 4-4B**.

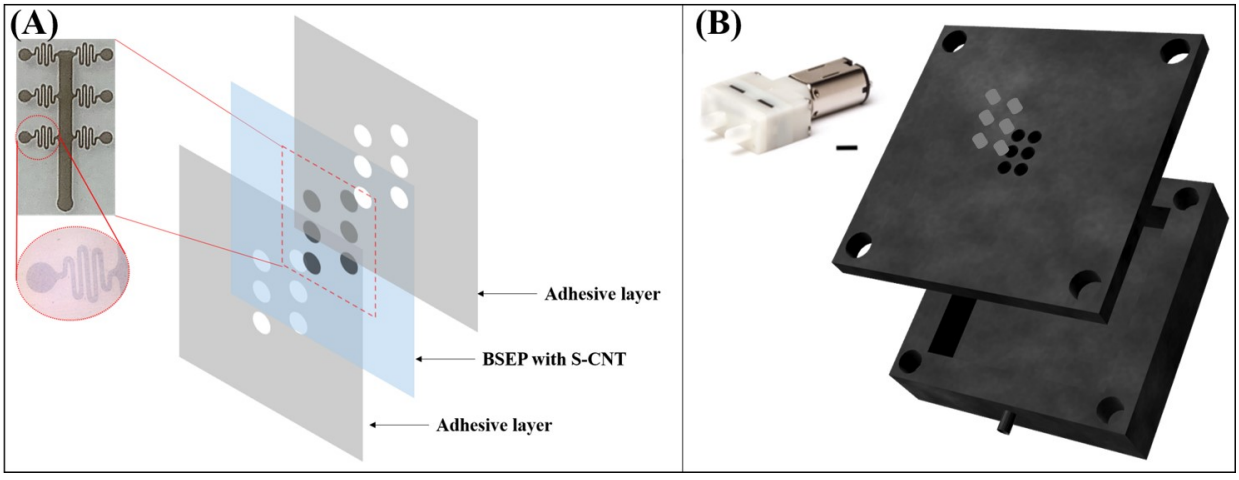

Figure 4-4 Details of a Braille cell architecture. (A) BSEP active film sandwiched with two adhesive layers. (B) Compact tactile display with 3 X 2 pixels array in the pneumatic system.

The tactile cell contains 6 tactile pixels (taxels) with 1.5 mm diameter and 2.5 mm center-to-center distance between adjacent taxels, which meets the Braille standard. The BSEP film can be locally heated within 1 second to 70°C by the serpentine-shaped CNT electrode heater with a 30V voltage supply as shown in **Figure 4-5A**. Infrared images of the S-CNT Joule heating electrodes in **Figure 4-5B** showed "U" "C" "L" "A" in Braille characters. The film showed uniform heat across the surface without cross talk among dots under Joule heating. After the BSEP film was softened, a low pneumatic pressure of 160 mmHg was applied which induce a large out of plane deformation of the BSEP film. The height of the diaphragm dot was raised by 0.7 mm. The BSEP film became rigid, and the out-of-plane displacement was preserved after the thermal stimuli was removed. The raised height matches the required displacement for Braille displays. [11]

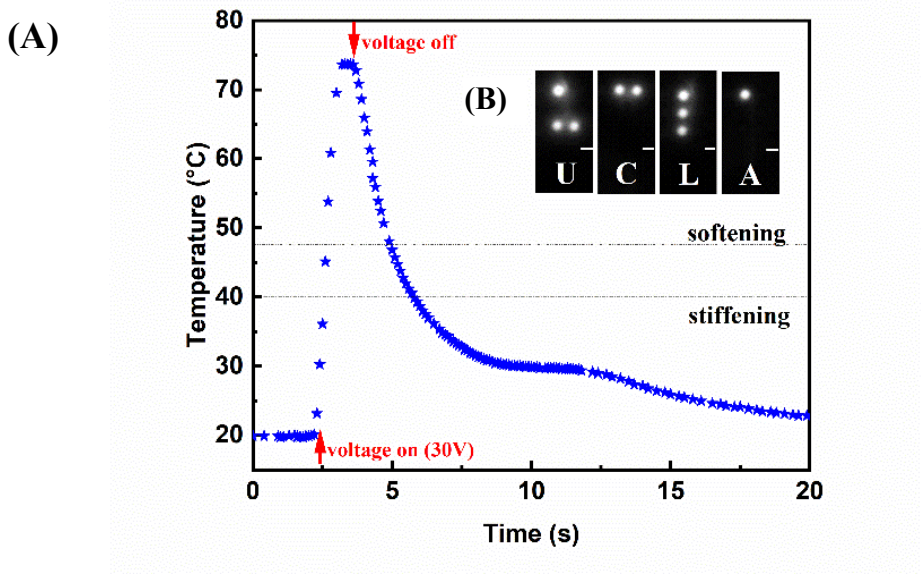

Figure 4-5 (A) Temperature profiles of S-CNT electrode under 30V. The "Softening" line indicates the temperature above which the polymer is soft, and the "Stiffening" line the temperature below which the polymer is stiff. (B) Demonstration by infrared images of the

corresponding S-CNT Joule heating electrode shows “U” “C” “L” “A” in Braille characters. The scale bars are 2 mm.

To examine the electrical continuity of the S-CNT electrode, the resistance of the electrode was measured as a function of biaxial deformation. **Figure 4-6A** shows that the resistance increases by 19% when the area expansion reaches 200%. Thus, the electrode can effectively heat the BSEP film at its maximum deformation. The resistance and Joule heating characteristics remained stable for over 100,000 cycles at a frequency of 0.8 Hz as shown in **Figure 4-6B**.

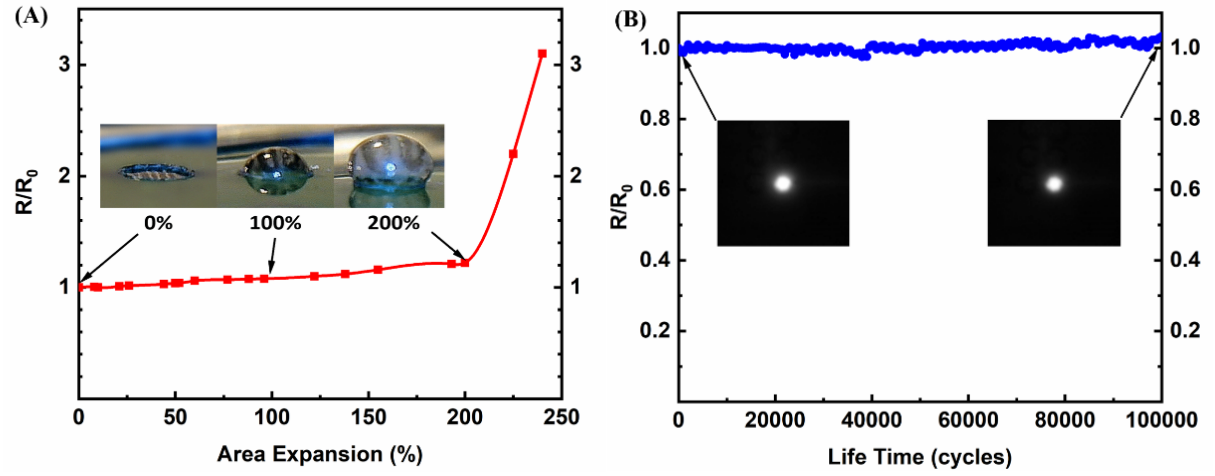

Figure 4-6 (A) Normalized resistance of one S-CNT electrode under different area expansions. (B) Lifetime test on the S-CNT Joule heating electrode with a 100% area expansion deforming and releasing cycle at a frequency of 0.8 Hz for over 100,000 cycles.

The blocking force of the taxels was tuned by using BSEP films of different thicknesses. The films were all actuated to a raised height of 0.5 mm. An incrementally increased force was applied to press on the tip of the raised dots until the dots became flattened. As shown in **Figure 4-7**, the measured blocking forces are 10, 51, and 95 grams for the BSEP films with thicknesses of 40 µm, 90 µm and 170 µm, respectively.

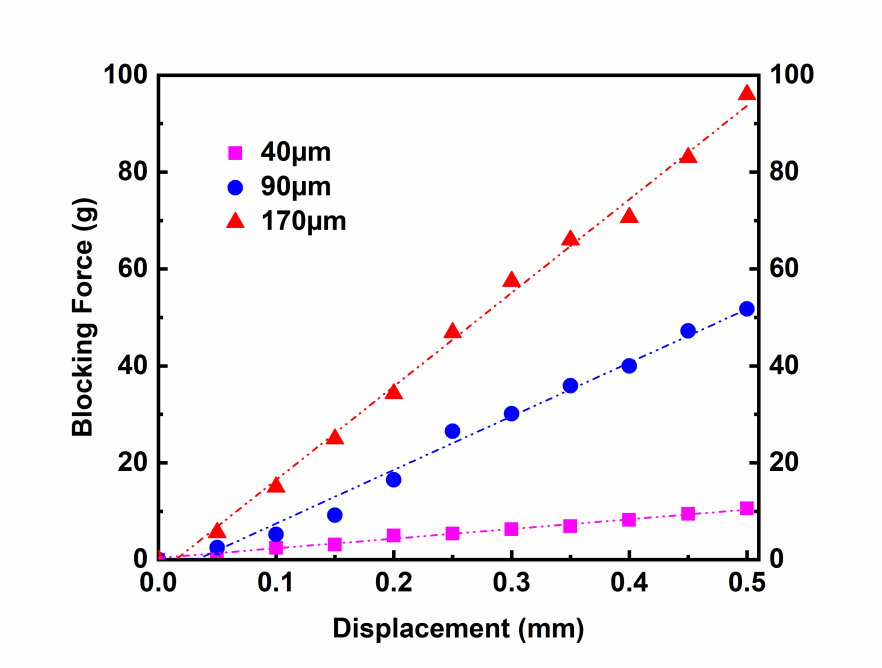

Figure 4-7 Forces applied to Braille dots originally raised by 0.5 mm and the displacements of the dot from the original raised height. Thickness of the BSEP films is specified.

4.4 Conclusions

BSEP's sharp transition temperature range allows rapid transition between its rigid and rubbery states by Joule heating. The transition temperature range is tunable by adjusting the polymer's composition. Above the transition temperature, the BSEP is in the rubbery state and exhibits large-strain deformation ability. This deformation is locked when it is cooled below the transition temperature. These unique properties make BSEP a suitable material for tactile display applications, such as Braille electronic readers. The tactile device we have developed can operate at a voltage supply as low as 30V. The serpentine-patterned carbon nanotube electrode enables uniform and high heating rates. The Braille dots can be operated repeatedly for over 100,000 cycles.

4.5 References

[1] R. Pelrine, R. Kornbluh, Q. Pei, J. Joseph, High-speed electrically actuated elastomers with strain greater than 100%. *Science*, **2000,** *287*(5454), 836.

[2] P. Brochu, Q. Pei, Advances in dielectric elastomers for actuators and artificial muscles. *Macromol. Rapid Commun.* **2010**, 31 (1), 10.

[3] J. Shintake, V. Cacucciolo, H. Shea, D. Floreano, Soft biomimetic fish robot made of dielectric elastomer actuators. *Soft Rob.* **2018**, 5(4), 466.

[4] F. Carpi, I. Anderson, S. Bauer, G. Frediani, G. Gallone, M. Gei, C. Graaf, C. Jean-Mistral, W. Kaal, G. Kofod, M. Kollosche, Standards for dielectric elastomer transducers. *Smart Mater. Struct.* **2015**, 24 (10), 105025.

[5] Z. Ren, W. Hu, C. Liu, S. Li, X. Niu, Q. Pei, Phase-changing bistable electroactive polymer exhibiting sharp rigid-to-rubbery transition. *Macromolecules* **2015**, 49 (1), 134.

[6] Yu, Z.; Yuan, W.; Brochu, P.; Chen, B.; Liu, Z.; Pei, Q., Large-strain, rigid-to-rigid deformation of bistable electroactive polymers. *Appl. Phys. Lett.* **2009**, 95 (19), 192904.

[7] N. Besse, S. Rosset, J. Zarate, H. Shea, Flexible active skin: large reconfigurable arrays of individually addressed shape memory polymer actuators. *Adv. Mater. Technol.* **2017**, 2(10), 1700102.

[8] National Federation of the Blind: Programs and Policy Research, "Statistical facts about blindness in the United States (2011)", https://nfb.org/factsaboutblindnessintheus, retrieved 2013-10-08.

[9] National Eye Institute, "Blindness, Statistics and Data [NEI]." Accessed April 12, 2013. http://www.nei.nih.gov/eyedata/blind.asp. Retrieved 2013-10-08.

[10] Y. Qiu, Z. Lu, Q. Pei, Refreshable tactile display based on a bistable electroactive polymer and a stretchable serpentine Joule heating electrode. *ACS Appl. Mater. Interfaces* **2018**, 10 (29), 24807.

[11] Y. Qiu, Z. Ren, W. Hu, C. Liu, Q. Pei, Bistable electroactive polymer with sharp rigid-to-rubbery phase transition. In Electroactive Polymer Actuators and Devices (*EAPAD*) **2016**, 9798, 97981U.

[12] Y. Kagami, J. Gong, Y. Osada, Shape memory behaviors of crosslinked copolymers containing stearyl acrylate. *Macromol. Rapid Commun.* **1996**, 17(8), 539.

[13] A. Matsuda, J. Sato, H. Yasunaga, Y. Osada, Order-disorder transition of a hydrogel containing an n-alkyl acrylate. *Macromolecules* **1994**, 27(26), 7695.

[14] N. Plate, V. Shibaev, B. Petrukhin, Y. Zubov, V. Kargin, Structure of crystalline polymers with unbranched long side chains. *J. Polym. Sci., Part A: Polym. Chem.* **1971**, 9(8), 2291.

[15] W. Yuan, L. Hu, Z. Yu, T. Lam, J. Biggs, S. Ha, D. Xi, B. Chen, M. Senesky, G. Grüner, Q. Pei, Fault-tolerant dielectric elastomer actuators using single-walled carbon nanotube electrodes. *Adv. Mater.* **2008**, 20(3), 621.

[16] W. Yuan, P. Brochu, H. Zhang, A. Jan, Q. Pei, Long lifetime dielectric elastomer actuators under continuous high strain actuation. In Electroactive Polymer Actuators and Devices (*EAPAD*) **2009**, 7287, 72870O.

Chapter 5 CONCLUSIONS AND FUTURE DIRECTIONS

5.1 Summary of this dissertation

This dissertation focuses on the research of dielectric elastomer actuation, including DE material synthesis, compliant electrode exploration, and multilayer DEA stacking processes innovation. A dielectric elastomer derivative named bistable electroactive polymer was also investigated, and its pneumatic actuation mechanism coupled with a stretchable Joule heating electrode was studied for a tactile display application.

The electrode exploration was mainly on improving the operational stability and durability under large actuation strains. To achieve that, an interpenetrating bilayer compliant electrode comprising a thin layer of a water-based polyurethane overcoated on an ultra-thin single-walled carbon nanotube layer was developed. The thin polyurethane layer serves as the dielectric barrier to suppress corona discharges of the nanotubes in air for reducing the localized breakdown events. The compliant bilayer electrode has the capability to self-clear at breakdown sites, enhancing the fault tolerance and mendability of the DEA at a large-strain actuation. Stable actuation at 150% area strain for 1000 cycles under square-wave voltage and 5.5-hours continuous actuation at a constant voltage have been achieved for acrylic elastomer-based DEAs.

In terms of dielectric elastomer materials improvements, the focus was on synthesizing a prestrain-locked high-performance acrylic thin films for avoiding the bulky prestraining structures. This thin film, when sandwiched with a compliant bilayer electrode, achieved a high actuation performance, fast response speed, and long-term actuation stability. Moreover, a hybrid manufacturing approach was developed and utilized to fabricate multilayer stacks based on the prestrain-locked DEs and

bilayer electrodes. The sets of stacking processes were demonstrated to be reliable, repeatable, and scalable, opening the door for high-performance multilayer DEAs fabrication.

BSEP, a derivative of dielectric elastomers, combines shape memory properties with large-strain actuation at the rubbery state for achieving the rigid-to-rigid actuation. The reversible melting-crystallization of polymer chains in the phase-changing BSEP leads to a narrow temperature change to complete the stiffness change of more than 1000 folds within ±3 °C. The application exploration was focused on tactile displays based on the pneumatic actuation mechanism for avoiding the high voltage of dielectric actuation. A serpentine-shaped compliant electrode was employed as the Joule heater and coated on a BSEP film to realize localized actuation for meeting the standard resolution of Braille electronics. After coupling with a pneumatic pressure source, diaphragm dots with 1.5mm base diameters were raised to heights up to 0.7 mm. The resulting tactile display can be actuated with low voltages, unlike conventional dielectric elastomer devices which operate at a few kV.

5.2 Future directions

The prestrain-locked high-performance DE materials coupling with stable compliant electrodes should facilitate the transition of the acrylate-based DEAs into practical applications. The hybrid manufacturing to fabricate multilayer stacks scales up energy and power outputs of the DEAs and the processing technique is quite scalable to produce a large number of devices.

From the actuator standpoint, DEAs have been explored in applications including biologically inspired robotics, tactile displays, tunable optics, and microfluidics. But almost all the related studies have been stopped at demo stages, mainly due to devices' lacking stability and durability. The combination of our prestrain-locked high-performance DE materials with stable compliant

bilayer electrodes, and scalable multilayer stack fabrication process could be a step forward towards real applications. Using tunable optic lens as an example, there are at least three requirements for a practical product: 1) The device function needs to be stable, 2) the lifetime needs to be long, and 3) the device needs to be safe to use. Our DE materials and electrodes have been shown to meet the first two requirements. For the last one, while DEAs typically require a driving voltage of several kV to reach required strains, we can take the advantage of multilayer stacks to scale up the energy and power outputs while reducing the driving voltages by using thinner DE films in stacks. Machines to automate the process in a cleanroom will be required, as handling and stacking ultrathin DE films in an ordinary lab setting is a nightmare.

Another interesting direction could be using our hybrid manufacturing to make stacks for dielectric elastomer generator-related applications. Opposite to the DEAs' converting electrical energy to mechanical energy, DEGs convert mechanical deformations into electrical energy based on the difference in capacitance in the DE films between the stretched and contracted states. Multiple factors would need to be considered to maximize the generated energy. The response speed of the DE materials cannot be slow to have a fast charge and discharge speed, and the coupling efficiency from the source energy to the mechanical deformation of the DE is a key for determining the generated energy. Our prestrain-locked acrylate-based DE material exhibits a small energy loss factor, high dielectric constant, and good elastic stretchability, and, therefore could be a good candidate for DEG applications.